Decarbonizing Freight Transport:

Mobile Carbon Capture from Heavy-Duty Vehicles

by

Christina D. Reynolds

A dissertation submitted in partial fulfillment
of the requirements for the degree of
Doctor of Philosophy
(Environmental Engineering)
in the University of Michigan
2019

Doctoral Committee:

Associate Professor Christian Lastoskie, Chair
Research Associate Professor Herek Clack
Assistant Professor Brian Ellis
Assistant Professor Gretchen Keppel-Aleks

Christina D. Reynolds

creyn@umich.edu

ORCID iD: 0000-0002-5512-409X

Dedication

To my father,

Thank you for instilling in me a love of learning and a desire to accomplish great things.

Acknowledgements

This work was funded by an Oak Ridge Institute for Science and Education (ORISE) fellowship, a Rackham Merit Fellowship, a Dow Doctoral Sustainability Fellowship, and a Student Program for Environmental Excellence in Design (SPEED) grant from the EPA National Vehicle and Fuel Emissions Laboratory (NVFEL).

I owe many thanks to my research advisor, Dr. Christian Lastoskie, who convinced me to stay when I thought I was ready to leave. I cannot thank you enough for seeing my potential. I also owe a great deal of thanks to my committee members, Dr. Gretchen Keppel-Aleks, Dr. Brian Ellis, and Dr. Herek Clack. Thank you for the guidance and genuine interest in my work.

I have had the pleasure of working with some wonderful people at the NVFEL. There are more than I could name here, but I would specifically like to extend my thanks to Dr. Matt Brusstar, Tom Veling, and Greg Davis, who have provided endless mentorship and inspiration to me.

My research group and friends have served as a lifeline both personally and professionally – supplying me with infinite resources, feedback, and conversation. I am all the better for it.

My parents, Clyde and Sherri, and brothers, Lance and Cameron, taught me to value and balance intellect and kindness. Without their unconditional love and support, I never would have begun this journey, much less finished.

My husband, Matt, supported me through indecisiveness, self-doubt, and sometimes obsessive work habits. Thank you for being my rock, and for giving me our wonderful kids. Fox and Jemma are, without a doubt, the very best parts of me.

Table of Contents

List of Tables

Table

List of Figures

Figure

Abstract

Predictions for future carbon dioxide emission reductions largely rely on power generation shifts to renewable energy sources and passenger vehicle electrification, while emissions from on-road freight shipping using heavy-duty vehicles (HDV) are expected to increase significantly over the coming decades. Mobile carbon capture (MCC) using porous solid adsorbents is a yet unexplored decarbonization strategy, the evaluation of which requires a study of the ideal materials and conditions for capture as well as the environmental, economic, and social implications of a global mobile carbon capture program for heavy-duty vehicles (HDVCC).

While many porous materials are researched as carbon capture adsorbents, their carbon dioxide storage capacity at higher temperatures, in the range of 40°C to 75ºC and representative of vehicle exhaust streams, is critical to assess performance under realistic conditions. To quantify the impact on uptake capacity of elevated temperatures characteristic of vehicle exhaust, pressure swing isotherms were conducted on eight commercially available porous adsorbents at temperatures from 25°C to 100ºC. The materials tested included two activated carbons, two zeolite molecular sieves, and four metal-organic framework (MOF) adsorbents.

An average decrease of 25% in the CO_2 adsorption capacity was observed for zeolites, activated carbons, and MOFs at 101 kPa pressure for each 15ºC stepwise increase in the measured isotherm. Isosteric heats of adsorption are obtained for each material using the Clausius-Clapeyron

equation and are in good agreement with adsorption enthalpies reported for these materials at similar temperatures. Among the materials considered, the reduction in CO_2 adsorption capacity with increasing temperature is least pronounced for zeolites 5A and 13X, which correspondingly have the largest heats of adsorption for carbon dioxide.

Candidate materials for HDVCC were then examined through a series of adsorption tests using dynamic flow of representative exhaust gas blends containing CO_2, CO, NO, and H_2O at temperatures and pressures characteristic of tailpipe exhaust. Of the materials tested, Zeolite 5A is a prime candidate for MCC, capturing approximately 11 weight % from representative wet diesel exhaust. Uptake can be further enhanced by cooling or removing water vapor from the exhaust gas; adding a high surface area heat exchanger prior to the adsorption bed accomplishes both, increasing capture to 15 weight %.

After establishing the technical feasibility of capturing carbon from HDV, we then explore if HDVCC is a viable and sustainable decarbonization strategy for the transportation sector. Publications addressing MCC claim it is cost-prohibitive because of high mass requirements, often offering direct air capture as a better means of indirectly reducing vehicle emissions. In the economic evaluation, we show that the hypothetical carbon abatement cost of HDVCC is competitive with both stationary carbon capture and battery electric vehicles at ~\$100/tCO_2 avoided.

The environmental impact of HDVCC was explored using an open-source simple climate model, the primary result of which is a range of warming (0.12°C – 0.15°C) that could be avoided if HDVCC is implemented between 2025 and 2040. Finally, a framework for the design of emerging technology was adapted to build an evaluation tool for consumers to compare HDVCC against traditional and electric HDV (using overhead catenary lines). The science and

sustainability components encompass a comprehensive assessment of HDVCC, which is found to be a practical, cost-effective, and sustainable approach to mitigating carbon emissions from on-road sources and would ideally be implemented and integrated alongside stationary carbon capture.

Chapter 1

Introduction

1.1 Carbon Emissions and Climate Change

Large scale efforts to quantify and understand climate change were initiated in the 1980s with the establishment of the Intergovernmental Panel on Climate Change (IPCC). Their five published summary reports have reached the same conclusions with increasing certainty: "warming of the climate system is unequivocal" and "human influence on the climate system is clear" (IPCC, 2013). Predictions for future emissions pathways are made by global climate models, based on socioeconomic assumptions like population, gross domestic product, and energy intensity (GCP, 2016).

As Figure 1.1 illustrates, historic emissions through 2014 (shown in black) match the steep increase of the highest emissions pathway, corresponding to a century-end temperature anomaly

between 3.2 and 5.4°C. More recently, emissions have begun to decrease as a result of the growth of renewable energy and a switch from coal to natural gas for stationary power generation; as of March 2019, atmospheric CO_2 is at 411 parts-per-million (ppm) (NOAA, 2019) and the global temperature anomaly is +0.86°C/+1.55°F (Energy, 2016). CO_2 emissions over the past decade have increased annually at a rate of 2.7% (Cuéllar-Franca & Azapagic, 2014); at this rate, atmospheric CO_2 would reach 500 ppm by 2050 and 800 ppm by 2100 (Wennersten et al, 2014).

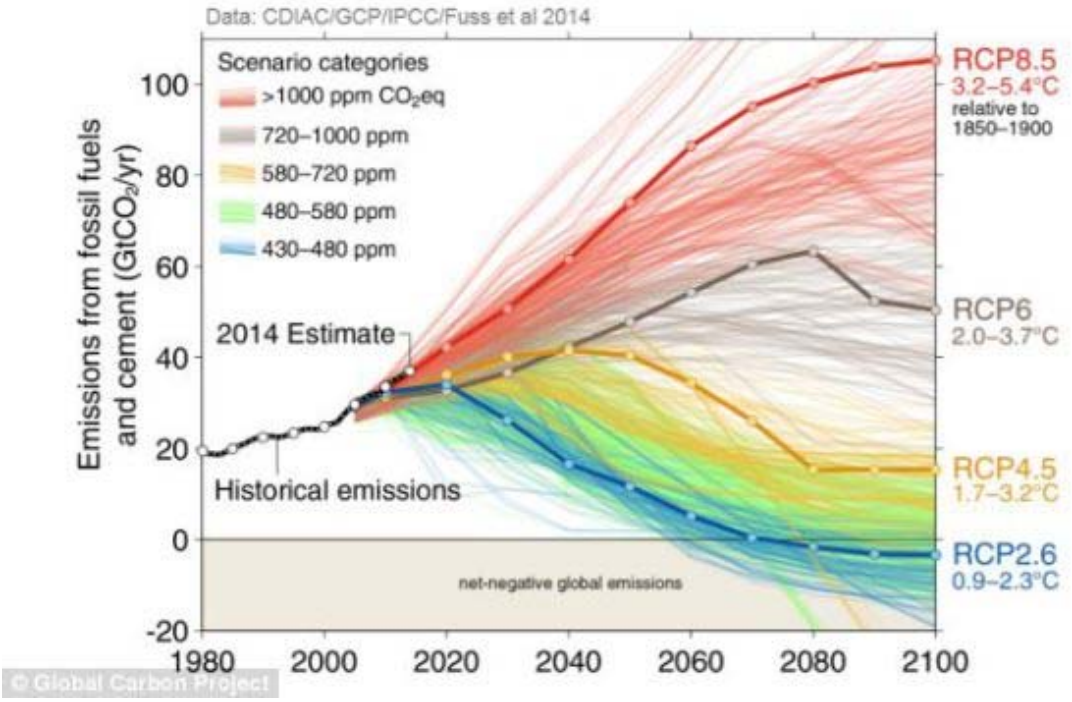

Figure 1.1 | Global CO_2 emissions projections to 2100 for four representative pathways, color-coded by the century-end range of atmospheric CO_2 concentration, incoming solar radiation, and warming (GCP, 2016)

Carbon-based fuels currently supply 85% of the global energy demand (Birol, 2014); existing infrastructure ensures that carbon fuels will remain central to the global economy for decades. Two of the six biggest polluters, China and India, are currently undergoing rapid economic development, fueled by cheap fossil fuels. Their abundant coal resources guarantee that

their CO_2 emissions will rise considerably in the coming years to decades (Wennersten et al, 2014), further exacerbated by exponential population growth.

Without definitive action to reduce these growing emissions, the Earth will be propelled into catastrophic climate change; at lower positive temperature anomalies, the impacts of climate change include more frequent hot days and heat waves, sea level rise, melting glaciers, ocean acidification, decreases in agricultural yield, heavier precipitation, and increased storm severity and drought (Lynas, 2008). Many of these changes are already happening; a new record for the highest global average surface temperatures has been set every year since 2014 (NOAA, 2019).

In 2016, the Paris Agreement was made by 196 state parties to limit global average temperature increases to well below 2°C above pre-industrial levels (UNFCC, 2016), which would benefit human health, ecosystem vigor, resource sufficiency, and energy resilience (IPCC, 2013). Strict and prompt emissions reductions are necessary to limit negative impacts of climate change, but there is not a single end-all solution. Rather, the answer lies in many smaller solutions that combat climate change via incremental reductions.

There are five general categories for CO_2 emissions reductions:

1. *Lower individual use*, which is most challenging in developed, affluent nations and involves conservation and reduced use of luxuries (air conditioning, air travel);
2. *Improvements in energy efficiency*, which has operational limitations and is less likely to be implemented in developing countries;
3. *Increases in nuclear power*, which encounter social acceptance and trust issues as a result of the nuclear disasters in Chernobyl, Ukraine and Fukushima, Japan;
4. *Renewable energy developmen*t, which has realistic limitations related to land and water availability and concerns about baseload power supply; and

5. *Carbon capture and storage* (CCS), which removes CO_2 from stationary or vehicle exhaust or directly from the atmosphere.

1.2 Methods and Materials for Carbon Dioxide Capture

CCS describes any process aimed at separating CO_2 from other gases, with a goal of lowering emissions or atmospheric concentrations (Pires et al, 2011). Three sectors where CCS could be deployed are stationary power generation facilities, on-board vehicles, and direct air capture. CCS has been shown to theoretically reduce the global warming potential from power plants, the highest point source for greenhouse gas (GHG) emissions, by 63-82% (Cuéllar-Franca & Azapagic, 2014). For direct air capture with carbon storage (DACCS), two distinct hurdles must be overcome to make it a cost-affordable emissions reduction option: high energy intensity (to separate diluted CO_2 from ambient air) and high water consumption (equivalent to 4% of annual crop cultivation use) (Damm & Fedorov, 2008).

Of the three general methods for CCS (pre-combustion, oxy-fuel, or post-combustion), post-combustion capture permits the continued combustion of fossil fuels, as the CO_2 capture is a separate process. The sorption process is either physical, where the gas adheres to a surface through van der Waals forces, or chemical, where bonds are created. The current standard for stationary post-combustion CCS is an absorption process called amine scrubbing, where a liquid solvent forms a chemical bond with CO_2. Solvent regeneration and CO_2 recovery are accomplished by heating the solvent with a counter-flow of steam or by raising the temperature or lowering the pressure of the absorbent bed (Metz et al, 2012).

There are several disadvantages of liquid capture processes: high energy penalty of regeneration, loss of solvent via evaporation, limited cyclic stability, equipment corrosion, solvent

degradation in the presence of oxygen, and unsustainable disposal methods (Pires et al, 2011). Additionally, the energy penalty incurred initializes a feedback loop: more fossil fuels must be burned to account for the energy diverted to regenerate the absorbent, thus increasing the emissions of CO_2 and increasing the amount of material that would need to be regenerated (Supekar & Skerlos, 2015). When the regeneration energy source is carbon-based, the capture process can never be truly sustainable.

To circumvent the problems associated with liquid absorption and to minimize the energy penalty for regeneration, a porous solid adsorbent can be used instead (Delgado et al, 2006). The process would be dry, stable over many cycles, require less energy, and would still retain high CO_2 capacity and selectivity in a regenerative process (Metz et al, 2012). The solid adsorption-desorption process is shown in Figure 1.2. For effective carbon capture, the material must have a low energy requirement for regeneration, cyclic stability, contaminant tolerance, good selectivity, high capacity, and low cost (Figueroa et al, 2008). Most commonly, activated carbons or zeolites are used for gas purification; they are affordable on a large scale, are porous, stable, and selectively adsorb carbon dioxide.

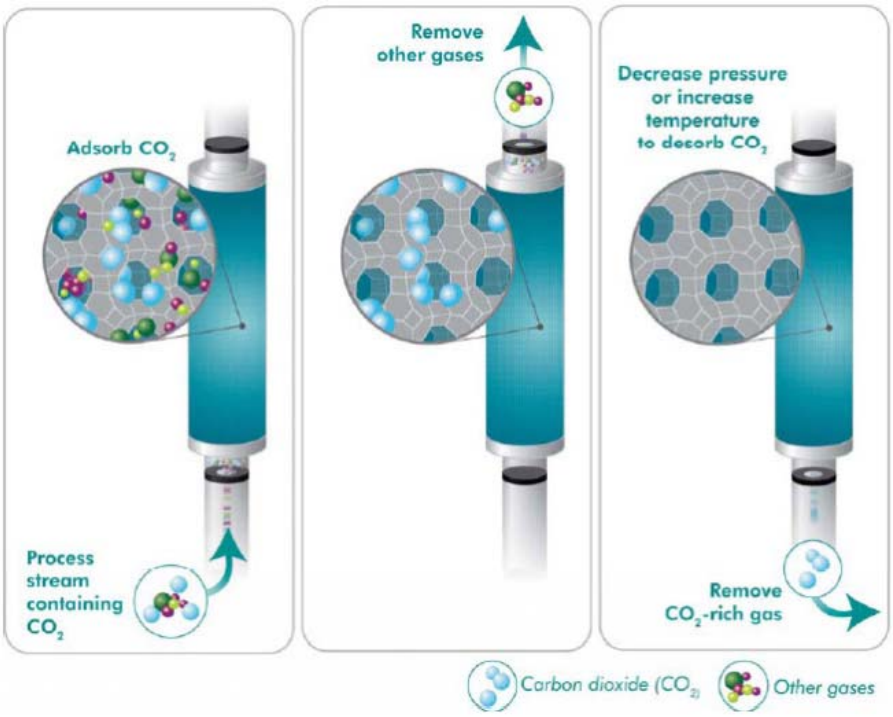

Figure 1.2 | CO_2 separation via adsorption on a porous solid material (CO2CRC, 2017)

Neither zeolites nor activated carbons completely satisfy the array of requirements necessary for large-scale affordable CO_2 separation due to their low storage capacity and/or gas selectivity, which is why the study of metal organic frameworks (MOFs) has recently received a remarkable level of attention in chemistry research. MOFs are characterized by metal centers surrounded by a charge-balancing counter-ion and connected via organic ligands (Kitagawa et al, 2004). The high CO_2 sorption capacity of MOFs is attributed to their high specific surface area and low density (Lastoskie, 2010). The size, shape, and coordination of the MOFs can be altered by changing the metal, counter-ion, or organic linker, thus allowing for a nearly infinite set of tailored MOFs designed for specific applications. The resultant frameworks are robust and permanently porous (Kitagawa et al, 2004). CO_2 affinity is further increased through the use of open metal sites, polarization, and quadrupole moments (Li et al, 2011).

Elastic-layered metal organic frameworks (ELMs) describe MOFs that exhibit a novel gating phenomenon, expanding from empty to saturated pores at their gate pressure. The isotherm of an ELM is a rectangular hysteresis loop, indicative of full desorption of captured CO_2 with a modest decrease in pressure (Kanoh et al 2009). Another category, called zeolitic imidazolate frameworks (ZIFs), covers an overlap between MOFs and zeolites; the metal centers are all connected via imidazolate and form a 145° angle characteristic of zeolites. ZIFs are known for their permanent porosity and stability under harsh conditions, along with a high capacity for CO_2 (Phan et al, 2010).

Some MOFs have shown remarkably high storage capacity at atmospheric pressures and room temperature, holding over 50 liters of CO_2 per liter of material (Wang et al, 2008; Banerjee et al, 2008). Compounds with extremely high storage capacity are only useful if these traits can be maintained in the presence of water over repeated cycles (Nguyen et al, 2014). Effective MOF testing for post-combustion capture is performed in the presence of a wet gas stream at conditions near ambient, with a concurrent evaluation of minimum energy requirements for regeneration (Fracaroli et al, 2014).

The synthesis procedures for most MOFs is complex and costly, involving the combination of a metal salt with an organic linker in an aqueous solvent. Depending on the components, the solution precipitates either immediately (facilitated by vigorous stirring), via slow diffusion over high contact area (left undisturbed for weeks), or by thermal degradation (heating to deprotonate the organic linker) (Eddaoudi et al, 2001; Phan et al, 2010; Cheng et al, 2011). The resulting yield is limited to milligrams; without the development of industrial processes to generate greater volumes, large-scale pilot testing is impractical. Instead, scaled testing of materials and conditions for carbon capture is limited to commercially-available adsorbents.

1.3 A Solution for Transportation Sector Emissions

More than two-thirds of global CO_2 emissions are from the transportation and small-scale distributed power sector, with 47% of transportation GHG emissions coming from passenger cars (Damm & Fedorov, 2008). Projections through 2040 have petroleum and other liquid fuels at the greatest usage, leading to the greatest source of CO_2 emissions (Conti, 2016), with transportation sector emissions becoming the largest source by 2035 (Kopp et al, 2013) and doubling by 2050 (Marchal et al., 2012). Reducing these emissions under a continuous carbon-fuel economy can be tackled in the same manner as stationary capture: mobile carbon capture (MCC) is post-combustion removal of CO_2 from vehicle exhaust.

Vehicles undergo transient operation, have a constrained size and weight, are often operated in harsh conditions, and require high efficiency to meet regulations. For these reasons, assumptions are often made that carbon sequestration from the transportation sector is not a viable option or is prohibitively expensive (Lackner, 2001; Damm & Fedorov, 2008; DeCicco, 2015). The most common concern regarding MCC is the large mass and volume requirements associated with capturing and storing the CO_2 and adsorbent; the mass from one gallon of gasoline increases 330% in equivalent CO_2 after combustion. Options that minimize on-board storage requirements include more frequent gas offloading or less total volume captured (Sullivan & Sivak, 2012).

A proposed MCC scheme, outlined in Figure 1.3, permits uninterrupted use of carbon fuels for vehicle transportation. The generated CO_2 would be collected and stored on-board the vehicle during the daily commute, and then the vehicle would be plugged in to a collection unit at home to regenerate the adsorbent and siphon the collected CO_2. The collection unit would rely on electricity to generate heat, avoiding parasitic mass on the vehicle, and the source of energy for regeneration would be CO_2-free electricity, thus minimizing overall emissions. The ability to

integrate this system with existing technology would allow for a more sustainable transportation energy system and would greatly reduce total CO_2 emissions.

The reduction potential of MCC is downplayed because of the longevity of CO2 in the atmosphere; carbon dioxide results in a peak warming about 10 years after emissions occur (Ricke & Caldeira, 2014), meaning the benefits from a reduction in emissions would be realized by the same society/generation that enacted the reductions. Thus, **actions to limit CO_2 emissions from vehicles would have a direct impact on today's drivers**.

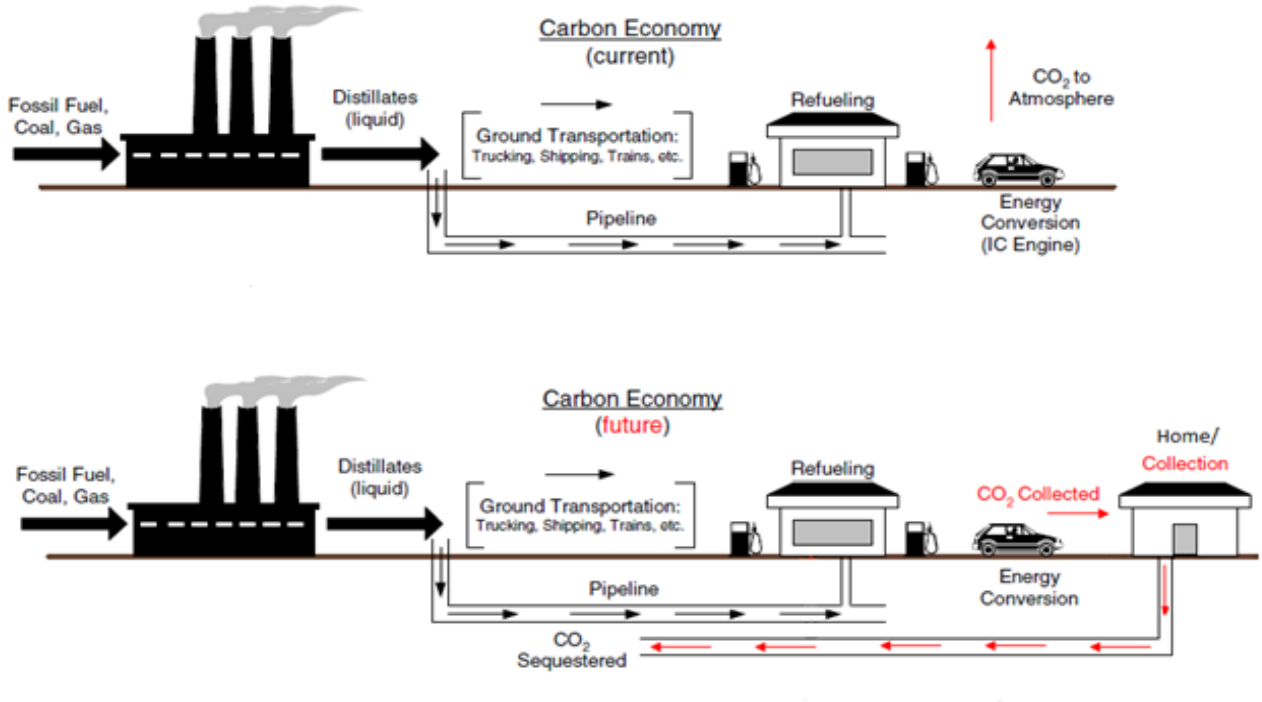

Figure 1.3 | CO_2 collection system proposed in an MCC scenario for passenger vehicles, with regeneration infrastructure occurring at home and CO_2 transport via pipeline (Damm & Fedorov, 2008)

1.4 Designing a Sustainable MCC System

In global climate policy architecture, effective incentives that ensure low cost must be made for participation and compliance. The global consensus is that the industrialized world must

make binding emissions commitments before the developing world (Aldy et al, 2003). A scientific effort to limit emissions, with a focus on technological advancements, is best realized in a developed, high income country. The assumption, which has proven true in regard to developed versus developing countries' adaptations, is that air pollution policies increase proportionately with income (van Vuuren et al, 2011).

Several note-worthy events have occurred in recent years as a result of former President Obama's Climate Action Plan and global calls for climate change action: the EPA passed a ruling in 2013 that all new power plants would be limited on carbon emissions; the US made a joint announcement with China in 2014 about ambitious emissions targets for 2025 that cut pollution by 26-28 percent from 2005 levels (White House, 2014); in 2015 the EPA's Clean Power Plan was established to set carbon pollution standards for existing power plants (EPA, 2015); and, in 2016, the US joined over 190 other countries in support of the Paris Agreement to combat climate change (White House, 2016).

There are two paths to societal influence on CCS ventures: either policy and regulations prompt public support, or public support prompts policy and regulations. For CCS from vehicles, policy would be necessary to promote a transformation shift in the transportation sector. Most likely, that policy would not occur without wide public acceptance. Any successful mitigation strategy must have a high abatement potential with a low abatement cost (Nauclér & Enkvist, 2009). Most CCS options have a high abatement cost for a moderate abatement potential; to ensure the abatement potential of the higher cost alternatives, climate models are used herein to illustrate the environmental benefits of such a venture.

Public participation in the decision-making process around MCC is vital to success. A driver opinion survey (Sullivan & Sivak, 2012) evaluated potential mobile carbon capture

technology by surveying drivers on what options would be preferable regarding maximum cost, reduction in fuel economy, storage lost, preference over electric vehicles (Table 1.1).

Table 1.1 | Driver opinion regarding mobile carbon capture preferences

Capturing 20% of CO_2 Emissions				**Capturing 80% of CO_2 Emissions**			
Cost	Reduction in Fuel Economy	Loss of Storage	Preference over BEV/Hybrid	Cost	Reduction in Fuel Economy	Loss of Storage	Preference over BEV/Hybrid
$200	8%	10%	33%	$500	15%	16%	67%

Respondents were willing to pay more for the capture system if they already drove a hybrid, were educated (beyond high school), had smaller cars, or were female. The authors asserted that "respondents have limited ability to place a sensible value on this new and unfamiliar capability," which is justified considering the lack of information on this emerging technology. Any evaluation of public perception must focus on education in addition to other impacts (cost, benefit, or consumer decision-making).

1.5 Scope and Outline of Thesis

A comprehensive evaluation of MCC as a potential solution to rising carbon emissions in the transportation sector must cover all of the following components:

1. *Technical feasibility*
    a. Optimal storage capacity under ideal conditions
    b. Realistic performance under exhaust conditions
    c. Scaled testing to proof-of-concept

2. *Social responsibility*

    a. Environmental impact

    b. Economic assessment

    c. Public perception

Collectively, these components cover the two major questions surrounding MCC and the main motivations for this work – could we capture carbon dioxide emissions from vehicles under actual exhaust conditions and, more importantly, should we pursue MCC as a solution to rising transportation sector emissions?

In Chapter 1, carbon emissions, transportation sector challenges, and plans for evaluating MCC are summarized. Chapter 2 summarizes the commercially-available materials selected for the study, their performance at elevated temperatures, and the associated isosteric heats of adsorption based on loading. Chapter 3 covers a small-scale apparatus design, along with testing of candidate materials under dual (N_2+CO_2), dry (N_2+CO_2+CO+NO), and wet (dry blend + H_2O) gas blends.

In chapter 4, an economic evaluation of MCC is performed based on the thermodynamic energy requirements and the calculated carbon abatement cost is compared with similar low-carbon ventures. Chapter 5 expands on the sustainable design of an MCC system through the use of a simple climate model to evaluate the environmental response, an emerging technology framework to assist with consumer decision making, and a cost-benefit analysis using the social cost of carbon. The final chapter summarizes the important findings of this work and plans for how it could be continued in the future.

Chapter 2

A Comparative Study on CO_2 Uptake in Porous Solid Materials at Elevated Temperatures

2.1 Introduction

The main driver of climate change is an increase in the concentration of carbon dioxide (CO_2) in the atmosphere. Natural sources and sinks produce and utilize CO_2 on a much larger scale but have existed in a carbon cycle equilibrium for thousands of years (IPCC, 2013). It was only after the Industrial Revolution- when the practice of fossil fuel combustion became commonplace- that atmospheric CO_2 levels began to increase (Ritchie & Roser, 2019). To prevent the emission of CO_2, carbon capture and storage (CCS) is used to remove CO_2 from exhaust gases before it is discharged into the atmosphere. An abundance of materials, both solid and liquid, exist that can

selectively capture and temporarily store carbon dioxide. The most promising of these are deemed "next-generation" materials and are synthesized and studied at laboratory scale; few are available commercially and commonly used in industrial gas separation.

Various publications examine porous materials suitable for carbon capture. Most focus on the synthesis and characterization of novel materials or the comparison of materials at specified conditions, often standard temperature and pressure (STP: 298 K, 101 kPa). A review of CO_2 adsorption by metal organic frameworks (MOFs), benchmarked against activated carbons and zeolites, at conditions near ambient (pressure from 0.85 to 1 bar, temperature from 273 to 318 K) provides a baseline for adsorption at STP (Keskin, van Heest, & Scholl, 2010). Other studies (Yazaydin et al, 2009; Singh & Kumar, 2016; Burchell et al, 1997; Song & Lee, 1998; Yong, Mata, & Rodrigues, 2001) examine multiple compounds for CO_2 capture at pressures (0.1 bar = 10% CO_2) and/or temperatures (298K – 338K) that are more representative of realistic exhaust conditions. A comparison of experimental results and published data can be found in Table 2.9.

Common adsorption isotherms report the pressure swing performance of materials, but rarely is the focus on the performance of multiple compounds at temperatures above ambient. Real-world CCS applications from exhaust gases would involve elevated temperatures; in the transportation sector, average tailpipe exhaust (measured post-tailpipe using an infrared thermometer) ranges from 50 to 75°C.

2.2 Materials and Methods

2.2.1 Methodology

To assess the impact of real-world exhaust temperature on the CO_2 uptake capacity of carbon capture materials, a series of commercially-available adsorbents were analyzed for their

capacity at temperatures of 25, 40, 55, and 70°C, while molecular sieves (zeolites) were further tested at temperatures of 85 and 100°C.

Using a Micromeretics ASAP 2050 Extended Adsorption Gas Analyzer, the compounds were subjected to a vacuum under 0.03 kPa and concurrent heating to 180ºC for 2 hours. Pressure swing adsorption measurements were made using a range of 5 to 120 kPa of CO_2 while the samples were immersed in a Thermo Fisher AC150 water bath. Physical adsorption is an exothermic process; as temperature increases, Le Chatelier's principle dictates that the system will adsorb less to reach equilibrium. A quantification of this equilibrium shift is herein evaluated at partial pressures corresponding to the volumetric CO_2 concentration in vehicle exhaust (0.12 – 0.14 kPa, equivalent to 12-14% CO_2).

2.2.2 Materials

The eight compounds under consideration include two activated carbons, two molecular sieves, two MOFs, one zeolitic imidazolate framework (ZIF), and one elastic-layered MOF (ELM). A MOF is characterized by a metal center that is charge-balanced by a counter-ion and connected by organic linkers. A ZIF is a crossover between a MOF, having the same metal-organic structure with imidazolate as the linker, and a zeolite, having the same characteristic 145º angle. An ELM is a category of MOF that exhibits a novel gating phenomenon from closed to open at a compound-specific gate pressure. All materials exhibit selective uptake of CO_2 and have significant storage capacity under specified conditions.

Tables 2.1-2.4 show the physical appearance and chemical characteristics of the activated carbons and zeolites included in the study. Darco KB-M (powdered) and BPL (granular) are affordable industry standard activated carbons commonly used for gas separation due to their high

porosity and surface area, but this does not correspond to high selectivity or CO_2 storage capacity. Several papers evaluating carbon capture materials have included BPL as an activated carbon benchmark; most relevant is the evaluation of pressure swing adsorption of CO_2, CH_4, and N_2 on BPL at 25ºC (McEwen, Hayman, & Yazaydin, 2013).

Table 2.1 | Characteristics of Darco KB-M PAC

Chemical Name	C
Type	Powdered Activated Carbon
Manufacturer	Cabot-Norit
Molecular Weight [g/mol]	12
Density [g/mL]	0.45
BET Surface Area [m^2/g]	~1000

Table 2.2 | Characteristics of BPL 6x16 GAC

Chemical Name	C
Type	Granular Activated Carbon
Manufacturer	Calgon
Molecular Weight [g/mol]	12
Density [g/mL]	0.60
BET Surface Area [m^2/g]	1068

Zeolites are another class of porous solids, comprised of crystalline aluminosilicates that function as molecular sieves and are typically named by their pore size (5A has 5 angstrom pore openings). Zeolites are noted for their high capacity, selectivity, and thermal stability but low porosity leading to slow internal gas transport (Hao, Li, & Lu, 2011). Zeolite 5A (powder) and Zeolite 13X (4-8 mesh beads) selectively capture CO_2 because their open pores are larger than the

diameter of a CO_2 molecule (3.30 angstroms) (Li et al, 2011). Both zeolites have been studied for their pressure swing performance at temperatures up to 250ºC (Lee et al, 2002; Wang & LeVan, 2009; Mulloth & Finn, 1998; Saha et al, 2010). There are reported inconsistencies when comparing zeolite performance at high temperatures and pressures (Dirar & Loughlin, 2013), but this could be attributed to variations in materials purchased and testing methods.

Table 2.3 | Characteristics of Zeolite 5A Powder

Chemical Name	$CaO + Na_2O + Al_2O_3 + SiO_2$
Type	Molecular Sieve
Manufacturer	Sigma-Aldrich
Molecular Weight [g/mol]	162
Density [g/mL]	0.48
BET Surface Area [m^2/g]	550

Table 2.4 | Characteristics of Zeolite 13X 4-8 Mesh

Chemical Name	$Na_2O + Al_2O_3 + SiO_2$
Type	Molecular Sieve
Manufacturer	Sigma-Aldrich
Molecular Weight [g/mol]	162
Density [g/mL]	0.69
BET Surface Area [m^2/g]	488

Zeolites and activated carbons are out-performed by MOFs in total CO_2 storage capacity in systems where pressure and temperature can be manipulated. Their high CO_2 capacity is attributed to high specific surface area and low density (Kitagawa, Kitaura, & Noro, 2004). Tables 2.5-2.8 show the four commercially-available MOFs included in this study.

Several MOFs have pores that only open under high pressure. An example is MIL-53, which has an adsorption capacity for CO_2 of approximately 40 weight percent (wt%) above 5 atmospheres but reaches a plateau at about 10 wt% below this pressure (Couck et al, 2009). It has large and narrow pore openings, and the extent that the pores open is a stress function of temperature and pressure (Boutin et al, 2010). Several MOFs have open metal sites for preferential bonding of CO_2; HKUST-1 has unsaturated Cu(II) centers. Small amounts of water in HKUST-1 increase CO_2 loading, but that all storage capacity is lost when the relative humidity of the gas stream reaches ~67% (Liu et al, 2010).

Table 2.5 | Characteristics of MIL-53 / Basolite A100

Chemical Name	Aluminum terephthalate, $C_8H_5AlO_5$
Type	Metal Organic Framework
Manufacturer	BASF
Molecular Weight [g/mol]	208.1
Density [g/mL]	0.40
BET Surface Area [m^2/g]	~1300

Table 2.6 | Characteristics of HKUST-1 / Cu-BTC / Basolite C300

Chemical Name	Copper benzene-1,3,5-tricarboxylate, $C_{18}H_6Cu_3O_{12}$
Type	Metal Organic Framework
Manufacturer	BASF
Molecular Weight [g/mol]	604.9
Density [g/mL]	0.35
BET Surface Area [m^2/g]	~1500

ZIFs have high chemical and thermal stability, along with a permanent porosity, permitting an extremely high CO_2 storage capacity with correspondingly low heat-energy requirements for regeneration (Phan et al, 2010). ZIF-8 has 11.6 angstrom pore openings, ideal for large guest molecules (Fairen-Jimenez et al, 2011). ELM-11 exhibits a unique gating isotherm containing a rectangular hysteresis loop, with higher temperature resulting in increased gating pressure (Kanoh et al, 2009).

Table 2.7 | Characteristics of ZIF-8 / Basolite Z1200

Chemical Name	2-methyimidazole zinc salt, $C_8H_{12}N_4Zn$
Type	ZIF
Manufacturer	BASF
Molecular Weight [g/mol]	229.6
Density [g/mL]	0.35
BET Surface Area [m^2/g]	~1200

Table 2.8 | Characteristics of (pre) ELM-11

Chemical Name	$Cu(bpy)_2(BF_4)_2$, $C_{20}H_{20}B_2CuF_8N_4O_2$
Type	Elastic-layered MOF
Manufacturer	Tokyo Chemical Industry
Molecular Weight [g/mol]	585.6
Density [g/mL]	~0.37
BET Surface Area [m^2/g]	~1100

2.3 Results and Discussion

2.3.1 Elevated Temperature Isotherms

Across all materials tested, carbon dioxide uptake ranges from 30 to 230 milligrams of CO_2 adsorbed per gram of material (equal to 3 - 23 wt%) at an atmospheric pressure of 101 kPa. At 12-

14 kPa, shown by the vertical gray bar in Figures 2.1-2.8, CO_2 uptake for both activated carbons remain under 2% by weight, even under ambient temperature (Figures 2.1-2.2).

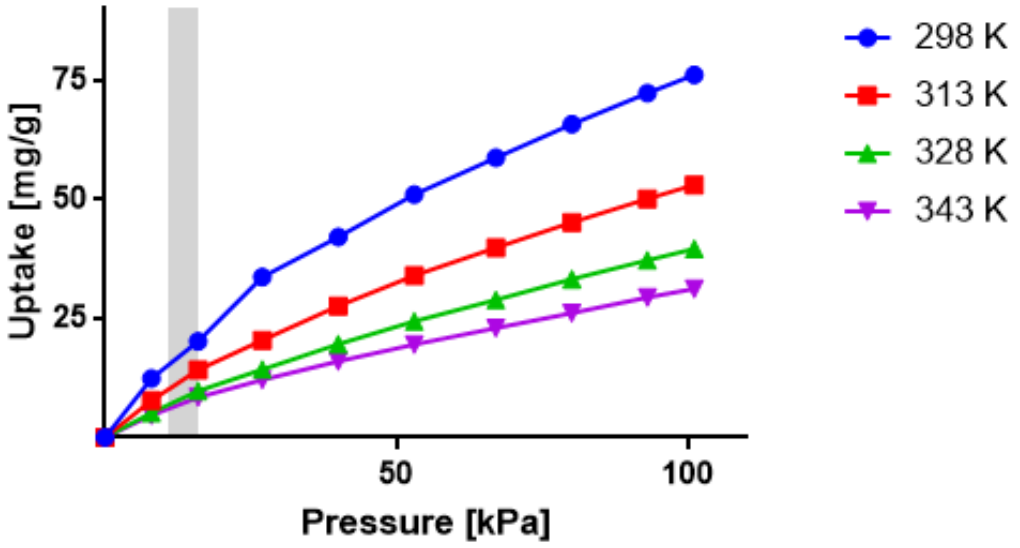

Figure 2.1 | Pure CO_2 pressure swing isotherm for BPL 6x16 mesh GAC, with a partial pressure corresponding to 12-14% CO_2 represented by the gray vertical bar

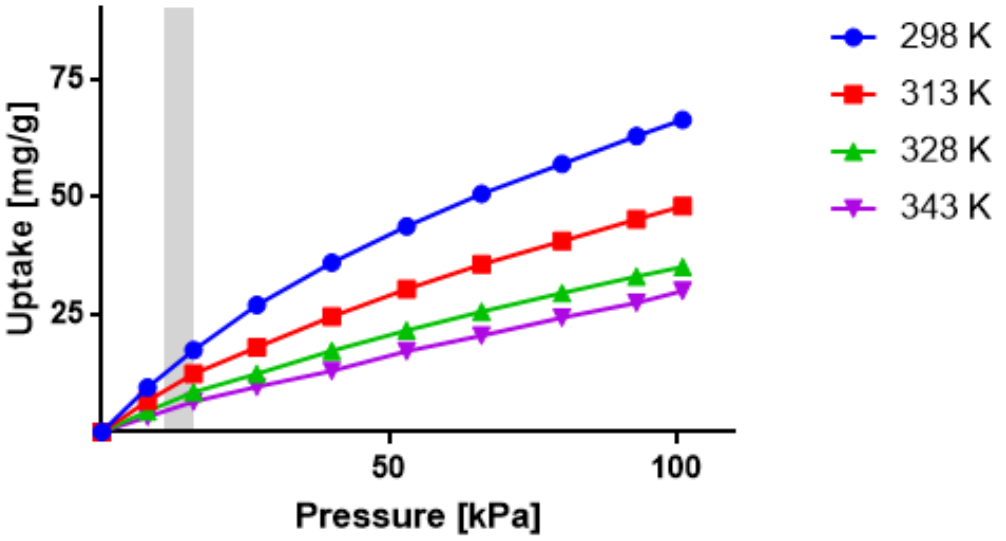

Figure 2.2 | Pure CO_2 pressure swing isotherm for Darco KB-M PAC, with a partial pressure corresponding to 12-14% CO_2 represented by the gray vertical bar

At these pressures and temperatures, the highest uptake capacity for CO_2 is found in the zeolite materials (Figures 2.3-2.4); their steep uptake at low pressures is highly beneficial for most exhaust streams, where the CO_2 concentration is less than 15%. Uptake at ambient temperature and at the partial pressure of interest (gray bar) is ~15-20% by weight. Even at 70ºC, uptake for Zeolite 5A at 14 kPa remains around 10 wt%. At the same pressure but a temperature approaching 100ºC, uptake decreases to 5 wt%. Under the same conditions (14 kPa, 70ºC and ~100ºC), Zeolite 13X only achieves 6 and 3 wt%, respectively.

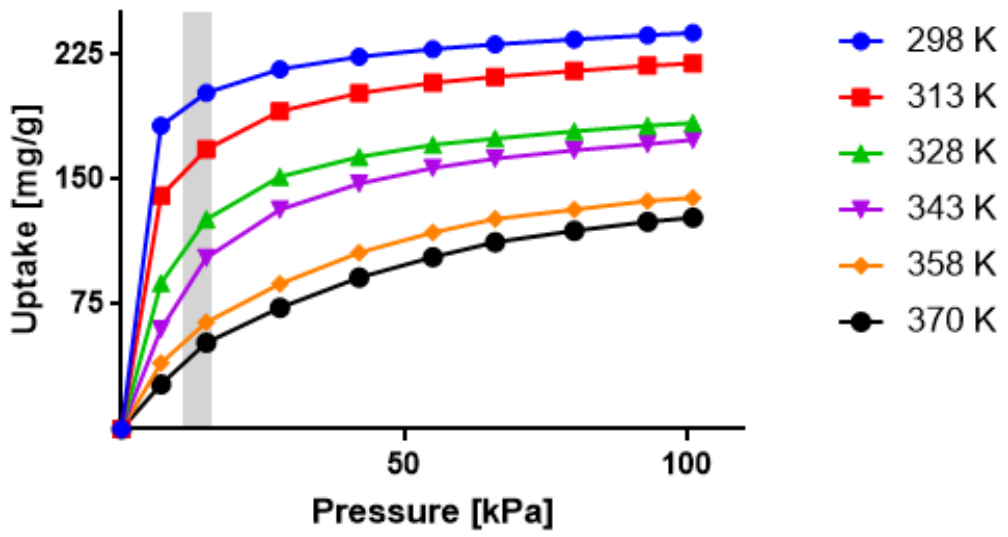

Figure 2.3 | Pure CO_2 pressure swing isotherm for Zeolite 5A, with a partial pressure corresponding to 12-14% CO_2 represented by the gray vertical bar

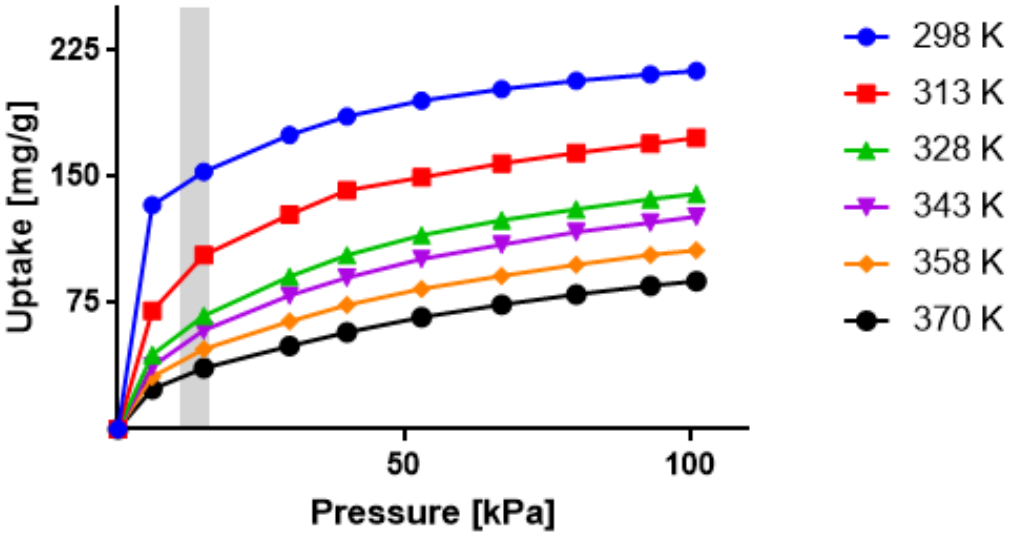

Figure 2.4 | Pure CO_2 pressure swing isotherm for Zeolite 13X, with a partial pressure corresponding to 12-14% CO_2 represented by the gray vertical bar

Adsorption onto MIL-53 (Figure 2.5) remains under 10 wt%, even at ambient temperatures, whereas HKUST-1 (Figure 2.6) can achieve almost 20 wt% under the same conditions. The growth of this curve is linear, however, giving a performance at 12-14 kPa of only ~3 wt% at ambient temperature and under 1 wt% at 70ºC.

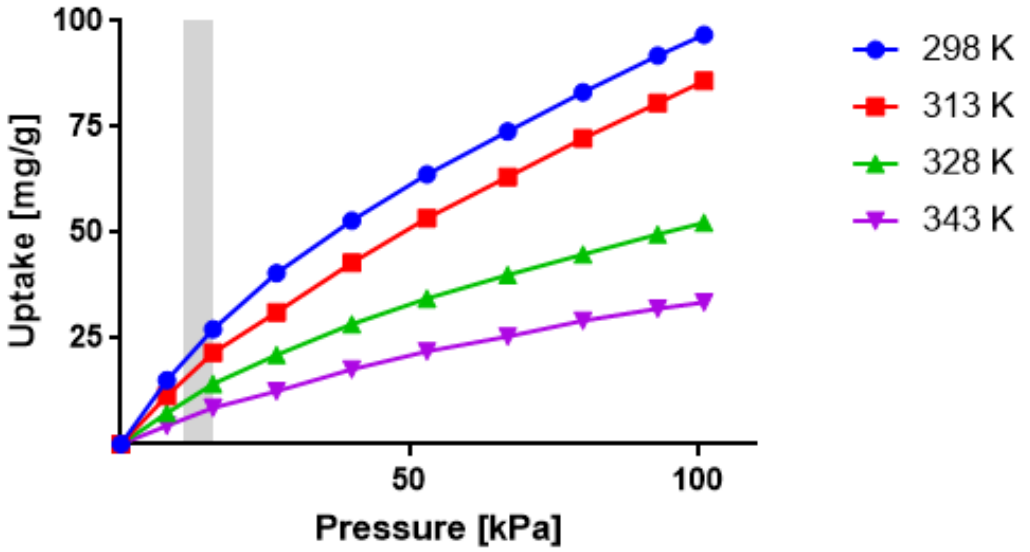

Figure 2.5 | Pure CO_2 pressure swing isotherm for MIL-53, with a partial pressure corresponding to 12-14% CO_2 represented by the gray vertical bar

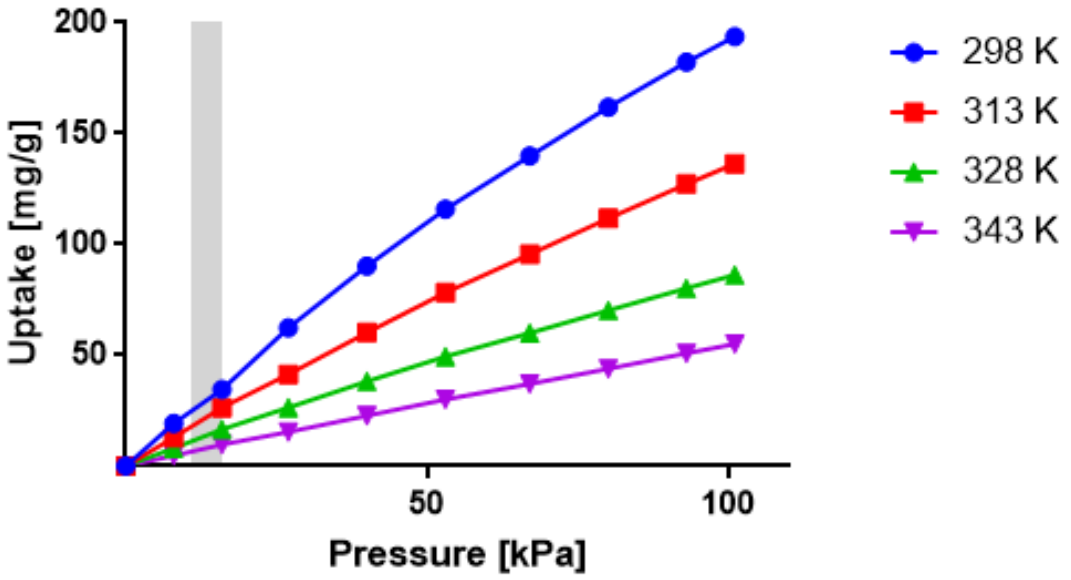

Figure 2.6 | Pure CO_2 pressure swing isotherm for HKUST-1, with a partial pressure corresponding to 12-14% CO_2 represented by the gray vertical bar

The remaining two compounds show poor CO_2 uptake even under ambient temperatures. ZIF-8 (Figure 2.7) captures only 3 wt% at STP. ELM-11 (Figure 2.8) is more promising, achieving 14 wt% at STP with a gate opening above 60 kPa (equal to a CO_2 concentration above 60%). At temperatures above ambient, the gate pressure exceeds 101 kPa, rendering uptake negligible. Thus, ELM-11 was deemed an outlier and removed from the comparison analysis.

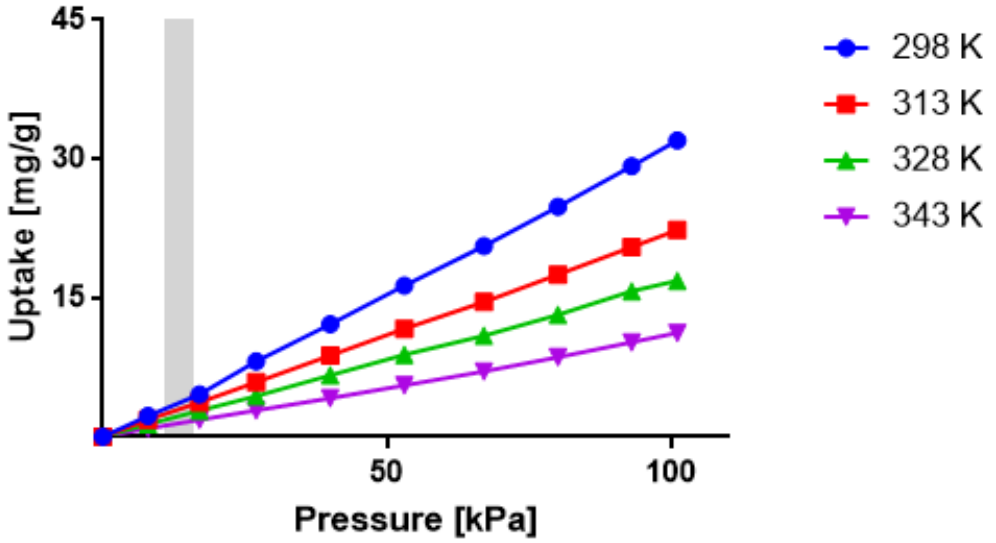

Figure 2.7 | Pure CO_2 pressure swing isotherm for ZIF-8, with a partial pressure corresponding to 12-14% CO_2 represented by the gray vertical bar

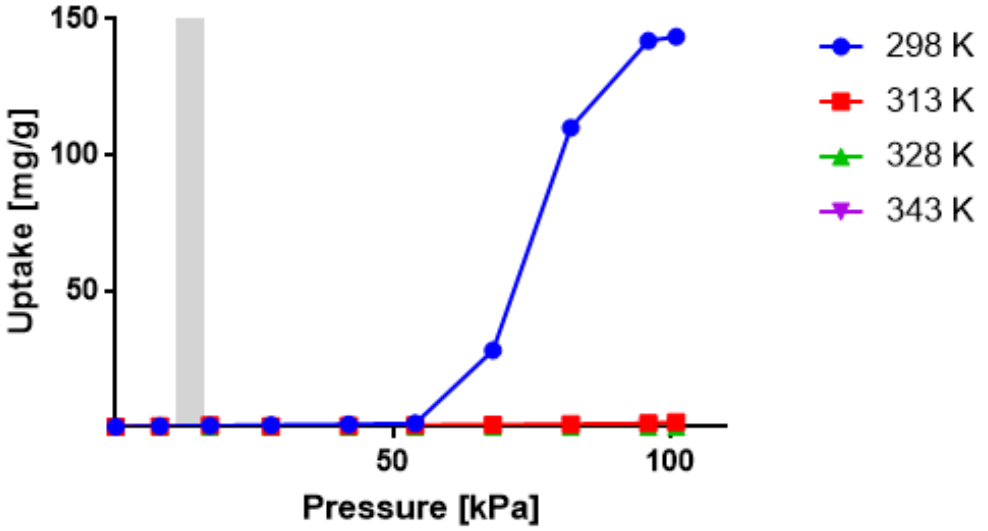

Figure 2.8 | Pure CO_2 pressure swing isotherm for ELM-11, with a partial pressure corresponding to 12-14% CO_2 represented by the gray vertical bar

The performance at each temperature step is illustrated in Figure 2.9, shown as the percentage of uptake capacity based on maximum uptake at STP (25°C, 101 kPa). The desired effect is minimal loss of uptake, which is best displayed by the zeolites (5A having the lowest loss of uptake).

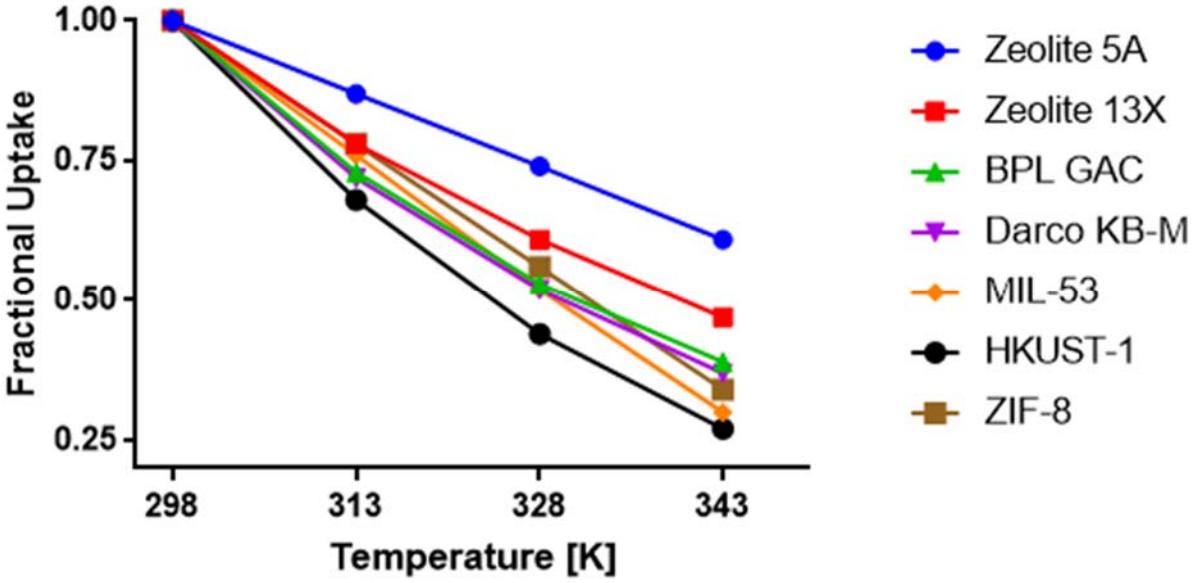

Figure 2.9 | Fraction of uptake capacity at constant pressure and 15K temperature steps, compared to maximum at 298K

The average fractional uptake for every +15ºC increase in temperature is 83, 73, and 68% for zeolites, activated carbon, and MOFs, respectively. Performance at 70ºC and atmospheric pressure for Zeolite 5A is 61% of maximum, or approximately 14 wt%. Table 2.9 summarizes material performance at STP compared to various published results as listed in section 2.1. The maximum error is found with ZIF-8, which could be attributed to different activation procedures. Darco KB-M is not included in the list but performs as expected for a powdered activated carbon (slightly less than Norit RB2 as reported by (Keskin, van Heest, & Scholl, 2010)).

Table 2.9 | CO_2 uptake at 298K and 101kPa and percent error for candidate materials, compared with results from published literature

	Findings	Literature	Error
	mmol/g		%
ZIF-8	0.73	1.02	0.28
BPL GAC	1.75	2	0.13
MIL-53	2.2	2	0.10
ELM-11	3.25	3.18	0.02
HKUST-1	4.45	5	0.11
Zeolite 13X	4.85	4.7	0.03
Zeolite 5A	5.4	4.89	0.10

2.3.2 Experimental Validation

The experimental results of the pure CO_2 isotherms were validated using a triple derivative mathematical proof (Kaplan, 2002), applied as shown in equation 1:

$$\left(\frac{\partial P}{\partial Q}\right)_T \left(\frac{\partial T}{\partial P}\right)_Q \left(\frac{\partial Q}{\partial T}\right)_P = -1 \tag{2.1}$$

where P is pressure (kPa), Q is uptake (mg/g), and T is temperature (K).

Each of the three derivatives is plotted and regression modeling gives the equation for the line of best fit; Figures 2.10-2.12 show the plots and regression lines for Zeolite 5A: Figure 2.10 is an isotherm, reflecting constant temperature; Figure 2.11 is an isostere, reflecting constant loading; and Figure 2.11 is an isobar, reflecting constant pressure. Regression analysis confirms the model and equations are a good fit for the experimental data, with an average root mean square error of 7% (with a corresponding range of 3% to 9%). Regression fits and equations for other materials can be found in Appendix A.

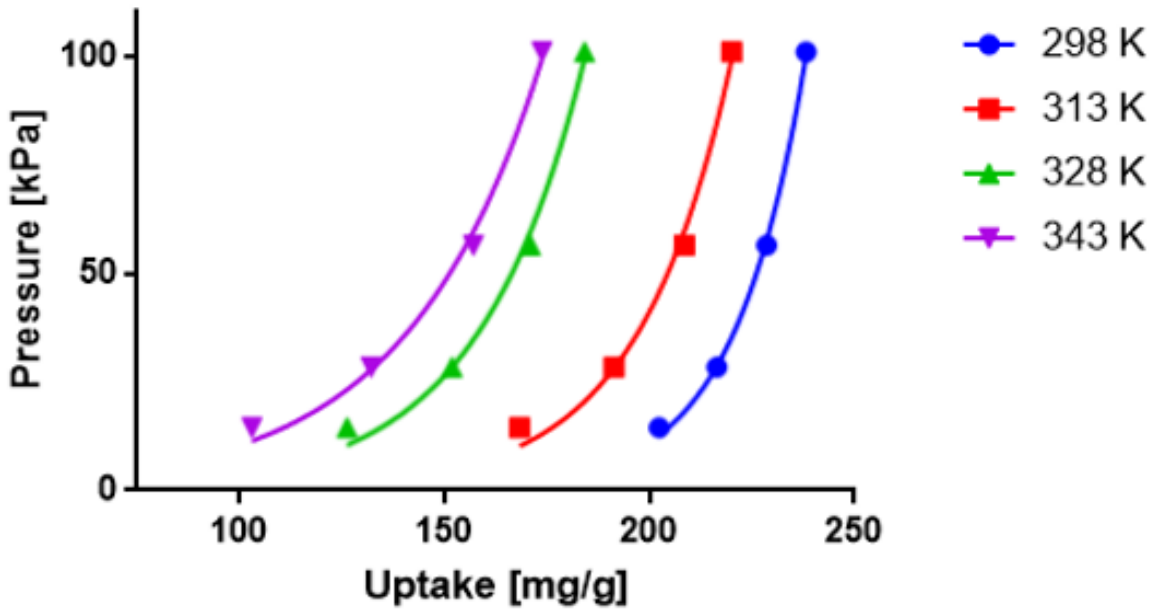

Figure 2.10 | Isotherm and regression lines for Zeolite 5A

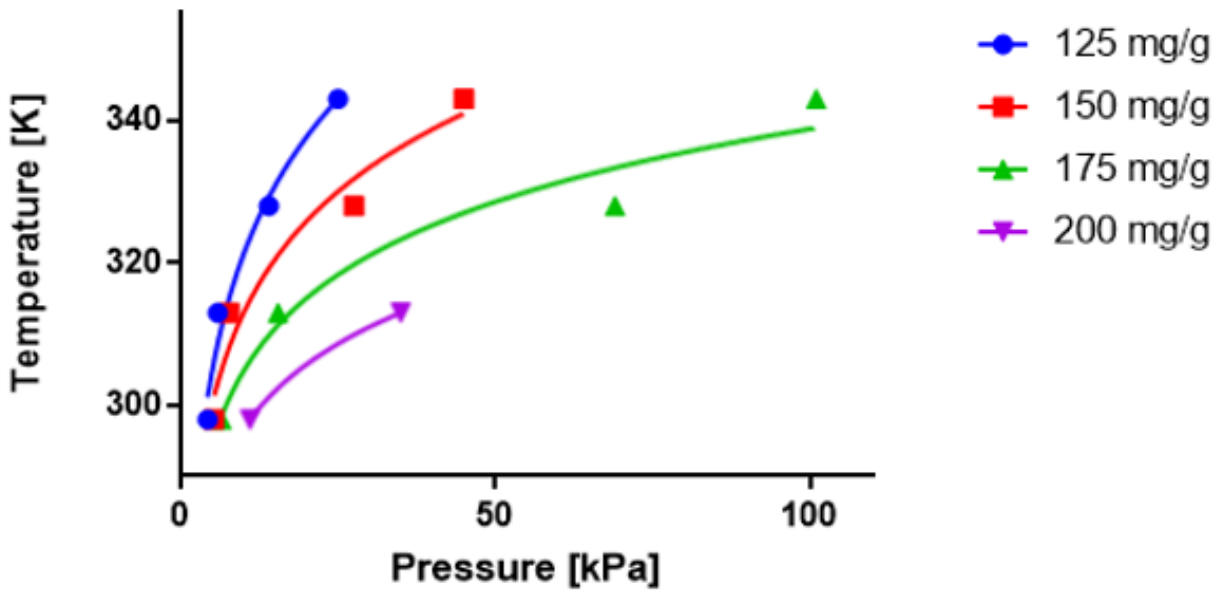

Figure 2.11 | Isostere and regression lines for Zeolite 5A

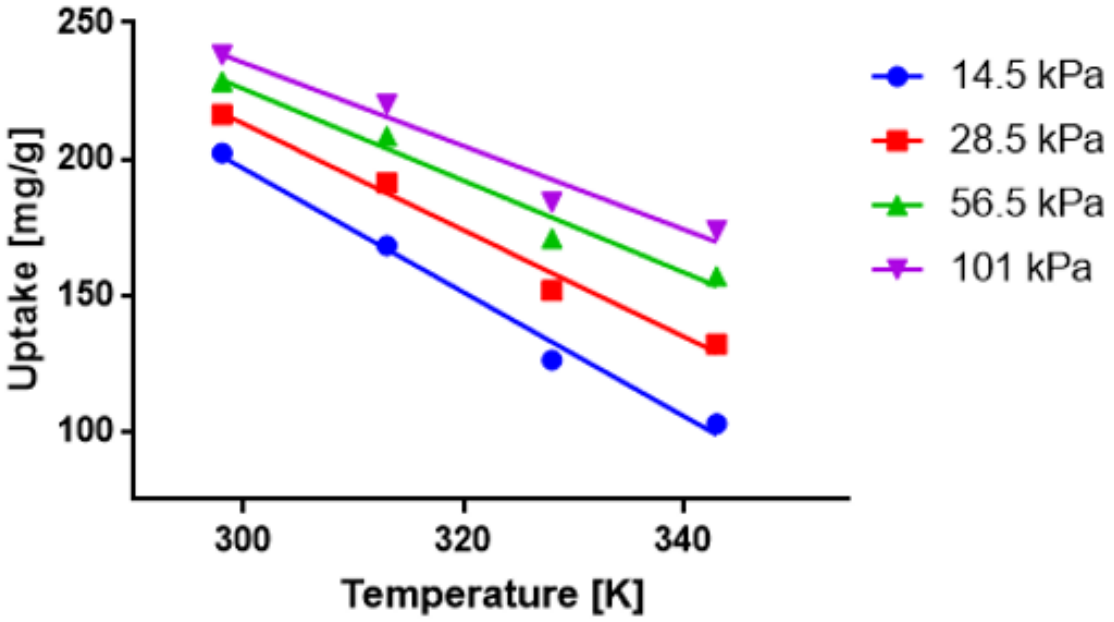

Figure 2.12 | Isobar and regression lines for Zeolite 5A

2.3.3 Isosteric Heat of Adsorption

The relationship between pressure and temperature under constant loading (equation 2.2), defined via the Clausius-Clapeyron equation, permits an examination of the isosteric heat of adsorption, which indicates the strength of the interaction between the gas adsorbate (CO_2) and the solid adsorbent. This parameter is critical in evaluating how much energy would be required to release captured CO_2 from an adsorbent. The heat value is found through linear regression on the plot of the natural log of the pressure against the inverse temperature (Pan, Ritter, & Balbuena, 1998) to find the isosteric heat, ΔH_{ads}.

$$\left(\frac{\partial lnP}{\partial(1/T)}\right)_{Q=constant} = \frac{\Delta H_{ads}}{R} \qquad \textbf{(2.2)}$$

where R is the gas constant of 8.314 J/K-mol (0.189 kJ/K-kg). Results for Zeolite 5A are shown in Figure 2.13; plots for other materials are located in Appendix A.

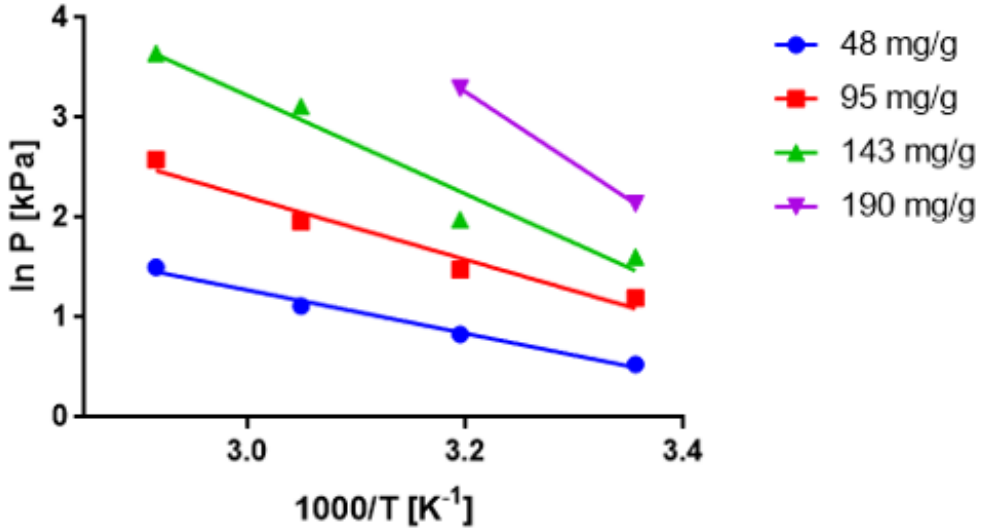

Figure 2.13 | Plot of the natural log of pressure versus inverse temperature at constant loading for Zeolite 5A

The isosteric heat plots, shown in Figure 2.14, were calculated at loading fractions of 0.2, 0.4, 0.5, 0.6, and 0.8, based on the maximum loading at STP. For the zeolite materials, isosteric heat is highest at low loading and reaches a steady value of 38 and 35 kJ/mol for 5A and 13X, respectively, at 0.4-0.6 loading. These values agree with published values (34-37 kJ/mol) for heat of adsorption at STP (Keskin, van Heest, & Sholl, 2010; Dirar & Loughlin, 2013). Constant heat of adsorption is indicative of uniform spatial interactions between gas and solids (Shen et al, 2000). Understandably, zeolites have the highest CO_2 storage capacity and corresponding isosteric heat.

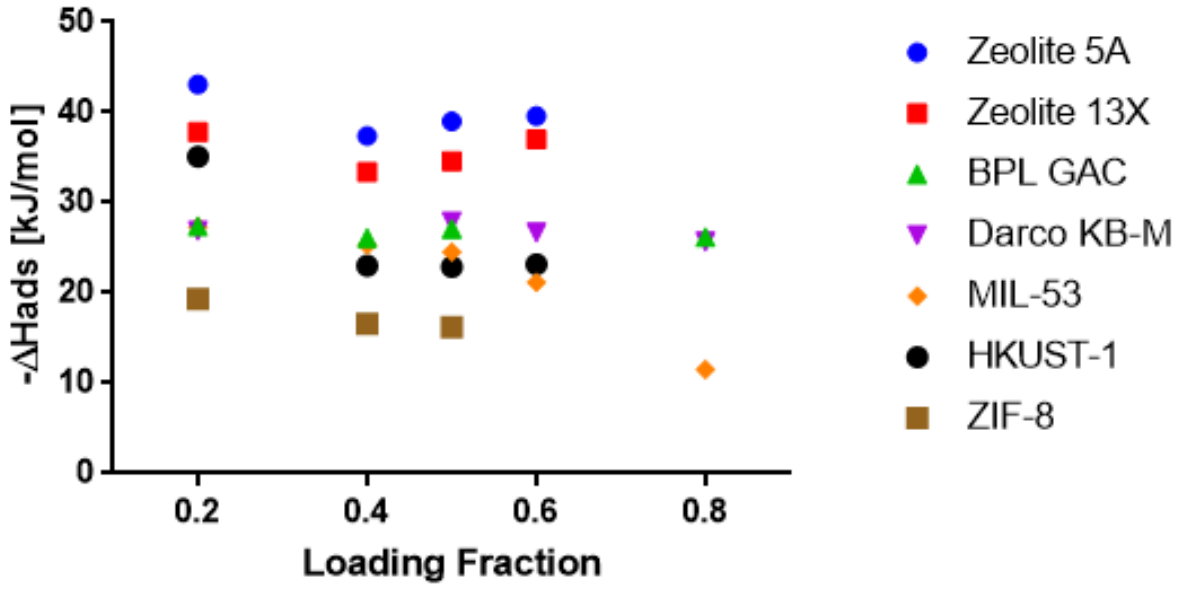

Figure 2.14 | Isosteric heats of adsorption at loadings of 20%, 40%, 50%, 60%, and 80% of maximum at STP

The rigid heterogeneous structure of the activated carbons dictates a constant isosteric heat (~26 kJ/mol) regardless of loading fraction, with a heat slightly higher than previously reported (23 kJ/mol) (Martin et al, 2011). The frameworks MIL-53, ZIF-8, and HKUST-1 exhibit isosteric heats that are dependent on loading fraction; $-\Delta H_{ads}$ decreases as loading fraction increases. The flexible pore structures of these MOFs permit rapid changes in isosteric heat, as the increasing presence of guest gas molecules show less attraction to the diminishing space remaining as the compound reaches saturation. At 50% loading, ZIF-8 and HKUST-1 exhibit heats of 16.2 and 26.6 kJ/mol, compared to published values of 15.5 and 25.4 kJ/mol, respectively (Bahamon & Vega, 2016). Results for MIL-53 average 25.6 kJ/mol, lying in the middle of the wide span of published results (12.5-39 kJ/mol) measured under much broader temperature and pressure ranges (Martin et al, 2011; Bahamon & Vega, 2016; Abid et al, 2016).

2.4 Conclusions

For mobile carbon capture applications, zeolites are the materials with the highest adsorption capacity and least loss of uptake with increasing temperature. The trade-off, however, is the higher heat needed to remove captured CO_2 once saturation has been reached. In addition to their beneficial storage capacity, zeolites are produced commercially in bulk and are affordable. This is not true for most of the materials tested; even with lower isosteric heats, their lower storage capacities and likely higher costs would exclude them as candidates for mobile carbon capture.

For all adsorbents, the decrease in performance at elevated temperature is of consequence when considering real-world carbon capture applications for exhaust gases, which would occur at temperatures of 50-75°C. At this anticipated temperature range, Zeolite 5A has a CO_2 storage capacity of 58-68% of maximum (at 298K). Winter climates and vessel design can work to further lower tailpipe exhaust temperatures and thus optimize conditions for carbon capture. An on-board capture system designed to remove CO_2 emissions from vehicle exhaust would therefore need to maximize the exposed surface area of the exhaust line to minimize operational temperatures for adsorption. This engineering design focus on lowering operational temperature would also have the added benefit of water vapor condensation, removing a prime competitor for CO_2 adsorption.

Chapter 3

Dynamic Adsorption of Carbon Dioxide from Multi-component Gases using Microporous Materials

3.1 Introduction

Traditional carbon capture methods target greenhouse gas emissions reductions from the electricity generation sector, long established as the highest emitting economic sector. In 2016, however, energy for transportation surpassed electricity generation for the first time since 1979 (EPA, 2018). While GHG emissions from other sectors decreased 24% between 1990 and 2009 (mainly attributed to the growth of renewable energy and the switch from coal to natural gas), transport emissions increased by 29% (Delft, 2012). The Organization for Economic Cooperation and Development projects that transport emissions will double by 2050 (Marchal et al., 2012),

while the World Bank estimates that transportation will be the single largest source of global GHG emissions by 2035 and 80% of total emissions by 2050 (Kopp et al., 2013).

Nearly half of all emissions can be attributed to liquid fuels; the transportation sector is fueled almost exclusively by petroleum and will continue to be fueled in this manner if internal combustion engines are the main power source for mobility. It is thus very likely that mobile power will continue to grow in both vehicles on the road and total miles travelled (EPA, 2018). While more stringent vehicle and emissions standards will reduce overall carbon dioxide emissions, the remaining options for further mitigating GHG emissions are either vehicle electrification with CO_2-free power or carbon capture from vehicle exhaust.

Similar to stationary carbon capture and storage (CCS), the method for removing CO_2 from exhaust can involve the use of either a liquid absorbent or a solid adsorbent that selectively pulls CO_2 from a complex gas mixture, where it is stored within the sorbent until it can be purged using heat or pressure. During the gas purge, the sorbent material is also regenerated so the capture cycle can be repeated (Wilcox, 2012).

To accomplish mobile carbon capture (MCC), a method is herein proposed to use porous solid compounds to adsorb carbon dioxide from the exhaust stream, where volumetric concentration is approximately 12-14% depending on the fuel. Candidate adsorbents for carbon capture must exhibit the following characteristics: high CO_2 capacity and selectivity, trace contaminant (carbon monoxide, nitrous oxides) tolerance, and hydrophobicity. In addition to these intrinsic properties, the materials must also perform under non-ideal conditions specific to mobile applications: elevated temperature, low operating pressure, high flow rates, and variable start-stop. All of these conditions are expected to lower the uptake capacity of the adsorbents.

3.2 Materials and Methods

3.2.1 Selection of Materials

Activated carbons and zeolites are the most well-known compounds for carbon capture, due to their affordability and bulk availability. There has been an extensive focus in recent years on next-generation materials for CCS – specifically, metal organic frameworks that can selectively adsorb CO_2. When synthesizing MOFs, the choice of metal center and organic linker can vastly differentiate the final compound: the choice of a metal cation with an open coordination site strongly favors CO_2 adsorption (Mason et al., 2015). While a plethora of MOFs exist that show high selectivity and storage capacity for CO_2, elaborate synthesis procedures and minimal yield exclude those materials from this study. Instead, the only compounds under consideration are those that show an affinity for CO_2 and are currently commercially available.

The eight compounds selected for dynamic bench-scale testing, as a continuation of elevated temperature isotherms reported in Chapter 2, are: Zeolite 5A, Zeolite 13X, BPL Granular Activated Carbon (GAC), Darco KB-M Powdered Activated Carbon (PAC), HKUST-1 (MOF), MIL-53 (MOF), ELM-11 (Elastic-layered MOF), and ZIF-8 (Zeolitic Imidazolate Framework). Physical structures include sticky powder, smooth micro-crystals, mesh pellets, charcoal powder, and granulated pieces. BPL was obtained from Calgon Carbon and Darco KB-M was obtained from Norit-Cabot. HKUST-1, MIL-53, and ZIF-8 were produced by BASF and obtained from Sigma Aldrich (Basolite C300, A100, and Z1200, respectively), along with Zeolites 5A and 13X. ELM-11 was obtained from Tokyo Chemical Industry as hydrous pre-ELM-11.

Table 3.1 | Relevant material properties for candidate porous solids

	Particle Size [µm]	Bulk density [g/mL]	(BET) SA [m²/g]
DARCO KB-M	40	0.46	-
BPL 6x16 mesh	1190	0.49	1068
Zeolite 5A (powder)	3.7	0.61	650
Zeolite 13X (4-8 mesh)	2380	0.78	600
Basolite A100 / MIL-53	31.55	0.43	1300
Basolite C300 / HKUST-1/Cu-BTC	15.96	0.78	1500
Basolite Z1200 / ZIF-8	4.9	0.22	1200
(pre) ELM-11	-	0.35	1100

Table 3.1 shows the large difference in particle size between the granular or mesh materials (BPL and Zeolite 13X) and also reports bulk (unloaded) density and surface area. Particle size and surface area were taken from manufacturer data while density was calculated using fresh unpacked material.

Activated carbons are composed of microcrystalline graphite stacked in a random orientation with a broad range of pore size distributions. They exhibit high porosity and surface area but poor CO_2 selectivity and capacity (McEwen et al., 2013).

Zeolites 13X and 5A are crystalline aluminosilicates that function as molecular sieves and are commonly studied because of their availability, affordability, and efficacy. They separate gases based primarily on kinetic diameter, permitting the collection of smaller-diameter species within their pores (approximately 1 and 0.5 nanometers (nm) for 13X and 5A, respectively). The kinetic diameter, listed in nm, of CO_2, CO, NO, N_2, and H_2O are 0.330, 0.376, 0.317, 0.364, and 0.265,

respectively (Mason et al, 2015). The significantly smaller size of water, compared to other gases present in exhaust, means that it easily competes for adsorption.

When the adsorbent carries a charge (as MOFs and zeolites do), the interaction is not based solely on size. Instead, distance-dependent Van der Waals and electrostatic forces dictate the behavior of CO_2 as a gas adsorbate due to its quadrupole moment, which is higher than most other species present in exhaust gas. The exception is water, which has a dipole moment that CO_2 and N_2 do not possess. This enhances its electrostatic contribution and thus causes preferential adsorption of H_2O over CO_2 for most adsorbents (Wilcox, 2012): the effect of humidity ranges from a decrease in capacity to structural degradation (Cheng et al., 2009).

For zeolites, H_2O preferentially adsorbs over CO_2, even at low pressure/water content (Kim et al., 2003). In fact, Zeolite 13X shows high water uptake (100%) and only moderate CO_2 recovery (60%) at very low pressures (Li et al., 2008). In activated carbons, CO_2-hydrates form in the pore spaces under high pressure (>4450 kPa) and slightly elevated temperature (< 283.5 K), leading to high storage capacities (Sun et al., 2007). For MOFs, repeated adsorption-desorption cycles show a decrease in CO_2 storage capacity as relative humidity increases (Kizzie et al., 2011). HKUST-1, however, exhibits an increase in uptake after exposure to low levels (<4%) of water content (Soubeyrand-Lenoir et al., 2012). Perhaps because of the challenge it poses, removing CO_2 from high humidity streams is not well-reported (Li et al., 2008).

A summary of static CO_2 uptake under elevated temperatures is shown in Figure 3.1, which illustrates uptake capacity (weight %, meaning grams of gas per gram of material) for pure CO_2 under static conditions at 298K and pressures of 101 kPa (atmospheric) and ~14 kPa (partial pressure corresponding to the concentration of CO_2 in vehicle exhaust). The zeolites show the

greatest capacity for CO_2, even at low pressures. MOFs, however, show minimal uptake in the low-pressure region but significantly more at higher pressures.

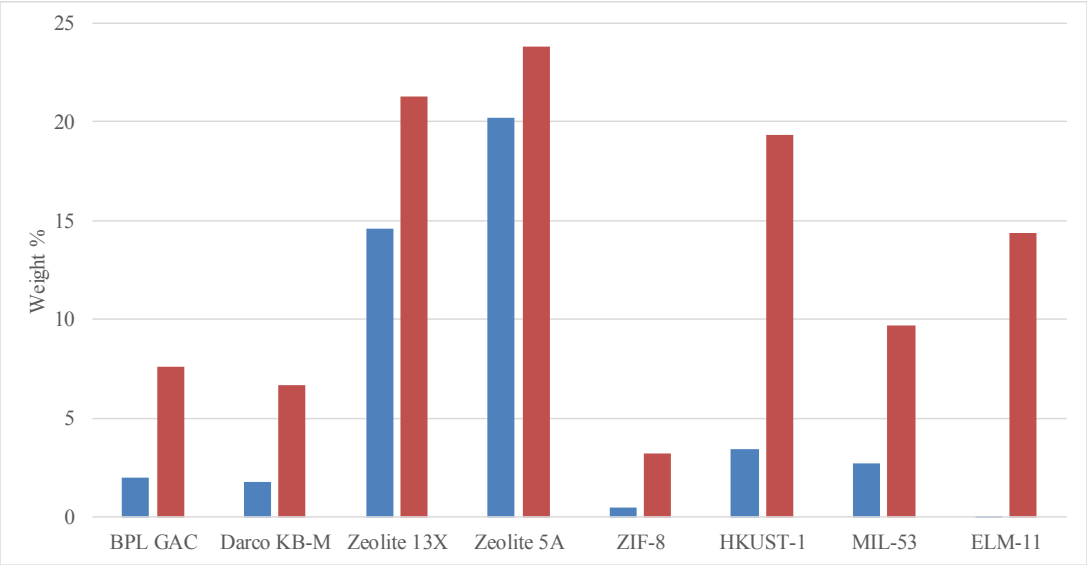

Figure 3.1 | Weight percent capture at 298K under partial pressures corresponding to 14% CO_2 (blue) and 100% CO_2 (red)

3.2.2 Operational Conditions and Constraints

The average composition of dry gasoline exhaust at the tailpipe is roughly 86% nitrogen (N_2), 13.5% CO_2, 400 parts-per-million (ppm) carbon monoxide (CO), 2-3 ppm nitric oxide (NO), 22 ppm total hydrocarbons, and 1992 ppm oxygen (O_2). For wet exhaust, H_2O would compromise 10-12% by volume. A gallon of diesel fuel will create about 15% more CO_2 emissions per gallon combusted than gasoline, but the higher fuel economy achieved by diesel vehicles more than offsets emissions on a gram-per-mile basis (EPA, 2018). For both wet and dry conditions, the percentages are relative since numerous environmental factors and operational parameters would directly influence the exhaust composition.

Vehicle certification testing undertaken at the U.S. EPA's National Vehicle and Fuel Emissions Laboratory (Ann Arbor, MI) does not typically include wet exhaust measurements for several reasons: (1) H_2O in exhaust gas is not a regulated pollutant; (2) the temperature of the exhaust line varies causing the water composition to vary both spatially and temporally; and (3) condensation in the tailpipe, sample bags, and exhaust gas analyzers would interfere with other measurements and damage equipment. Prior to vehicle certification testing, the exhaust stream is dried with a desiccant. For this work, however, the role of H_2O is critical in assessing material performance under realistic conditions.

3.2.3 Apparatus Design

The design of an appropriate testing apparatus and the development of experiments are constrained by the input requirements of the Semtech-G Exhaust Gas Analyzer (Sensors, Inc), which detects CO_2 and CO using non-dispersive infrared spectroscopy, NO_x using non-dispersive ultraviolet radiation, O_2 using paramagnetics, and hydrocarbons using flame ionization. The Semtech-G is designed for in-situ exhaust testing, requiring an incoming flow of four standard liters per min. However, at this flow rate, materials with small particle diameters would become compacted, causing significant backpressure to build in the system. This is avoided through the use of an air intake and mixing chamber, added after the adsorption bed, which dilutes the exhaust stream before it enters the gas analyzer (shown in Figure 3.2).

Actual vehicle exhaust has several properties that make it problematic for experimental carbon capture testing; most notably, high temperatures, flow rates, and water content are all detrimental to CO_2 uptake on porous solids. These variables were controlled through the use of pressurized cylinders that represent several exhaust gas blends, but at a limit of four gas species in

each blend. This allowed variable water content to be eliminated and temperature to be kept steady at approximately 25ºC. The flow of gas throughout the apparatus was controlled through step-down regulators and flow meters (Porter LB366).

Pressure drop across the adsorption vessel was measured using a Sensotec transducer and Fluke 189 multimeter, the latter of which was also used to monitor temperature using thermocouples at various points along the apparatus. For wet testing, a bubbler was used to add water to the exhaust blend until equilibrium was reached, confirmed by a General Eastern Hygro-M2 Dew Point Monitor with Chilled Mirror Sensor that measured dew point temperature and relative humidity (RH) of the gas stream. After equilibrium was reached, the hygrometer was relocated downstream of the adsorption vessel to measure changes in water content after material exposure. The optional wet testing is shown in blue in the apparatus diagram in Figure 3.2.

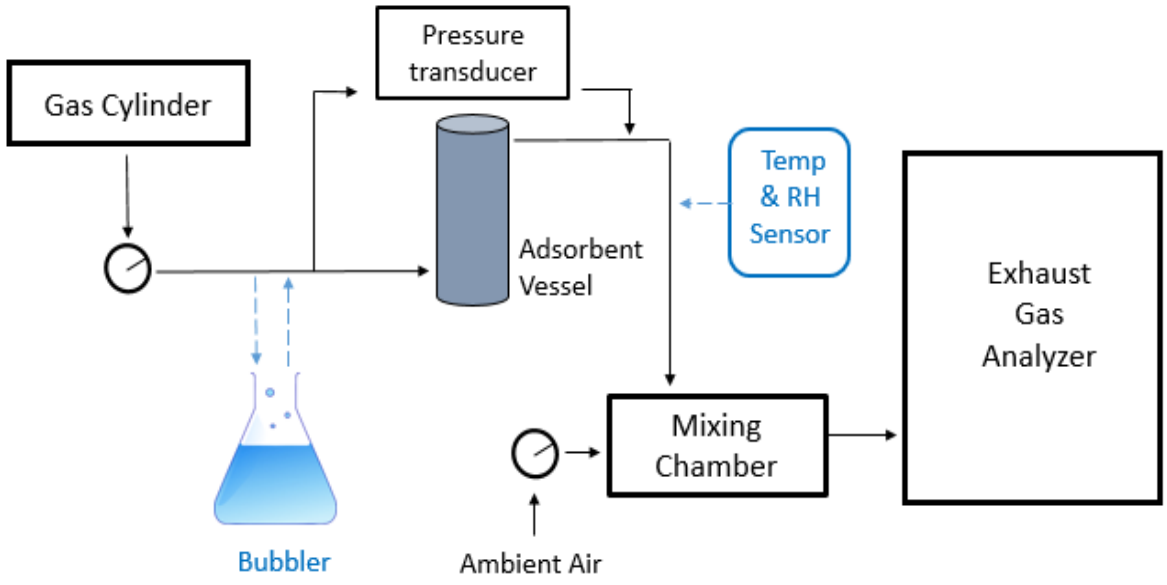

Figure 3.2 | Diagram of the bench-scale testing apparatus, showing gas flow through an adsorption vessel and air dilution in a mixing chamber (wet testing in blue)

Figure 3.3 shows a picture of the laboratory set-up, with the bubbler and RH sensor included. The adsorption vessel configuration was found to have a significant role in material performance, so it was designed to accommodate all materials and gas blends. The design, shown in Figure 3.4, permits an up-flow of gas through the material bed. As designed, the material sits on a mesh screen above the gas inlet and exits at the top of the vessel. To prevent compaction of the finest materials, gas stream lines are permitted around the perimeter of the screen. The outcome of this design choice is explored in detail in section 3.3.2.

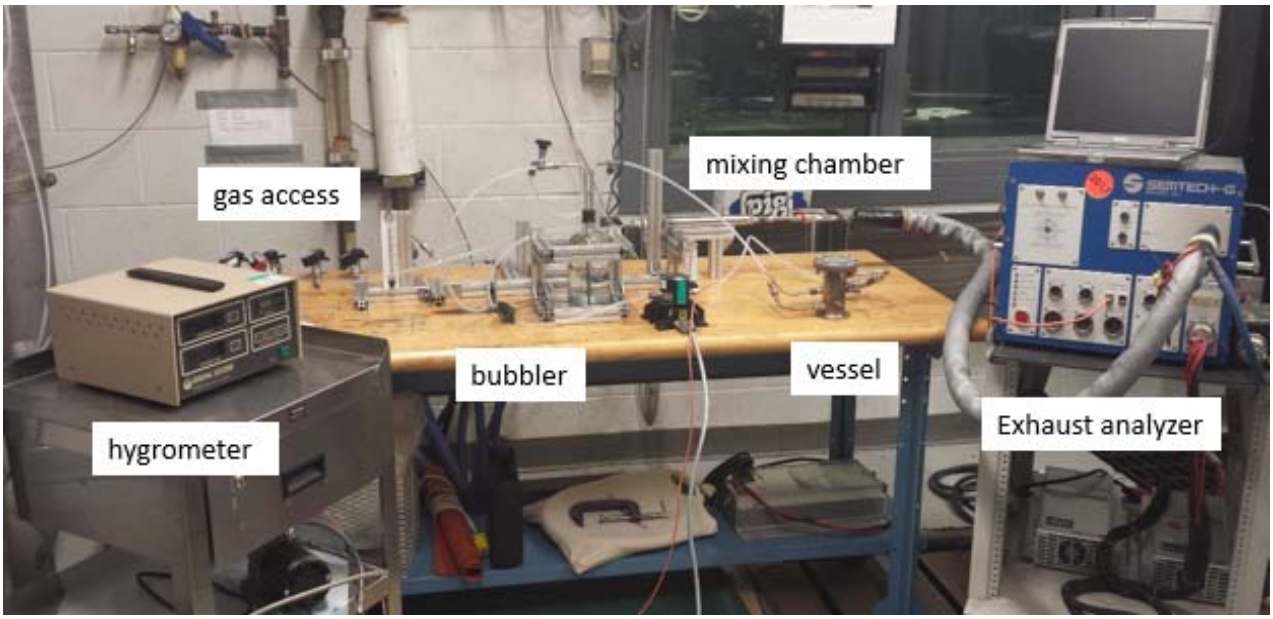

Figure 3.3 | Laboratory experimental set-up of bench-scale testing apparatus

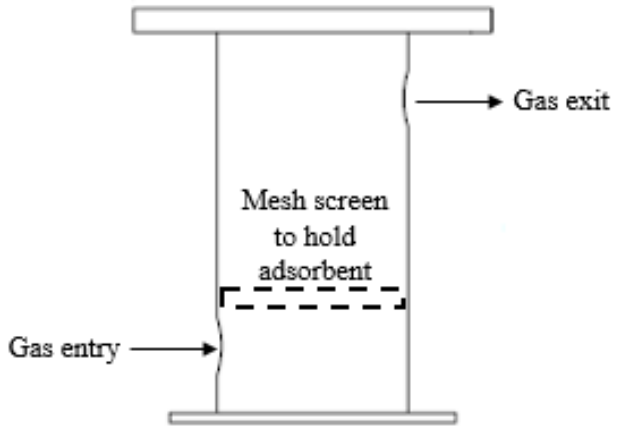

Figure 3.4 | Engineering drawing of the adsorption vessel

3.2.4 Test Protocol

Prior to testing, the adsorbents were activated in vacuo (< 0.03 kPa) using a Micromeretics ASAP 2050 Extended Adsorption Gas Analyzer, with concurrent heating to 180ºC for 2 hours. The adsorption experiments were then run within 12 hours of activation with minimal exposure to ambient air. For each material, adsorption experiments were repeated until results were within 5% deviation. Outliers (2 tests out of 26 total) were omitted. Initial testing used a dual gas blend of 13.5% CO_2 and 86.5% N_2, meant to evaluate the dynamic CO_2 storage capacity at a concentration representing gasoline exhaust.

The adsorption affinity for both Zeolite 5A and 13X adhere to the following order: $SO_2 > CO_2 > NO > N_2$ (Deng et al, 2012). Sulfur standards for tier 3 gasoline have almost eliminated SO_2 emissions from vehicle exhaust (EPA, 2014). Even when present, SO_2 is vastly diluted by CO_2 and N_2. NO and CO were therefore included in a quad blend, intended to test trace contaminant tolerance. Diesel vehicle certification testing at the NVFEL in April 2017 showed average CO and NO concentrations of 5 and 10 ppm, respectively. This is nearly negligible for real-world

applications, but the selectivity of CO_2 over CO (where the molecules are understandably similar in composition and size) is a critical parameter for carbon capture from vehicle exhaust, so the concentration of CO was supplied in excess. Concentrations in the quad blend are 12% CO_2, 0.5% CO, 10 ppm NO, and 87.5% N_2.

Finally, material stability and CO_2 uptake in the presence of water was tested using the quad blend with water vapor added using a bubbler. Given the temperature, pressure, and flow constraints, the average equilibrium water content was limited to approximately 4%, resulting in a gas composition of 11.6% CO_2, 0.5% CO, 10ppm NO, 3.8% H_2O, and 84.1% N_2.

3.2.5 Calculations for Mass Uptake

The exhaust gas analyzer output is the volumetric concentration (% or ppm) for CO_2, CO, NO, and O_2 adjusted for wet conditions, where applicable, based on the water vapor condensed from the gas stream. The concentration is adjusted to molar fraction by dividing percent by 100 or parts-per-million by 10^6. The concentration of each gas species, system pressure, temperature, and volumetric flow rate are measured at the exhaust analyzer, before the adsorbent bed, and the air intake before the mixing chamber. Atmospheric controls built into the laboratory ensure the absence of carbon monoxide and nitric oxide in the ambient air (Dräger Polytron 2XP), while temperature and humidity are continuously monitored (Vaisala HMP233).

Mass of the loaded adsorbent vessel is measured before and after the experiment. The transducer is pre-calibrated to a voltage-flow-pressure curve (Figure 3.5) and measures pressure drop across the adsorption bed, so the voltage quantifies the loss in flow or pressure across the bed. Once the exhaust analyzer readings for CO_2 have reached the bypass concentration (maximum at equilibrium) recorded prior to testing, the experiment is complete.

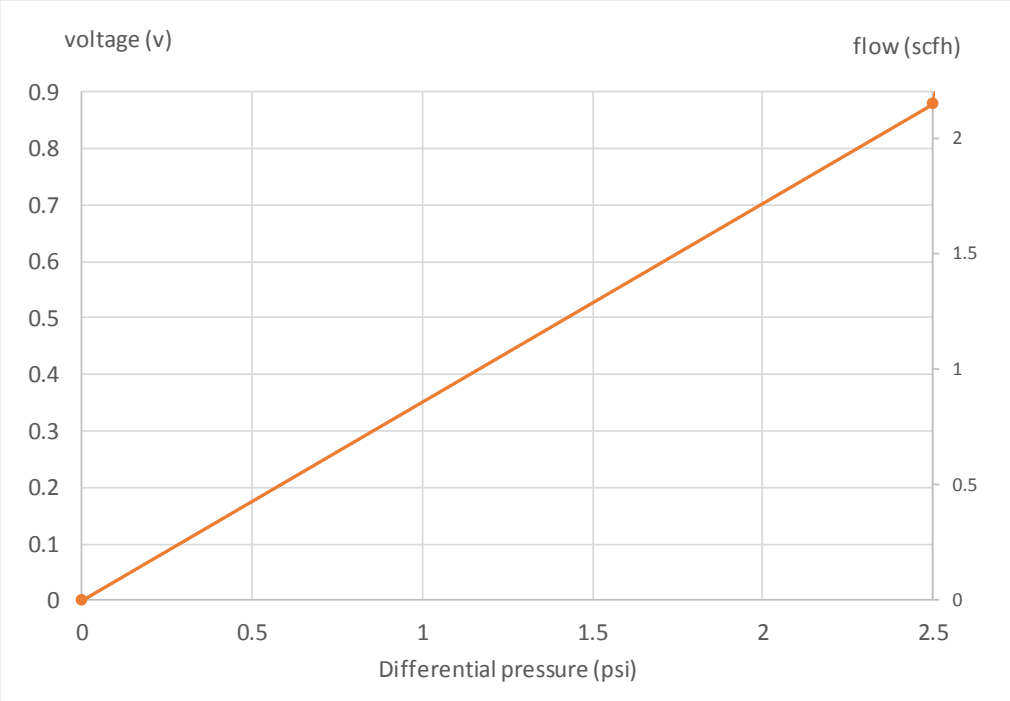

Figure 3.5 | Pressure-voltage-flow calibration curve

Molar flow rates are calculated using the ideal gas law. Moles of CO_2 exiting the system at the exhaust gas analyzer are computed based on the air dilution. The total moles of CO_2 captured are then determined by the sum of the feed rate minus the exit rate, over the duration of the adsorption test. The same equations and methods are used to compute mole balances for all gas species. Water content is calculated using saturation pressure (from steam tables), relative humidity, and temperature. The total mass of water retained is calculated as the summation of water retained over time, using molecular weight and volume.

3.3 Results and Discussion

3.3.1 Experimental Results

For the dual CO_2-N_2 blend, exhaust gas analyzer results (volumetric % post-adsorption) for the different adsorbents and their respective performance were normalized by time to compare the shape of the breakthrough curves (Figure 3.6), with the x-axis reporting the fraction of testing time over equilibrium time (when the material reaches saturation). Zeolite 5A (blue) and MIL-53 (black) best illustrate the expected delayed breakthrough (occurring after ~30% of the time has elapsed) but this effect is muted for most of the materials as the bed vessel design permitted uniform gas stream lines on the exterior of the packed bed. As illustrated, the area above the curve shows the total quantity of CO_2 adsorbed.

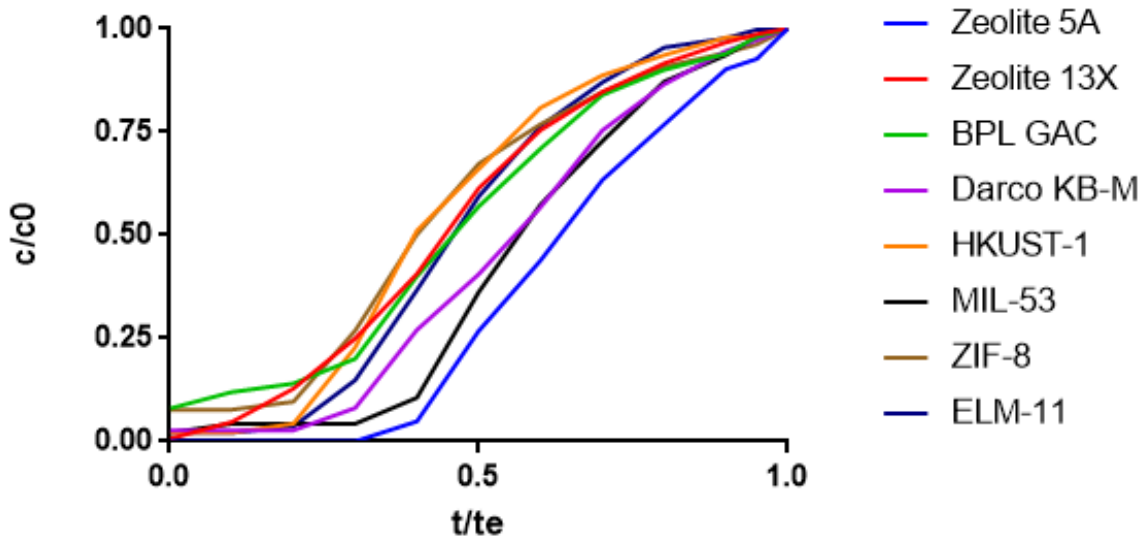

Figure 3.6 | Normalized breakthrough curves for 13.5% CO_2 at 25°C and 101kPa total pressure

In the evaluation of competitive adsorption by CO, NO, and H_2O, the cumulative mass adsorbed was calculated for each gas species based on the molar flow rates and assuming an ideal

gas. Figure 3.7 summarizes the mass uptake (g/g, gram of gas per gram of material) for CO_2 (blue bars) and CO (orange bars). Beyond the inherent affinity for CO_2 characteristic of these materials (shown with blue bars in Figure 3.8, indicating CO_2 adsorption, are all significantly higher than orange bars), the predominant uptake of CO_2 can also be attributed to the volumetric concentration ratio between CO_2 and CO of 24. Despite the low concentrations in the feed stream, all of the adsorbents still capture a portion of CO. Results for NO, however, were omitted because uptake was approximately zero (<0.008 g/g).

To separate the adsorption affinity of two gases onto the same adsorbent, selectivity is used to demonstrate how the relationship between CO_2 and CO changes during adsorption; higher values for selectivity are preferable for CO_2 capture. Selectivity is calculated as the molar ratio of CO_2 to CO in the adsorbed phase over the molar ratio in the feed gas.

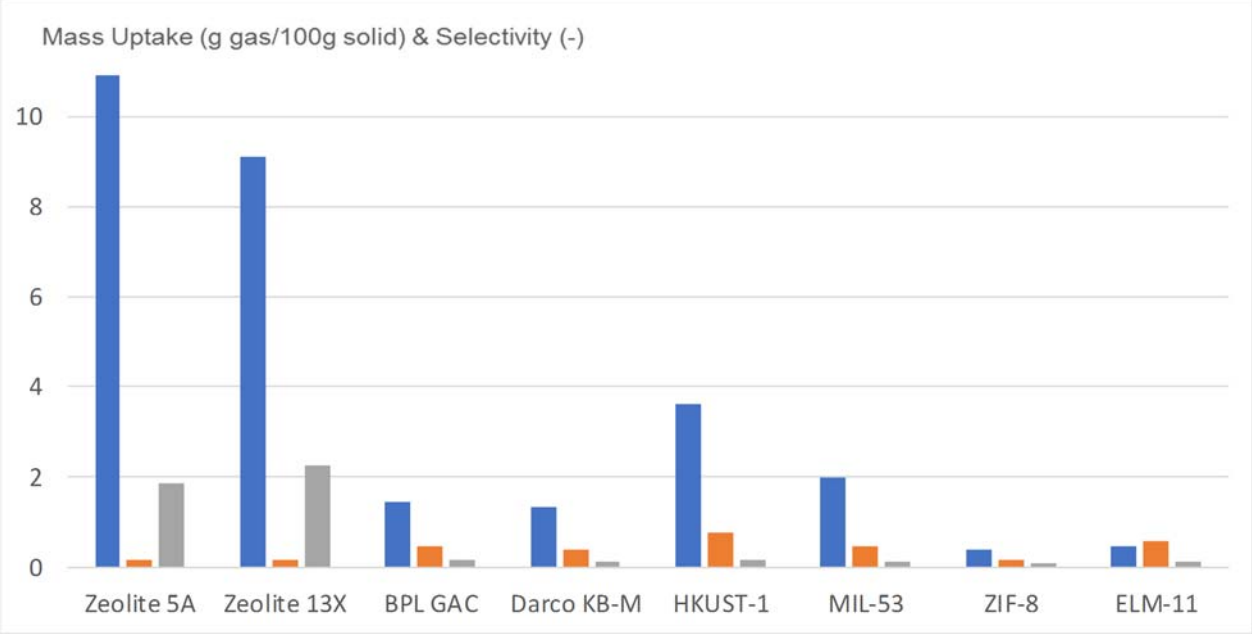

Figure 3.7 | Results for mass uptake (g/100g) for CO_2 (blue) and CO (orange) and selectivity (gray) for dry blend testing at 12% CO_2 and 0.5% CO

In the wet blend testing (Figure 3.8), the addition of water to the dry blend alters the selectivity of CO_2 over CO slightly but does not impede the mass uptake of CO_2 (as the blue bars are still significantly higher than orange (CO) or yellow (H_2O)). All materials except HKUST-1 exhibit preferential adsorption of water (CO_2/H_2O selectivity less than 1), competing for capture with CO_2 despite having a volumetric concentration ~3 times less. In this case, the water content is the limiting factor for uptake; at a higher water content (like the expected >10% in vehicle exhaust), the CO_2/H_2O selectivity would be even less. As expected, the CO_2 capacity increases in HKUST-1 with low levels of humidity in the gas stream, resulting in a CO_2/H_2O selectivity greater than one.

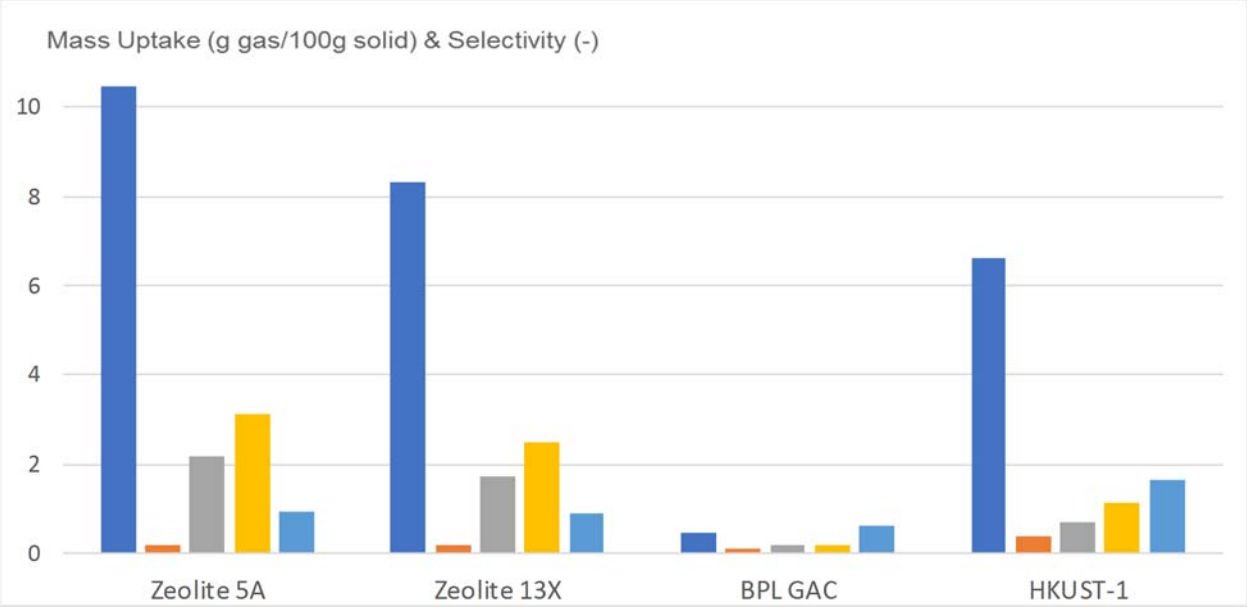

Figure 3.8 | Results for mass uptake (g/100g) for CO_2 (blue), CO (orange), CO_2/CO selectivity (gray), H_2O (yellow), and CO_2/H_2O selectivity (light blue) for wet blend testing at 11.6% CO_2, 3.5% H_2O, and 0.5% CO

At standard temperature and pressure, activated carbons show minimal uptake of CO_2. An example of this is shown using BPL GAC in Figure 3.9a, illustrating the expected breakthrough

curve of gas uptake from the dry quad blend. While CO_2 is captured until saturation (blue S-curve), CO and NO remain near their initial concentration (with some expected "noise" due to the sensitivity of the gas analyzer).

Zeolites have the highest mass uptake of CO_2 from any gas blend but show a decrease in capacity when additional gas species are present in the exhaust stream. This is an inherent property of molecular sieves: they will capture all molecules smaller than their pore opening. As Figure 3.9b illustrates, breakthrough curves for CO_2 and CO in Zeolite 13X follow a similar curve. Uptake of the smaller CO molecules is rapid, whereas the larger CO_2 molecules take longer to fill the open pore space.

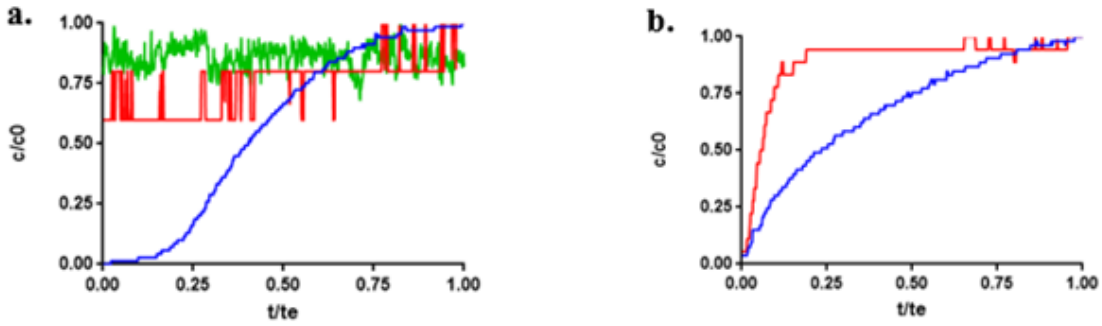

Figure 3.9 | Breakthrough curves for (a) BPL and (b) Zeolite 13X showing competitive adsorption of CO_2 (blue), CO (red), and NO (green) for dry quad blend testing

For the MOFs (excluding HKUST-1) and Darco KB-M PAC, wet blend testing results are excluded because they were below the limit of detection and/or water was known to degrade the chemical structure. As stated previously, HKUST-1 exhibits an increase in performance when exposed to low levels of humidity (Soubeyrand-Lenoir et al., 2012), which is confirmed here for water concentrations around 4%. The potential of HKUST-1 as an adsorbent for MCC is limited

by its performance (which is expected to decrease) at higher water concentrations, along with the capacity and costs of mass production.

Despite the competitive adsorption between CO_2 and H_2O in the wet blend, the zeolites experienced an average loss in storage capacity of only 11% compared to the dry blend. Meanwhile, BPL GAC experienced a 69% capacity loss, as water vapor saturated the carbon surface. HKUST-1, on the other hand, increased 84% in storage capacity (although this increase is expected to decline as humidity increases).

For a large-scale MCC program that used zeolites for carbon capture, it would be beneficial to remove H_2O from the exhaust gas prior to adsorption to increase CO_2 uptake. Based on the mass of adsorbent and the mass of adsorbate removed from the gas stream, the total weight percent for carbon capture was calculated (Table 3.2). For each calculation, the uncertainties in measurements were tabulated using errors from the exhaust gas analyzer, mass comparator (Mettler Toledo PR10003), and hygrometer.

Table 3.2 | Dynamic CO_2 weight percent and uncertainty at 298K and 101kPa total pressure

	wt % CO_2 adsorbed		
	13.5% CO_2	**12% CO_2 + CO, NO**	**Blend + H_2O**
Zeolite 5A	12.43 ± 0.58	10.89 ± 0.56	10.45 ± 1.40
Zeolite 13X	11.12 ± 0.40	9.09 ± 0.22	8.35 ± 1.25
BPL GAC	1.65 ± 0.13	1.46 ± 0.10	0.45 ± 0.07
Darco KB-M	2.35 ± 0.20	1.35 ± 0.11	-
HKUST-1	3.80 ± 0.30	3.62 ± 0.21	6.65 ± 1.00
MIL-53	1.85 ± 0.24	1.98 ± 0.24	-
ZIF-8	0.50 ± 0.08	0.42 ± 0.05	-
ELM-11	0.45 ± 0.13	0.48 ± 0.13	-

3.3.2 Parameter Fitting

The variable flow rates, temperatures, pressure gradients, air dilution ratios, and run time of experiments make comparisons across materials and gas blends challenging. Furthermore, the ability of the gas stream to bypass the packed bed adds uncertainty to the quantification of breakthrough and equilibrium times. Based on the *Carbon Capture* text by Wilcox (2012), mass transfer zone parameters are calculated to compare performance and scale the design from bench to proof-of-concept.

In the breakthrough curve illustrated in Figure 3.10, c/c_0 is the ratio of output concentration to initial concentration, t_b is the breakthrough time, t_e is the time to equilibrium (material saturation), and t* is the time for ideal adsorption. This is represented by the dashed lines, which correspond to a vertical breakthrough curve at t*, showing an abrupt shift to saturation. In reality, mass-transfer resistance and axial dispersion dictate an S-curve (solid line) for breakthrough.

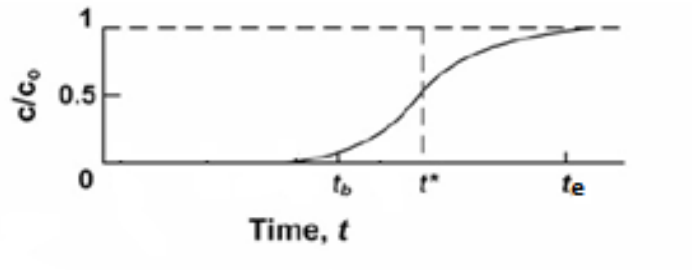

Figure 3.10 | A typical breakthrough S-curve showing time to breakthrough (t_b), to equilibrium (t_e), and ideal time (t^*) for "perfect" uptake (adapted from Wilcox, 2012)

The ideal time, t*, can be determined from,

$$t^* = \frac{L\rho_b(W_{sat}-W_0)}{u_0 c_0} \qquad \textbf{(3.1)}$$

where L is the length of the packed bed (m), ρ_b is the bed density (g/mL), W_{sat} is the equilibrium saturation value (mmol/g), W_0 is the initial saturation value (mmol/g), u_0 is the superficial velocity (m/min), and c_0 is the concentration of CO_2 in the feed (mmol/mL). Bed length, density, CO_2 concentration, and superficial velocity were obtained experimentally. W_{sat} was taken from the static adsorption isotherm at 298K and at the CO_2 partial pressure corresponding to the feed value (Figure 3.1). All sorbent material was pristine, so W_0 was set equal to zero.

To compare the materials across tests using the same gas blend, uptake was normalized to equivalent mass and flow rates so that corresponding breakthrough times could be fitted based on the experimental S-curves. After calculating the normalized t*, equations 3.2 and 3.3 were used together to solve for t_e and t_b:

$$[Total\ adsorbed] = Qy_{CO2}t_b + \frac{1}{2}\,Qy_{CO2}(t_e - t_b) \tag{3.2}$$

$$\theta = \frac{t_b}{t_b + \frac{1}{2}(t_e - t_b)} = \frac{2t_b}{t_b + t_e} \tag{3.3}$$

where total adsorbed is the volume (mL), Q is the feed volumetric flow rate (mL/min), y_{CO2} is the molar fraction of CO_2, and Θ is the fraction of bed saturated. The static versus dynamic uptake at 13.5% CO_2 and 298K was used to obtain Θ (Figures 3.1 and 3.6).

Table 3.3 | Characteristic times and relevant parameters for [dual blend | dry blend] testing

	W_{sat}, mmol/g	t*, min	t_b, min	t_e, min
Zeolite 5A	4.590	68.7 | 76.7	34.4 | 38.4	103.1 | 115.1
Zeolite 13X	3.295	63.1 | 70.4	37.9 | 42.3	88.3 | 98.6
BPL GAC	0.459	5.5 | 6.2	4.4 | 4.9	6.6 | 7.4
Darco KB-M	0.396	4.5 | 5.0	4.5 | 5.0	4.5 | 5.0
HKUST-1	0.787	15.1 | 16.8	15.1 | 16.8	15.1 | 16.8
MIL-53	0.619	6.5 | 7.3	4.6 | 5.1	8.5 | 9.5

Results for characteristic times for dual and dry blend tests are shown in Table 3.3 (excluding ELM-11 and ZIF-8 due to their limited CO_2 uptake capacity). Characteristic times are illustrated in Figure 3.11 for BPL GAC, MIL-53, and Zeolites 13X and 5A, with Darco KB-M and HKUST-1 excluded because their characteristic times are approximately equal. Calculations of t* are dependent on W_{sat}, as the total gas loading represents how long the material takes to reach saturation under otherwise equal conditions.

The higher ratio of breakthrough to ideal time (and ideal to equilibrium time) indicates a narrower mass transfer zone for BPL GAC and MIL-53 (blue and purple lines in Figure 3.11). The opposite is true for the zeolites, but Zeolite 13X (red line) slightly outperforms Zeolite 5A (green line) in this regard.

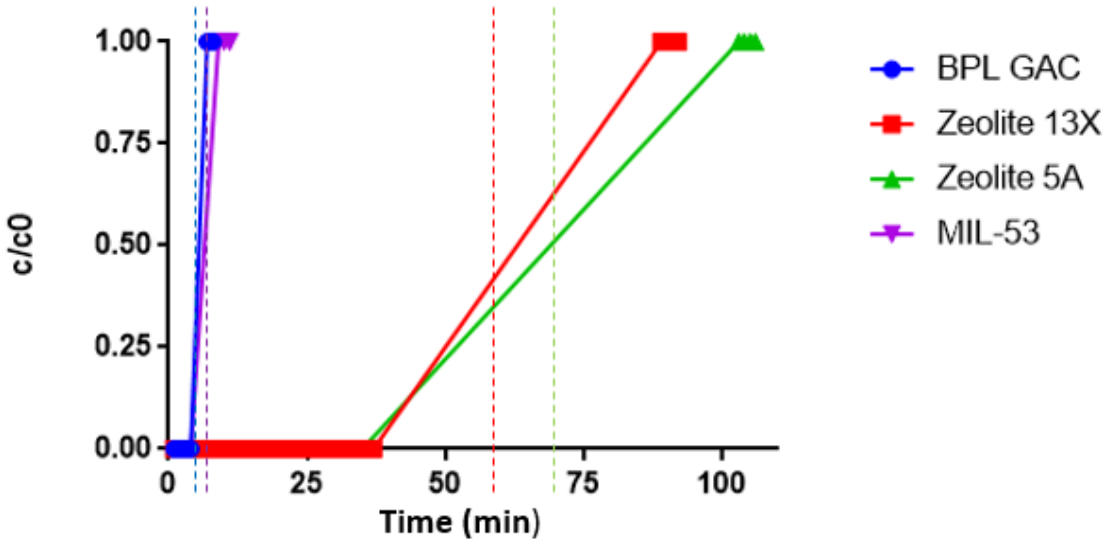

Figure 3.11 | Breakthrough curve fitting showing t* (dotted vertical line), t_b (c/c0 > 0), and t_e (c/c0 = 1) for CO_2 capture from the dual blend

3.3.3 Pressure Drop Calculations and Scaled Design Considerations

To evaluate laminar flow across a packed bed of solid material, assuming gas stream lines travel through small capillaries, the Kozeny-Carman equation (3.4) is used:

$$\frac{\Delta p}{L} = \frac{150 u_0 \mu}{\Phi^2 d^2} \frac{(1-\varepsilon)^2}{\varepsilon^3} \tag{3.4}$$

where Δp is the pressure gradient across the bed (Pa), μ is the fluid viscosity (Pa-s), Φ is the sphericity (-) or surface-to-volume ratio of a sphere of minimum diameter, d (m), and Ɛ is the external bed void fraction (-). While the pressure drop across the bed was measured experimentally, it was not a true packed bed and thus underestimates the actual pressure drop. Velocity was obtained experimentally, diameter was taken from the chemical data sheets, sphericity was assumed based on known particle shape, void fraction was assumed based on experimental packing, and the total fluid viscosity was calculated using equation 3.5:

$$\mu_{ga} = \frac{\sum_{i=1}^{N} y_i \mu_i \sqrt{M_{gi}}}{\sum_{i=1}^{N} y_i \sqrt{M_{gi}}} \quad \textbf{(3.5)}$$

where yi is the molar concentration of each gas species i (mol/L), μ is the viscosity at the desired temperature and pressure (pa-s), and M_g is the molecular weight for each gas species (g/mol). Using equations 3.4-3.5, an anticipated pressure drop per unit length can be computed for each compound (Figure 3.12). The pressure drop is highly sensitive to particle diameter; gas flow causes microporous materials to agglomerate into tight groupings, resulting in limited gas stream lines and higher backpressure.

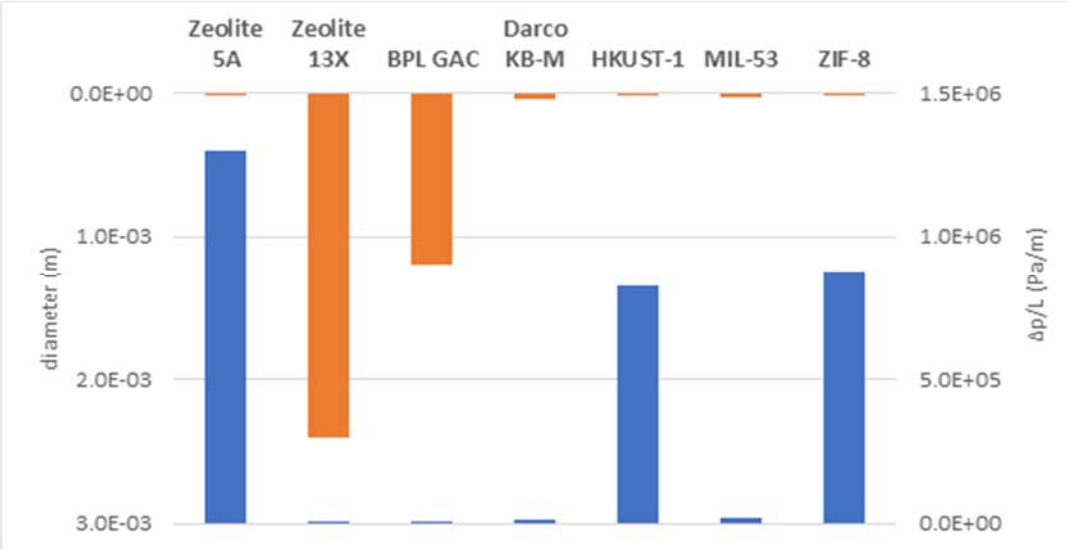

Figure 3.12 | Results for minimum particle diameter (orange) and pressure drop per unit length (blue) for candidate materials, excluding ELM-11

3.3.4 Kozeny-Carman Equation Sensitivity

A general void fraction of 0.4 and sphericity of 0.9 was used for most materials in the Kozeny-Carman equation (3.4), but the random granulation of BPL and the deliberate sphericity

of Zeolite 13X beads are reflected in void fractions of 0.36 and 0.31 and sphericities of 0.7 and 1.0, respectively. Volumetric flow ranged from 118 – 192 mL/min. A sensitivity analysis, summarized in Table 3.4, verifies the importance of particle diameter in the Kozeny-Carman equation. Materials with micro-scale particle diameters correspond to extremely high backpressure, reflecting material compaction and partial gas blockage. Fortunately, most of these materials can be formed into beads/pellets of any diameter with the use of a binding agent (see section 3.3.5).

Table 3.4 | Sensitivity analysis of the variables in the Kozeny-Carman equation

	velocity	Viscosity	Void	sphericity	diameter	Δp/L
average	1.30E-03	1.73E-05	0.35	0.85	5.00E-04	184
high velocity	1.60E-03					227
low velocity	1.00E-03					142
high viscosity		1.80E-05				191
low viscosity		1.65E-05				176
high void			0.40			105
low void			0.30			339
high sphericity				1.00		133
low sphericity				0.70		271
high diameter					2.38E-03	8
low diameter					3.70E-06	3.E+06

Based on their low anticipated pressure drop, high breakthrough and equilibrium times, and storage capacity for CO_2 under dynamic flow conditions, Zeolite 13X or 5A would be suitable candidates for a proof-of-concept scale apparatus. Particle diameter can be tailored for molecular sieves using a chemical binder and should be selected large enough to minimize pressure drop but also small enough to permit intra-pellet transport, which is notably slow in zeolites (illustrated in Figure 3.13).

3.3.5 Zeolite Particle Diameter versus Uptake

As tested, Zeolite 13X is a 4-8 mesh with a 2.38mm particle size, while Zeolite 5A is a fine powder with a 3.7µm particle size (spanning the high and low diameter range in Figure 3.12). Since the material is permitted to reach equilibrium, regardless of elapsed time, the result is an almost doubling of test time when beads are used instead of powder (Figure 3.13). If desorption is also considered, the time more than doubles to purge the captured CO_2. The significance of this would come in proof-of-concept or pilot testing, where the tailpipe flow rate would dictate exposure time between the zeolite and the exhaust gas; without slowing the flow, there may not be sufficient retention time to ensure maximum adsorption.

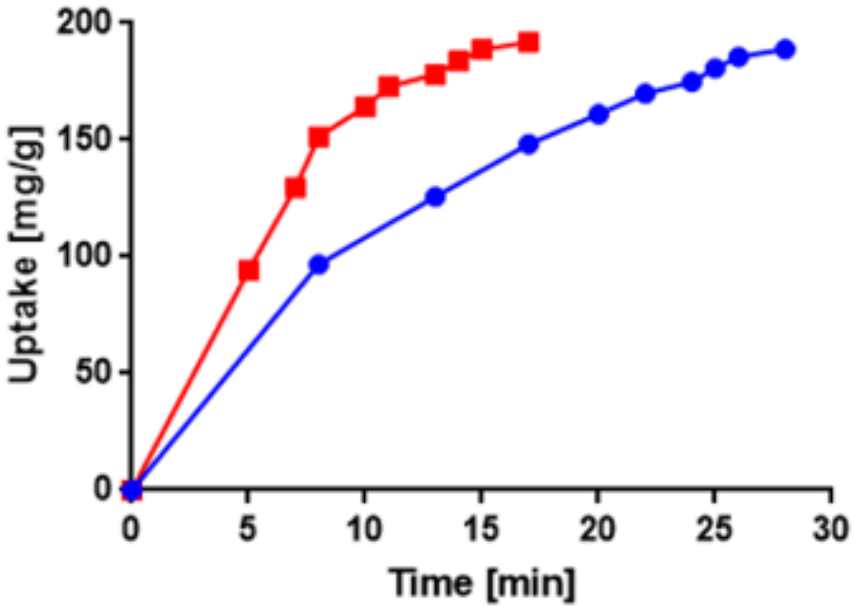

Figure 3.13 | Pure CO_2 isotherms for Zeolite 5A beads (blue) and crushed powder (red)

Once material size is selected, the pressure drop can then be manipulated via the choice of vessel length and diameter (dictating the superficial velocity) and by packing method (dictating the void fraction). Other factors to consider include energy requirements; when compared to 13X,

the specific heat consumption for Zeolite 5A is 19% less while the capture rate is 18% better (Merel et al., 2008). This translates to higher capture and less energy needed for regeneration.

3.3.6 Preliminary Testing for Proof-of-Concept

A proof-of-concept system was designed and built in partnership with the EPA NVFEL. The prototype canister was designed at 1:8 scale (for capture from a full tank of gas), with a storage target of 2.3 kg CO_2. It was loaded with Zeolite 13X pellets and connected to a Chevrolet Silverado pick-up truck during idle operation, where the measured CO_2 concentration was 6-8% by volume at equilibrium. The backpressure threshold was calculated at 2.5 kPa, approximately 25% of the typical exhaust system at idle. Tests were run on exhaust gas with no further pretreatment, with the understanding that heat and water content would impact CO_2 uptake.

The breakthrough time for CO_2 was approximately 13 minutes, with an equilibrium time of 17 minutes. For the duration of testing, H_2O (at 2-3 % by volume) was preferentially captured by the adsorbent. A small percentage of CO, present in the feed at roughly 200 ppm, was also captured but reached an almost immediate breakthrough and saturation after 5 minutes. The measured backpressure was 85% of the expected value.

Total mass capture was approximately 0.9 kg, which is less than half of expected based on the design parameters. A molar flow balance shows that mass capture by Zeolite 13X was 73% CO_2 and 26% H_2O; it is assumed that water plugged the pore openings, lowering the total CO_2 capacity.

The same adsorbent canister was used in another prototype test to evaluate heat applications for gas purge and zeolite regeneration. COMSOL Multiphysics was used to model gas flow through the canister; preheated nitrogen gas was found to be the most consistent and well-

distributed heating method. An alternative design with lower potential cost and energy requirements was used for testing: heat tape was wrapped around the internal perimeter of the vessel, which was then wrapped in fiberglass insulation, and a slow flow of nitrogen gas (4 L/min) was used to carry released CO_2 out of the vessel.

The target temperature for desorption was 135°C. Using saturated zeolite, testing involved concurrent measurements of centerline vessel temperature and volumetric CO_2 concentration in the purge gas. Desorption of captured CO_2 was found to commence at temperatures over 50°C, reaching a final peak at approximately 150°C. The temperature ramp rate was ~1.5°C/min and the vessel took about 2 hours for complete desorption and material regeneration.

The early release of captured CO_2 indicates that a lower temperature could be used for regeneration over a longer time period or a higher temperature over a shorter time period. Further examinations into regeneration should focus on the simultaneous optimization of temperature and timing.

3.3.7 Design of a Heat Exchanger for Exhaust Pretreatment

A model of heat transfer and flow was conducted, again using COMSOL Mulitphysics, to explore various configurations for a heat exchanger that would reduce temperature and remove moisture from the exhaust flow of a diesel tractor-trailer. Post-tailpipe diesel exhaust is approximately 50°C and the CO_2 and H_2O are approximately equal, at about 10% by volume.

Based on previous findings from a customer discovery course offered through the Center for Entrepreneurship at the University of Michigan, carbon capture equipment is limited to the trailer of the truck, as any modifications on the tractor portion would void the manufacturer's warranty.

Under tailpipe exhaust flow of 0.8m/s, travel speed of 70mph, and ambient air at 20°C, the dew point temperature of the exhaust is roughly 43°C. The area available for the heat exchanger is limited in height, width, and length to 0.075m, 2.6m, and 14.6m, respectively. The most effective design that achieves a centerline exit temperature under 40°C consists of a 15.8m long piping system constructed of 3in diameter (5.5mm thickness) steel piping with serpentine channels along the width of the trailer.

The exhaust flow rate is increased significantly in this configuration, although it drops rapidly after exiting the heat exchanger and entering the adsorption vessel. The design can be further enhanced using fluid dynamics to limit the flow rate and using brackets on the bottom of the heat exchanger to allow for air flow on the bottom as well. Collectively, an MCC capture unit and heat exchanger placed on the bed of a HDV trailer would account for approximately 15% of both the payload mass and the trailer bed volume.

3.4 Conclusions

The infancy of explorations into the technical feasibility of MCC result in a highly flexible system design, with dozens of variables (relating to capture, regeneration, storage, transport, and infrastructure) to optimize. This study, however, focuses on initial laboratory-scale testing to determine what commercially-available adsorbents could remove CO_2 from vehicle exhaust. Eight solid porous compounds were evaluated for the ability to selectively remove CO_2 from surrogate gas streams.

Zeolite 5A and 13X exhibited the highest uptake across all gas blends, with the former retaining a storage capacity above 10 weight % despite the addition of CO, NO, and H_2O. In wet blend testing, water is adsorbed preferentially over carbon dioxide for all materials except

HKUST-1. A higher affinity for water means that a steam displacement purge for regeneration would easily displace any captured CO_2. After cooling and removing any condensed water, the end product would be high purity CO_2 gas.

Chapter 4

A Baseline Economic Evaluation of Mobile Carbon Capture

4.1 Introduction

In the United States, transportation sector emissions are currently 34% of all carbon dioxide emissions from fossil fuel combustion, with on-road vehicles comprising ~74% of all transportation-related emissions. On-road combustion emissions have surpassed stationary CO_2 emissions from coal combustion as of 2015; the latter of which was the premier target for emissions regulations as the largest single point-source (EPA, 2017). The recent shift in U.S stationary power generation from coal to natural gas has resulted in a decline in industry emissions, whereas lower fuel prices have inadvertently supported an increase in transportation sector emissions. Total stock of personal vehicles (OICA, 2017) and total vehicle miles travelled (FHA, 2017) are increasing

annually, along with the energy required to power those vehicles. In 2016, emissions from transportation surpassed electric power generation for the first time since 1979 (EIA, 2017).

Transportation sector emissions are predominantly from gasoline and diesel fuel sources; these fuels will continue to be the preferred power source for mobility due to their higher energy density (permitting a higher range for travel), lower cost, and ease of transport and storage when compared to other liquid and gaseous transportation fuels.

Emissions from transportation are projected to remain as the top emitting sector through 2040 (EIA, 2017). The stabilization of greenhouse gases is dependent on a drastic reduction in carbon dioxide emissions from all sectors (IPCC, 2013). To reach climate targets by 2050, further emissions reductions beyond those already in place are necessary and must begin by 2025 at the latest for the U.S. automotive sector (Supekar & Skerlos, 2017); a reduction of 50-80% in GHG emissions means vehicle efficiency must drastically increase while carbon content of fuels decreases (Lutsey & Sperling, 2009), which is unlikely given recent trends. As Figure 4.1 shows, near-term vehicle and fuel technologies are not adequate in this regard; long-term and higher-cost interventions are necessary to achieve global climate goals. Carbon capture and storage (CCS) is a method to capture carbon dioxide from exhaust gas before emitted to the atmosphere; it is most commonly researched for stationary power sources but can be applied to vehicles to mitigate CO_2 emissions.

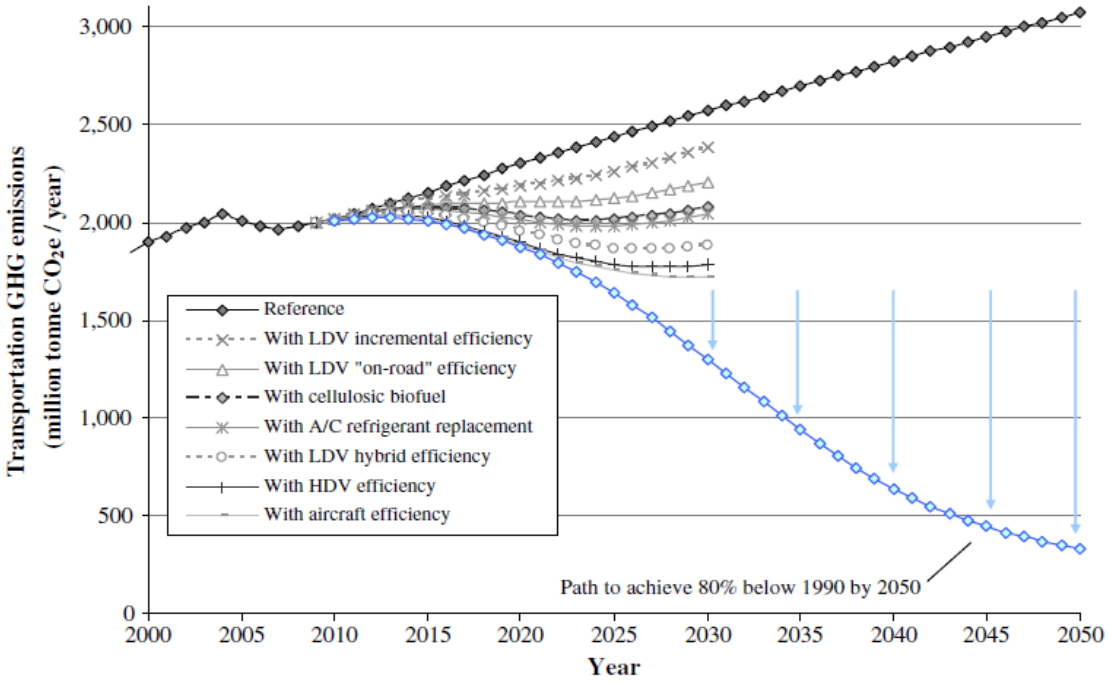

Figure 4.1 | Transportation sector GHG emissions projections and mitigation options (Lutsey & Sperling, 2009)

Mobile carbon capture (MCC) refers to the on-board separation of CO_2 from vehicle exhaust, where the concentration is 12-14% by volume (depending on the fuel). This type of carbon capture has been discounted in previous studies due to the feasibility challenges and presumed high costs (Ruthven, 2014; Goeppert et al, 2012; Boot-Handford et al., 2014), typically without any supporting calculations or citations. The oft-used reasoning is that the on-board capture system would be detrimental to vehicle performance and the infrastructure investment would be costly, rendering MCC impractical and uneconomical. While any large-scale effort to capture carbon dioxide emissions would require a substantial infrastructure investment, the high initial capital costs for MCC can be vastly mitigated by operating the CO_2 collection, transport, utilization, and/or storage in tandem with stationary carbon capture operations.

4.2 Building an MCC Program

The limited studies that have explored MCC (Damm & Fedorov, 2008; Bilger & Wu, 2009) have proposed various alternatives to carbon capture from automobiles, but none have included an economic component which is critical to the evaluation of MCC as an emerging, transformative technology. The hypothetical program established for mobile capture, based on modeling and laboratory testing, relies on a solid adsorbent to separate CO_2 from the vehicle exhaust gas. Various alternatives exist for capture, regeneration, and transport of CO_2 – the choice of power for separation and compression can come from low carbon electricity off-board the vehicle or from the fuel-powered internal combustion engine; the captured CO_2 can be transported to a collection site or injection well via pipeline or via canisters using truck delivery; and, lastly, the system can be regenerated and capture repeated at various travel intervals (daily, by miles travelled, or by refueling).

The components used to make a baseline cost estimate are outlined in Figure 4.2, with three major components that define the stages of carbon capture: capital cost expenditures, capture (covering work for gas separation and regeneration), and transport and storage (separate from the capture process but necessary additions to a capture estimate).

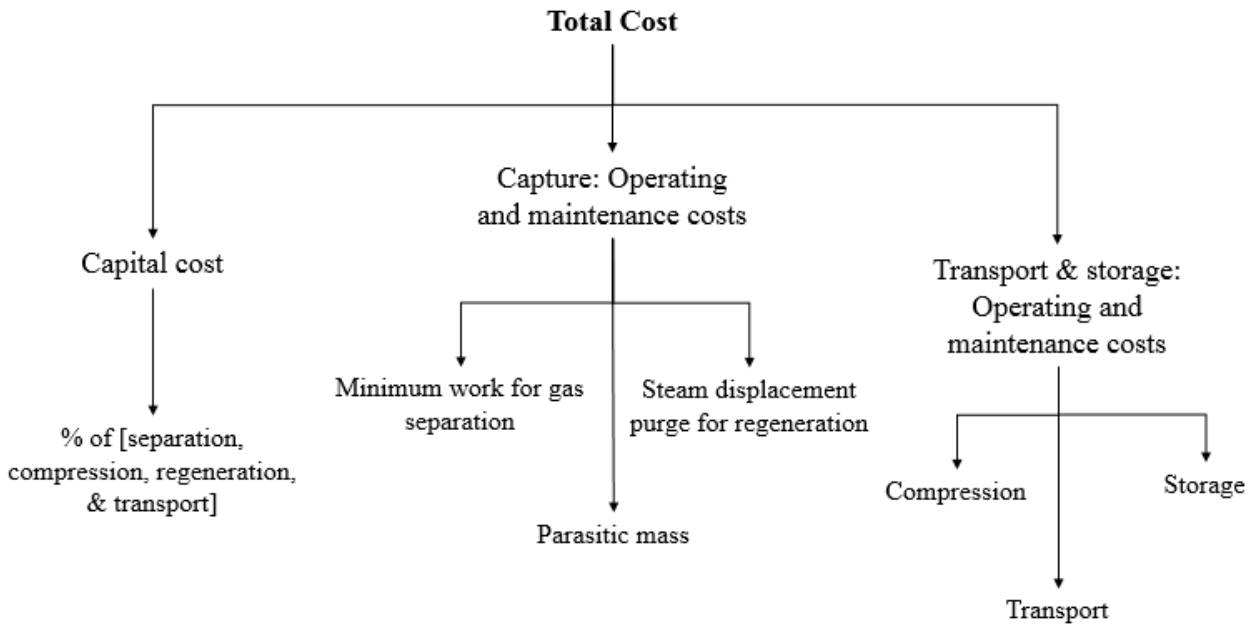

Figure 4.2 | Categories for carbon abatement cost estimation for mobile carbon capture

The premise for capture for this model uses porous solid materials to selectively remove CO_2 from vehicle exhaust post-tailpipe. Commercially-available materials have CO_2 adsorption capacities similar to liquid absorbents at 50-200 grams per kilogram (kg) of material (Keskin et al, 2010). Using a typical zeolite (5A, 13X), a capacity of 20 weight % (1 kg of CO_2 captured per 5 kg of zeolite) is assumed. Next-generation materials for carbon capture and conversion show much higher storage capacity, up to 240 weight % for expanded metal organic frameworks (Furukawa et al, 2010).

4.2.1 Separation

Based on the initial work done by (Sotomayor, 2016), an energetic-economic evaluation is constructed using principles of gas separation; the basis for estimating energy requirements stems from the thermodynamic minimum work, which is equal to the difference in Gibbs free energy

between the initial and final states. In the simplified case of ideal gas streams in an isothermal and isobaric process, a feed stream [A] is separated into two product streams [B and C]. The minimum work (kJ, kilojoules) is thus:

$$W_{min} = RT\left[n_B^{CO_2} \ln\left(y_B^{CO_2}\right) + n_B^{B-CO_2} \ln\left(y_B^{B-CO_2}\right)\right]$$
$$+RT\left[n_C^{CO_2} \ln\left(y_C^{CO_2}\right) + n_C^{C-CO_2} \ln\left(y_C^{C-CO_2}\right)\right]$$
$$-RT\left[n_A^{CO_2} \ln\left(y_A^{CO_2}\right) + n_A^{A-CO_2} \ln\left(y_A^{A-CO_2}\right)\right] \quad \textbf{(4.1)}$$

where R is the ideal gas constant (8.314 J/mol-K), T is temperature (K), $n_i^{CO_2}$ is the moles of CO_2 captured, $y_i^{CO_2}$is the mole fraction of CO_2 in the gas stream, and $y_i^{i-CO_2}$ is the non-CO_2 mole fraction of a given gas stream.

The variable of interest in gas separation is the minimum work per unit mass of CO_2 captured. If 100% capture of pure CO_2 is assumed, the minimum work per unit mass of CO_2 captured (kJ/kg) is reduced to:

$$w_{min} = -\frac{RT}{yM_{CO2}} \left[y \ln(y) + (1-y)\ln(1-y)\right] \quad \textbf{(4.2)}$$

where y is the mole fraction of CO_2 in the feed stream and M_{CO2} is the molecular weight of CO_2 (44 g/mol) (Wilcox, 2012).

As the adsorbate concentration in the feed decreases, the minimum work required to separate the adsorbate from the gas stream increases (Figure 4.3). For mobile capture from gasoline exhaust at 13.5% CO_2, the minimum work requirement is equal to 165 kJ per kg CO_2 removed (46 kWh/tonne or 48 kWh/tonne for diesel exhaust). Stationary capture from a coal-fired power plant at 12% CO_2 requires slightly more work, at 172 kJ/kg. Capture directly from ambient air, where the CO_2 concentration is a mere 0.04%, would require three times as much energy (497 kJ/kg).

The strong correlation between initial gas concentration and work required for removal is a concept widely understood and reported in estimates for gas separation costs (House et al., 2011).

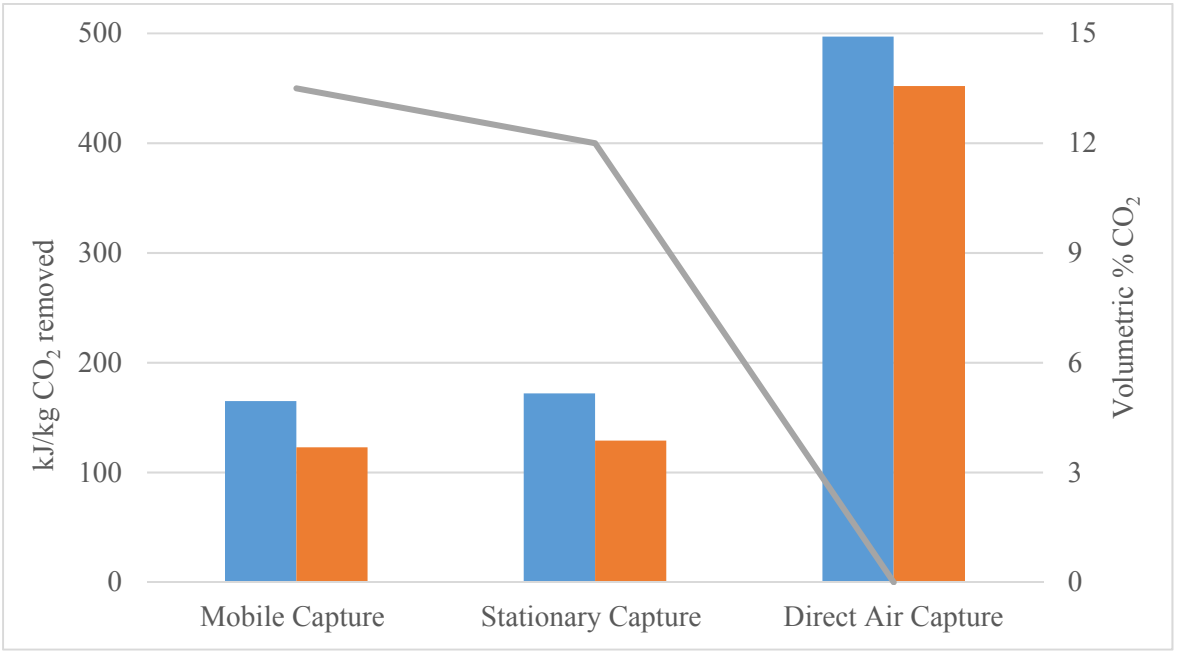

Figure 4.3 | Minimum work required to separate CO_2 from mobile, stationary, and direct air sources at 298K for 100% purity at 50% (orange) and 100% (blue) capture, based on the volumetric concentration of CO_2 (grey line, secondary axis)

4.2.2 Compression

The industry standard for pipeline transport is to keep CO_2 at supercritical phase, so a final pressure of 110 bar is used. For a large-scale MCC program to be effective, the CO_2 compression infrastructure would mimic that of power plants, where the average cost is estimated at $6-8/tonne CO_2 (Wong, 2005).

4.2.3 Second Law Efficiency

While the thermodynamic minimum work provides a baseline energetic evaluation of separation and compression, no system can achieve 100% efficiency. Actual work is governed by the second-law efficiency, which compares theoretical (thermodynamically perfect) to actual power consumption and is generally 5-40% (House et al, 2011) for a combined separation and compression process.

For a pulverized coal power plant with a volumetric CO_2 concentration of 12% capturing a 99.5% pure CO_2 stream, the average second-law efficiency is 24% compared to ~5% for direct air capture at the same purity but at a CO_2 concentration of 0.04% (Wilcox et al., 2017). Assuming future technological advancements, the second law efficiency is set at 40%. For every 10% reduction in efficiency, the corresponding cost estimate increases by approximately 11%.

4.2.4 Energy Source

Once CO_2 is captured, thermal regeneration is one of several methods for gas desorption. By using heat from the internal combustion engine as the source of energy for CO_2 desorption and adsorbent regeneration, the amount of capture that can be accomplished on-board the vehicle increases. Unfortunately, parasitic mass also increases (with a negative impact on fuel economy), resulting in a decrease in effective engine work (already at 15-30% efficiency under regular operating conditions) (An & Santini, 2004).

When comparing two scenarios that only differ in the source of energy – gasoline or electricity – the choice to regenerate the system on-board using liquid fuels results in a total cost two to four times higher than regeneration using electricity. This system would have significant

costs in added fuel and would have the greatest negative impact on consumers, as vehicles would operate less efficiently.

Therefore, the better economic choice is to use low-carbon or CO_2-free electricity as the energy source for CO_2 desorption and adsorbent regeneration. If a renewable energy source such as wind turbines or solar panels are used, the power is CO_2-free and costs are assumed to range between $0.10 and $0.20 per kilowatt-hour (kWh) (House et al, 2011). Assuming cost of power of $0.13/kWh is used in the model.

4.2.5 Parasitic Mass

The effect of added mass is detrimental to the performance of the vehicle; for a 10% increase in mass, fuel economy is reduced by 5-9% (Brooker et al, 2013; Cheah & Heywood, 2011) for light-duty vehicles (LDV, covering passenger cars and trucks). For heavy-duty vehicles (HDV, covering class 7/8 tractor-trailers), the impact is calculated from chassis dynamometer testing as a 3% reduction in miles per gallon for every 10% increase in payload mass. The payload, using a KW T-700 model tractor-trailer, was measured at 46,000 pounds (lb) for a gross vehicle weight rating of 80,000 lb (Reinhart, 2015). In the model, the parasitic mass is computed at full capacity for adsorbent saturation. This conservative estimate is necessary as any commute beyond the intended range will involve a saturated adsorbent bed.

4.2.6 Regeneration Methods

Periodically the capture system must be regenerated to prepare for repeat cycles. This is accomplished by either reducing the pressure within the system (to a vacuum), increasing the temperature (for a set duration), or using a hot inert gas or steam to displace the captured CO_2

(Wilcox, 2012). The procedure for regeneration depends on the adsorbent material and can vary widely. The choice of regeneration for this system is a displacement purge.

For regeneration via steam purge, the change in temperature is higher (steam is at ~130ºC) and the steam consumption is assumed to be 0.3 kg/kg CO_2 (Wilcox, 2012). There are a few benefits to this option: there is no added cost for a vacuum pump, the captured gas is of high CO_2 purity after the water condenses, and the process takes only a few minutes.

4.2.7 Regeneration Frequency

The frequency of CO_2 off-loading and adsorbent regeneration is based on a daily commute for passenger vehicles of 30 miles, so a home regeneration unit could handle desorption, regeneration, and compression overnight (similar to charging a battery electric vehicle). If regeneration was instead delayed until refueling occurred – roughly every 300-350 miles – the total cost for carbon capture would increase 250%, with a corresponding fuel penalty about fifteen times higher. Relying on daily regeneration accomplishes several goals simultaneously: less volume sacrificed for the on-board system, less mass penalty and thus higher fuel economy, minimal impact on consumers, and more convenient CO_2 storage and transport.

A National Household Travel Survey, conducted in 2009 and summarized in Figure 4.4, shows that 62% of drivers commute less than 30 miles per day (DOT, 2009; Krumm, 2012). A system that captured the emitted CO_2 from the first 30 miles of all daily commutes would capture approximately 80% of passenger vehicle emissions.

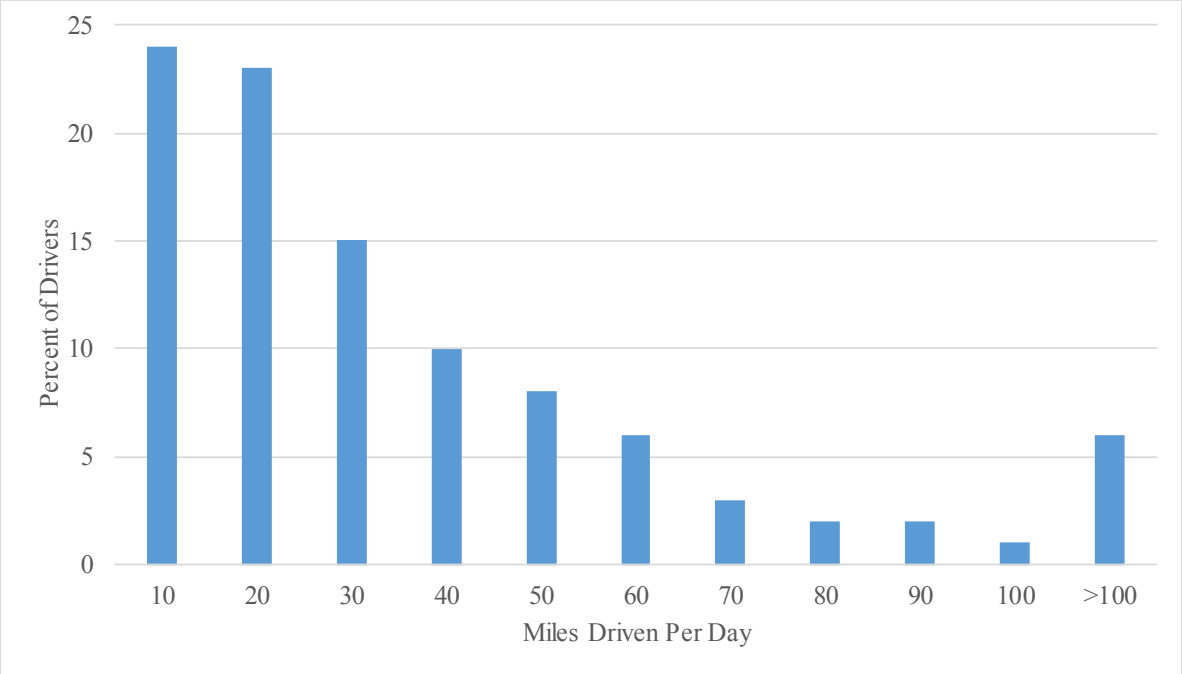

Figure 4.4 | Histogram of daily miles driven for passenger vehicles (adapted from DOT, 2009)

The approach is slightly different for regeneration frequency of long-haul heavy-duty tractor-trailers, as the expected daily commute is in excess of 500 miles. In this case, regeneration would occur twice daily, after 250 miles of travel. A distance shorter than this would be inconvenient for truck drivers, who already have limitations on their driving and travel times. While the weight penalty for HDV is less, a compromise is made in loss in total payload mass.

4.2.8 Transport, Utilization, and Storage

Once the captured CO_2 has been successfully purged from the adsorbent bed, it must be transported to another location for utilization or storage. This can be accomplished either by pipeline – similar to natural gas supply lines to residential homes – or by truck – similar to curbside waste removal. Truck transport would require less infrastructure and could be operational

immediately. Historic costs for freight transport by truck were $0.37/ton-mile (DOT FHA, 2005) while future costs are an estimated $0.15/tonne-kilometer (km) (Perez et al, 2012).

Truck transport has lower capital costs compared to pipeline transport, but higher and permanent maintenance costs. Estimates for transportation of CO_2 via pipeline and injection into deep geological storage are on average $10-$15 per tonne of CO_2 avoided (David & Herzog, 2000; Dooley et al, 2008; Grant et al., 2013) and differ based on pipeline length, basin range, and storage volume. In the U.S., cost per ton for pipeline transport ranges from 1.03 to 2.63 (McCoy & Rubin, 2008). Pipeline transport of CO_2 is assumed to cost $2/tonne (under 150 kilometers) and storage is an additional $10/tonne.

Transport in the model assumes a total travel distance of 100 kilometers for pipelines and 30 kilometers for trucks (as multiple canisters would be picked up along a single trucking route). Both transport options are initially considered to establish the most economically sound approach to CO_2 transport. Practically, the capital costs associated with pipeline transport would be significantly higher while the long-term operational costs of truck transport would be higher. For both transport methods, associated emissions are assumed to be null - the pipeline distance is small enough to minimize the impact of any leaking CO_2 and the collection trucks would be fitted with MCC to avoid more emissions.

Captured CO_2 would ideally be utilized for enhanced oil recovery (EOR), which refers to various techniques that increase crude oil extraction. EOR is a mature technology that has been practiced for decades; in the U.S. in 1998, ~43 million metric tons of CO_2 were injected across 67 commercial EOR projects (Herzog, 2001). As CCS projects grow, captured CO_2 is expected to provide 43% of EOR needs by 2020 (Wallace et al., 2015). The Global CCS Institute (Godec, 2011) estimates a delivered cost for CO_2 at EOR sites of $40-$45/tonne of CO_2 (tCO_2) if oil prices

remain above $100 per barrel. With average oil prices currently at half this amount, the estimated return for CO_2-EOR is $20/t$CO_2$.

4.2.9 Fuel and Vehicles

Projections for retail gasoline and diesel fuel in 2020 are $2.56 and $3.15 per gallon, corresponding to the production of 8.89 and 10.15 kg CO_2, respectively (EIA, 2018). For LDV, corporate average fuel economy (CAFE) standards were set to reduce carbon emissions to 163 grams CO_2 per mile in 2025, equivalent to an average fuel economy of 54.5 miles per gallon (mpg) (EPA, 2012). Recent changes to future CAFE standards will result in an on-road fuel economy of approximately 36 mpg. The range of LDV mass (compact to pick-up truck) is 2,900 to 4,700 lb. The distribution of vehicle types is not even, so the average passenger vehicle weight is set at 3,500 lb.

HDV, specifically class 7/8 diesel trucks, are predominantly used for the transport of goods across the U.S. (EPA OTAQ, 2008). They have a projected fuel economy of 6.8 mpg (EPA, 2016) to 9.1 mpg in 2025, corresponding to CO_2 emissions reductions of 15-27% per ton-mile of freight moved between model years 2017 and 2027 (Sharpe et al, 2016). The maximum gross vehicle weight for this class is 80,000 pounds with a tare weight of ~15,000 pounds.

The lifetime of a heavy-duty vehicle is often 20 years or more (Law, Jackson, & Chan, 2011), making the ability to retrofit MCC technology a primary goal. The growth of freight activity, which doubled between 1990 and 2013 and is expected to double again by 2040 (SmartWay, 2017), reinforces the need to promptly mitigate freight emissions.

4.2.10 Capital and Contingency Costs

MCC capital costs are difficult to assess in a hypothetical system, so cost estimates rely on assumptions from literature on post-combustion capture at power plants and direct air capture (Socolow et al, 2011). A need for extensive infrastructure means greater capital costs, while the synergies between existing stationary carbon capture and EOR sites would decrease the capital investments needed for a nationwide MCC program (Law, Jackson, & Chan, 2011).

With evidence that modular technologies have faster learning rates and thus lower costs (National Academies, 2018), the future capital cost expenditure for MCC can be assumed less than 100% of operational and maintenance (O&M) costs as on-board capture systems and regeneration units would be mass-manufactured. The sensitivity of an MCC program operating under a range of capital costs is explored, over a range of 50 to 200% of the sum of separation, compression, regeneration, and transport costs.

Because this is an emerging and potentially transformative technology, there is an added degree of uncertainty in the operation and maintenance costs as well. To account for this, a contingency of \$25/tCO_2 is included in each estimate.

4.3 Results and Discussion

The MCC capture unit would be installed in the trunk, bed, or trailer of the vehicle. Operation would continue normally. After a predetermined distance (30 miles for LDV, 250 miles for HDV), the driver would connect their capture unit to a regeneration unit at home or at a gas station. CO_2 would be siphoned out of the capture unit, and an alert would inform the driver when the regeneration process finished. The siphoned CO_2 would then be compressed and periodically

transported via pipeline to an injection well or EOR site. For truck transport, the system would automatically alert the manufacturer that a canister exchange was necessary; a delivery truck would bring an empty canister and pick-up the full one.

Table 4.1 lists MCC system parameters used for the cost estimate for both light-duty (LDV) and heavy-duty vehicles (HDV). Parameters that differ between vehicle classes include those pertaining to the fuel (CO_2 intensity, fuel cost, and minimum work for separation) and the vehicle (weight, fuel economy, capture distance, and fuel penalty).

Table 4.1 | MCC system parameters for cost estimation

	LDV	HDV	
CO2 intensity: gasoline | diesel	8.89	10.15	kg-CO2/gallon
Car Weight | Payload Weight	1300	20718	kg
Fuel Economy	36	6.8	MPG
Capture Distance	30	250	miles
Adsorbent wt%	20%	20%	
MPG/Weight Equivalency	7	3	%/10% mass(payload) change
Fuel Cost	2.56	3.15	$/gallon
Minimum Work Separation	46	48	kWh/tonne
2nd Law - Separation	40%	40%	
Cost of CO2 Compression (power plant)	7	7	$/tonne
Cost of Power	0.13	0.13	$/kWh
CO2 Intensity of Electricity	0	0	kg-CO2/kWh
Pipeline Transport	2	2	$/tonne
Pipeline Distance	100	100	kilometers
Truck Distance	30	30	kilometers
Trucking Cost	0.15	0.15	$/tonne-kilometer
Storage	10	10	$/tonne
CO2 supply for EOR	20	20	$/tonne
Cost of Steam Regneration	2.5	2.5	$/1000 lb steam
Steam Consumption	0.3	0.3	kg steam/ kg carbon

4.3.1 Carbon Abatement Cost

The pie chart in Figure 4.5 shows an example cost breakdown, excluding capital cost expenditures, for a passenger car fitted with MCC and relying on CO_2 transport via pipeline. The largest cost component is gas separation, which is based on a thermodynamic minimum. While the physics of that relationship will not change, advancements in research and efficiency will permit decreases over time. The second largest component is gas storage, which would decrease if the CO_2 was utilized in EOR rather than stored underground.

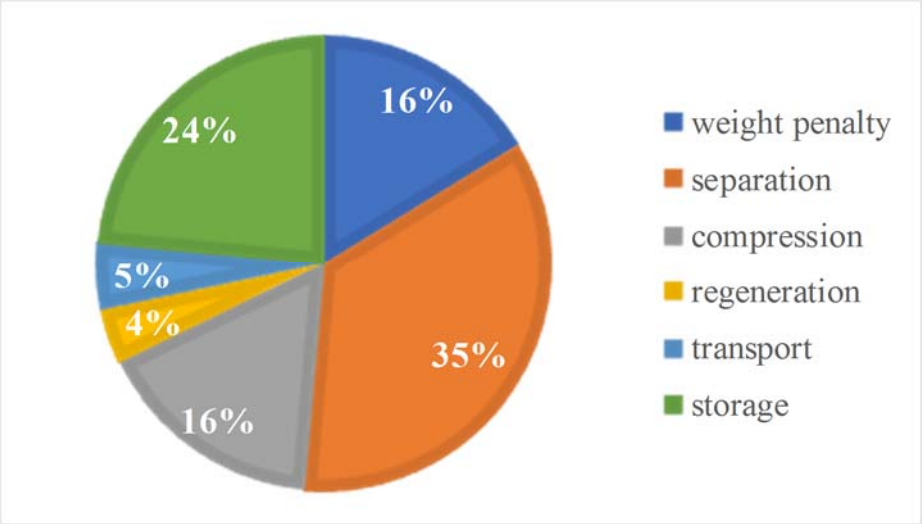

Figure 4.5 | Cost breakdown for LDV baseline case, showing O&M costs by category (without capital costs)

The use of EOR allows a shift from a parasitic and indefinite storage cost to a marketable end product. In addition to the cost benefit, this also allows the narrative surrounding CO_2 to switch from the cause of climate change to a usable product. Based on published estimates, the cost benefit for utilizing CO_2 is $20 per tonne (Figure 4.6, B and C).

Despite the shorter distance needed for truck transport, abatement cost per unit mass is higher, at $4.50/t$CO_2$ versus $2/t$CO_2$ for pipeline transport. The rationale for designing an MCC system that relies on truck transport is the avoidance of infrastructure investments for pipeline

transport from homes, where the wide distribution network would make implementation especially difficult. For transport of captured CO_2 by trucks instead of pipelines, total costs increase by 8% and 7% for LDV and HDV, respectively.

For comparable systems that use pipeline transport, the abatement costs for separation, compression, regeneration, and transport, which serve as the baseline for capital costs, total ~$27/t$CO_2$. Capital costs of 50-200% range from $14 to $54/t$CO_2$, producing total abatement costs at 200% capital of $119/t$CO_2$ for LDV and $128/t$CO_2$ for HDV (Figure 4.6, A).

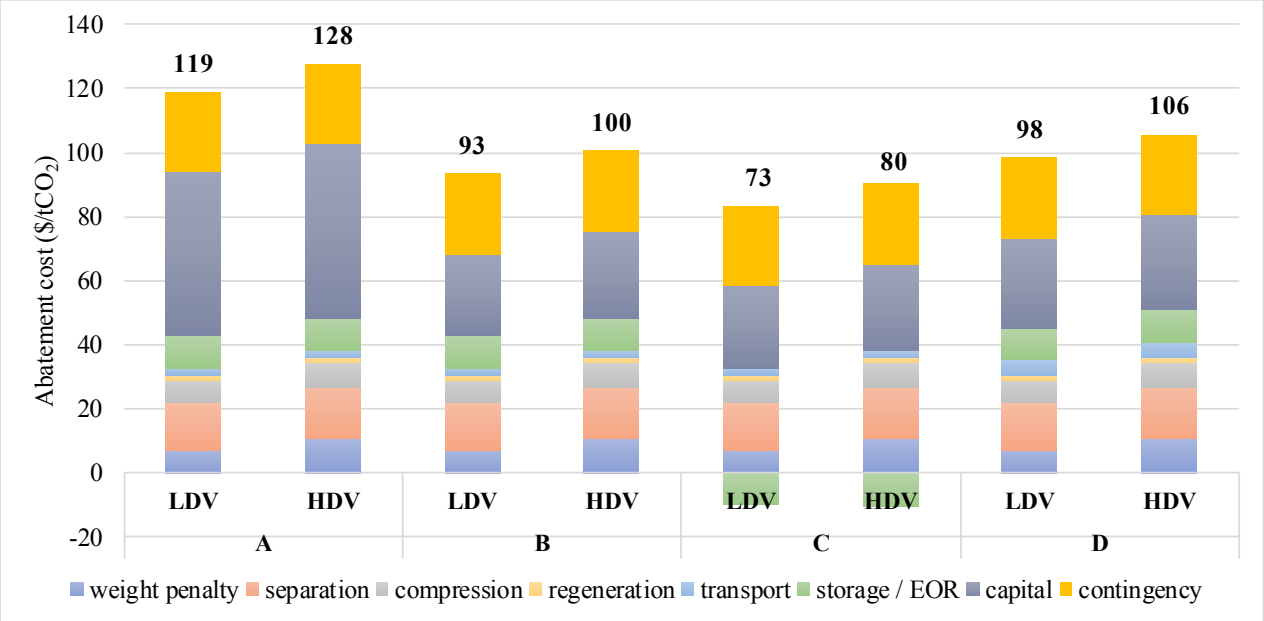

Figure 4.6 | Carbon abatement cost estimates ($/t$CO_2$) for Light-Duty (LDV) and Heavy-Duty (HDV) Vehicles assuming: (A) geological storage and 200% capital costs, (B) geological storage and 100% capital costs, (C) EOR and 100% capital costs, and (D) geological storage, 100% capital costs, transport via truck

In addition to CO_2 utilization via EOR, future technological advancements would decrease the expected total carbon abatement cost. Modular retrofit technology would permit mass

production and thus decrease capital costs, while next-generation adsorbents can achieve up to 240 weight % capture, vastly lowering the parasitic mass and associated fuel penalty.

Global anthropogenic emissions from road transport are about 6.5 Gt CO_2 (Kodjak, 2015), with the U.S. share at about 1.5 Gt (EPA, 2017). To capture 80% of on-road transport emissions at an average abatement cost of \$100/tCO_2 (100% capital costs with geological storage), the total cost is \$120B USD for a national program and \$520B USD for a global program. Gross domestic product for the U.S. is \$19 trillion USD and globally is \$80 trillion USD (World Bank, 2019), giving an average cost of MCC at only 0.6% of GDP.

To better relate to a single consumer (driver), the cost can be converted from per-tCO_2 to per-trip or per-mile. For the baseline case (geological storage, 100% capital costs) in a passenger car (\$93/tCO_2) and with current CO_2 emissions at ~200 g/mile, the cost per 30-mile trip is \$0.56. The regeneration infrastructure is included in that estimate, although the long-term O&M would be financed and managed at the state or federal level, which means that driver's cost is reduced to approximately \$0.34 per commute or \$124 annually (for 365 days of driving).

4.3.2 Sensitivity Analysis

The impact of variables taken from published literature is explored in Table 4.2, which lists the reported ranges for each variable and the resulting high and low abatement cost for that range in the baseline scenario (\$93/tCO_2). The most sensitive parameters, not counting capital costs, are the second law efficiency for separation and the cost for CO_2-free electricity, both of which could improve the total cost for gas separation. The least sensitive parameters are the cost of pipeline transport and the fuel penalty imposed for added weight. The model was run assuming operation

always took place at capacity, so the realistic impact of a fuel penalty would be even less than the model prediction.

Table 4.2 | Parameter sensitivity for baseline case: LDV with MCC

	Range	Low	High
CO_2 uptake [wt%]	0.1-0.6	$89	$99
% mpg Δ/ 10% mass Δ	5 - 9	$91	$95
fuel cost [$/gal]	2 - 4	$92	$97
second law, separation	0.2 - 0.5	$87	$123
cost of power [$/kWh]	0.08 - 0.2	$82	$109
cost of compression [$/t]	6 - 8	$91	$95
capital costs	50 - 200	$80	$119
pipeline transport [$/t]	1.03 - 2.63	$91	$94
storage [$/t]	8 - 12	$91	$95

It is helpful to note that there is also a minimal impact from variations in the cost of compression, geological storage, and fuel. As with electric batteries, geographic region will be a key determinant in the actual carbon abatement costs for MCC.

4.4 Other Low-Carbon Technologies

To mitigate the emissions of carbon dioxide and therefore its contribution to climate change, various alternatives exist that fall under three general areas: stationary capture, aimed at reducing emissions from power generation facilities; direct air capture, aimed at scrubbing CO_2 from the atmosphere; and battery electric vehicles, which do not burn fossil fuels and thus do not emit CO_2 during operation.

To compare MCC cost estimates (assuming pipeline transport and geological storage) with other decarbonization strategies, values of carbon cost abatement/effectiveness were taken from

literature. As Figure 4.7 illustrates, the total carbon abatement cost for on-road vehicles is competitive with several other low-carbon alternatives. The error bars on passenger cars and freight trucks reflect a capital cost expenditure up to 300% of separation, compression, regeneration, and transport costs.

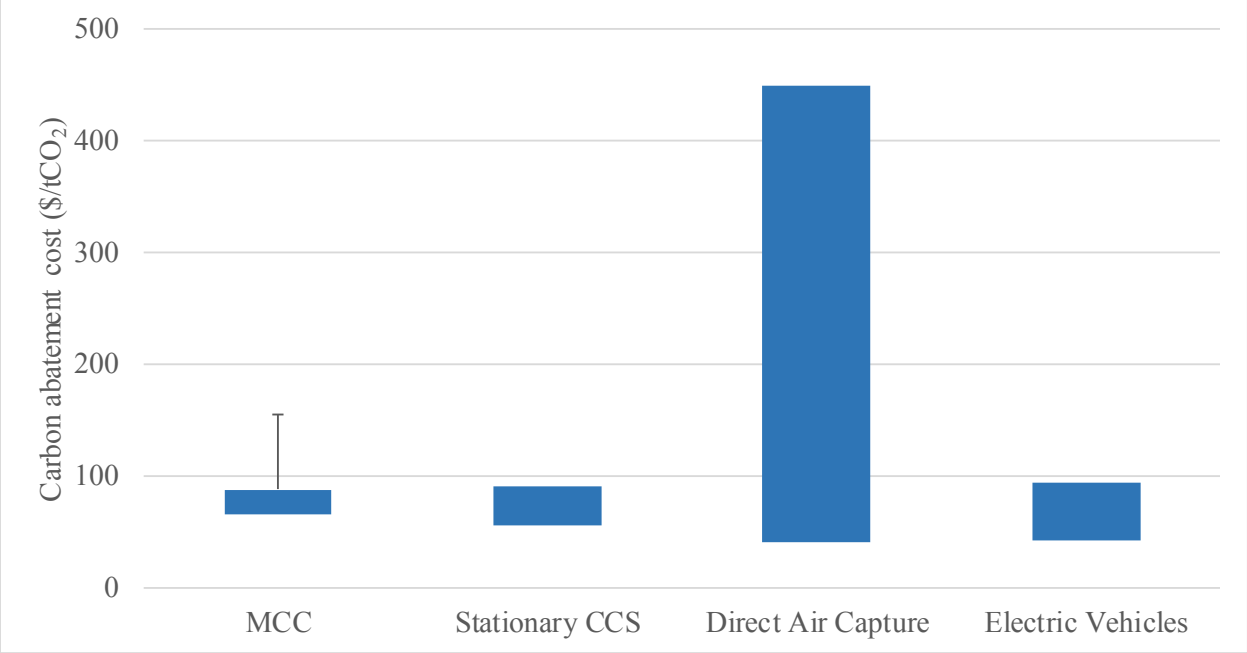

Figure 4.7 | Abatement cost comparison between mobile carbon capture and low-carbon alternatives, with estimates based on published literature

4.4.1 Stationary

Using current and available technology for capture and compression, the estimate for stationary capture is \$55-\$90/tonne CO_2 avoided (Socolow et al., 2011; House et al, 2011; Ranjan & Herzog, 2011), with an average of \$73/tCO_2. For stationary carbon capture, estimates of operational costs exceed capital costs by more than half, while the opposite was true for DACCS (capital costs exceeding operational) (Socolow et al, 2011).

4.4.2 Direct Air Capture

The most common technique for DACCS relies on scrubbers with very high surface area contact to remove CO_2 from the air. CO_2 concentrations are diluted significantly in the atmosphere (400 ppm versus 12-14% for vehicle or flue exhaust), increasing the work required for gas separation. The benefits of DACCS are that it reduces emissions from all economic sectors at a rate faster than the natural carbon cycle (Keith, Ha-Duong, & Stolaroff, 2006), providing a means for net negative emissions.

There have been several studies into the technical feasibility of DACCS using various chemical absorption processes (Baciocchi et al., 2006; Pritchard, 2015; Zeman, 2007). Relevant literature reports a wide range of cost estimates, ranging from \$20 to \$1000/tCO_2 avoided (Brandani, 2012; House et al., 2011; Pielke, 2009; Socolow et al, 2011; Zeman, 2014) with an interquartile range of \$40-\$449/tCO_2 but with less evidence and agreement in the lower cost estimates (IPCC, 2018).

DACCS proponents argue for higher-risk options that could potentially lower costs significantly, to ~\$27-136/tCO_2 (Holmes & Keith, 2012; Ranjan & Herzog, 2011), putting them on par with stationary capture, regardless of the higher costs of separation of a more dilute CO_2 stream. This higher cost and potential for net negative emissions make DACCS a prime alternative for widespread emissions reductions, but presumably only after stationary CCS has become commonplace (National Research Council, 2015). Predictions for cost-affordable DACCS start in 2060 at a price of \$600/tCO_2, reaching a capture rate of 21 $GtCO_2$ in 2100 (Marcucci, Kypreos, & Panos, 2017).

4.4.3 Electric Vehicles

Electric vehicles (EVs) are a fast-growing market of vehicles that operate on stored chemical energy in rechargeable battery packs, where the battery itself can be compared with the on-board MCC unit. Recently, the global EV market has seen several positive shifts towards increasing use: global EV sales doubled between 2011 and 2012 and average battery costs per kilowatt-hour reduced from $1000 in 2008 to $485 in 2012 (Trigg et al., 2013). Carbon abatement costs for EVs are estimated at $42 to $93/t$CO_2$ for the average and high estimate, respectively (Lutsey & Sperling, 2009).

With the introduction of the GM Chevy Bolt and Tesla Model 3, affordable electric vehicles with ranges over 200 miles per charge are now a reality. However, the U.S. Energy Information Administration (EIA) projects that alternative fuel vehicles will comprise only 7.6% of the total vehicle stock in 2040, with conventional gasoline cars comprising the majority of passenger vehicles (EIA, 2017).

Consumer adoption of EVs must overcome several barriers. Most relevant to this study is the time spent recharging the battery, which can range from 4-12 hours (9.3 hours for a Chevy Bolt and 12 hours for a Tesla Model 3, both at 220 volts) compared to only a few minutes to refuel a vehicle (Trigg et al., 2013). Furthermore, one of the biggest consumer hurdlers is the battery itself; a spent battery ceases vehicle operation. A saturated adsorbent bed would negatively impact vehicle performance if not regenerated, but it would not impede vehicle operation.

4.5 Conclusions

MCC using porous solid adsorbents is a feasible and economical approach to reduce carbon pollution from automobiles that could be cost competitive with other low-carbon technologies. The transportation sector is powered by carbon-based fuels and will continue to be fueled in this manner as long as fossil-fuel combustion is the main power source for mobility. Dangerous pollutants emitted from these vehicles, be they passenger cars or commercial freight trucks, must be reduced to meet future climate targets. As ICE engine costs increase to meet more stringent fuel economy and emissions regulations, MCC costs are predicted to decrease as technology advances and mass production capabilities increase (Moultak, Lutsey, & Hall, 2017).

While the need for carbon emissions reductions may be apparent, investments in carbon capture projects typically require prior federal policy or regulations (Sullivan & Sivak, 2012) and estimates for the infrastructure investments needed to decarbonize freight are approximately $150 billion USD (Moultak, Lutsey, & Hall, 2017). MCC can bypass this hurdle by marketing directly to consumers, where zero emission passenger vehicles already have a demand among environmentally-conscious drivers, or among freight shipping fleets, where clean transportation initiatives like SmartWay and Green Freight have had success (Hill et al, 2011). MCC offers an effective complement to stationary CCS and should be explored as a viable climate mitigation option before carbon dioxide removal techniques targeting net negative emissions.

Chapter 5

Environmental and Social Impacts of Mobile Carbon Capture from Freight Shipping using Heavy-Duty Vehicles

5.1 Introduction

It is quite often difficult to properly design emerging technology to fit society's needs at the early phases of development, where it has the greatest improvement potential (Miller & Keoleian, 2015) because of the inherent high uncertainty in what technological advances and societal changes may come to fruition in the coming decades. Even if comprehensive design factors, such as technology displacement and behavior changes, are used to inform development, a method to predict the environmental and social impact of the technology is still necessary to ensure its sustainability and global benefit.

Herein we attempt to quantify the environmental and societal impacts of mobile carbon capture for the freight shipping industry using heavy-duty vehicles (collectively HDVCC) by (1)

relating possible emissions reductions to the avoided temperature increase, (2) accounting for the social cost of carbon and comparing this against the carbon abatement cost, and (3) outlining a metric by which we can consider the benefits of an emerging technology like HDVCC against other similar decarbonization strategies.

5.1.1 Socioeconomic Pathways

In preparation for global climate model intercomparisons, climate scientists and economists developed a set of socioeconomic narratives that define future emissions pathways, grouped into five Shared Socioeconomic Pathways (SSPs) that collectively cover the spectrum of social and economic challenges associated with climate change mitigation and adaptation (Figure 5.1). The defining factors that differentiate the SSPs are population, economic growth, education, urbanization, rate of technological change, and personal lifestyle choices (Riahi, 2017). The pathways follow successful completion of national commitments already enacted under the Paris Agreement through 2030, but do not inherently include international efforts to combat climate change, relying instead on socioeconomic drivers like population and economic prosperity to spur climate change mitigation (Hausfather, 2018).

SSP1 and SSP4 represent futures with steep reductions in emissions, which are not expected given historic trends. Adversely, SSP5 and SSP3 better represent historic emissions, despite recent events indicative more climate-sensitive actions (Riahi et al, 2017; van Vuuren et al, 2017). The middle-of-the-road scenario, SSP2 (Figure 5.1, center) has limited levels of growth, development, and cooperation (Kriegler, 2012); it represents a continuation of historical patterns, specifically regarding carbon and energy intensity improvements, which decrease at historical rates (1.2% globally) (Fricko et al, 2017). Population peaks at ~9.4 billion around 2070 and

declines to 9 billion by 2100 (O'Neill et al, 2017). Urbanization increases from its current level of 54% to 80% at the end of the century, while energy demand more than doubles (Fricko et al, 2017).

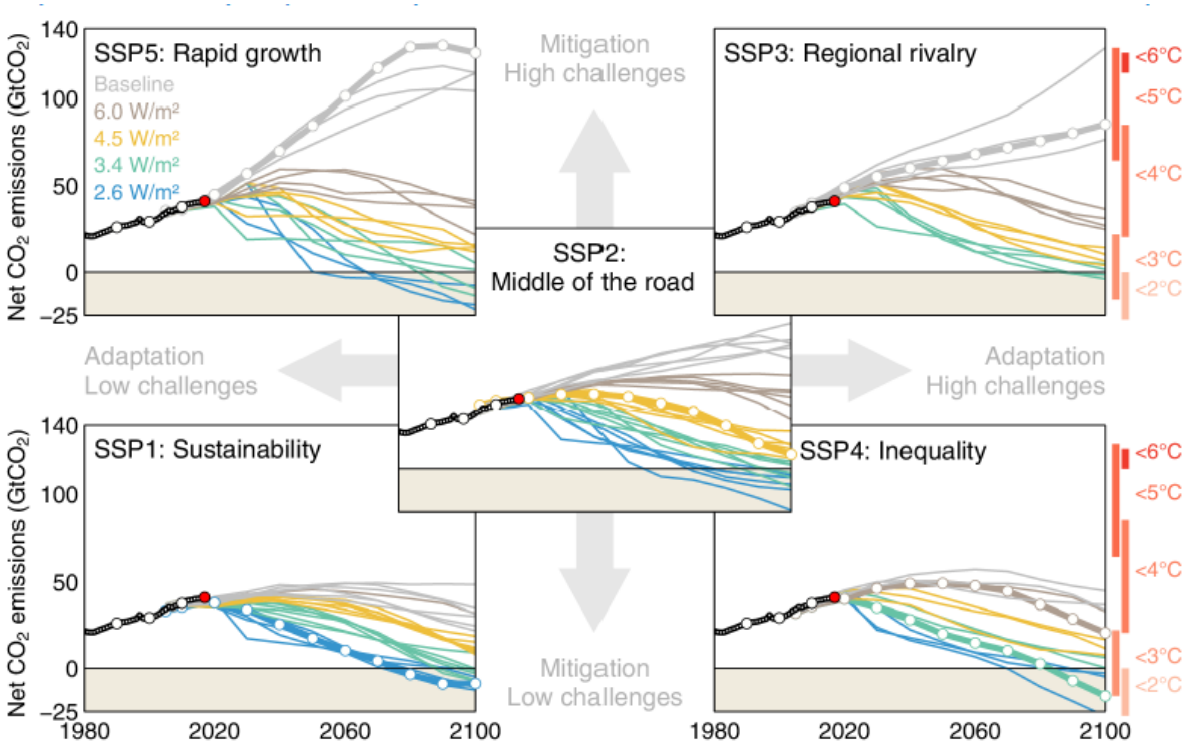

Figure 5.1 | Shared Socioeconomic Pathways showing net CO_2 emissions through the 21st century, defined by their climate change mitigation and adaptation challenges (Riahi et al, 2017); 1 GtC = 3.664 $GtCO_2$

In this pathway, CO_2 emissions double over the century from 40 gigatonnes of carbon dioxide ($GtCO_2$) in 2010 to 85$GtCO_2$ in 2100, despite 50% of the transportation sector being electrified. Temperature anomaly reaches 2ºC by 2050 and approximately 3.8ºC by 2100 (Hausfather, 2018). Although SSP2 does not assume any coordinated global climate change mitigation policy or transformative technological advancements, stringent global climate policies could limit temperature increases to below 2ºC if atmospheric CO_2 levels are capped at 426-491 parts-per-million (Fricko et al, 2017), corresponding to an emissions avoidance of ~1200 $GtCO_2$ (Riahi et al, 2017). The middle-of-the-road nature of SSP2, combined with its potential to reach

climate targets, makes it an ideal pathway for a study into future emissions pathways and mitigation potential.

The Intergovernmental Panel on Climate Change released a special report in 2018 that outlined dire consequences for global warming beyond 1.5ºC. This is a substantial deviation from the previous target of 2ºC used to inform climate policy and regulations worldwide (IPCC, 2013) and was necessary given recent advancements in our understanding of the global climate system and our ability to model it accurately (IPCC, 2018). To achieve this century-end 1.5ºC target would mean that global emissions must peak by 2020 and reach net zero between 2040 and 2055, although the report states that there has been "no documented historic precedent for the scale of system rate change needed to meet emissions reductions."

Further support for immediate emissions reductions comes from an analysis of the rate of temperature change over multi-decadal scales, which is found to be accelerating at an unprecedented rate. The global-mean temperature is presently increasing at a rate of 0.2ºC per decade (Smith et al, 2015); the higher the rate of change, the less time remaining for mitigation efforts to successfully keep global temperature rise under 2ºC.

5.1.2 Current and Future Emissions

The four nations that emit the most carbon pollution are China, the U.S., the European Union (EU), and India. Until 1990, the U.S. and the EU had similar emission rates. The EU enacted environmentally-friendly policies which reduced emissions around the turn of the century, but the same was not true for the U.S., which remained the top emitter until 2007. China's rapid economic development in the 21st century has resulted in an exponential growth of emissions, currently at

28% of the global total (Le Quéré et al., 2017); similar rapid growth is expected from nations undergoing significant economic development (Friedrich et al., 2017).

The changing share of emissions over time reinforces the necessity of global cooperation to the success of any climate mitigation strategies. Efforts to limit emissions from high-emitting nations will only see a corresponding rise in emissions from developing nations that have yet to achieve the same level of economic advancement. This is further reinforced by the synergy between low global emissions and global cooperation/convergence explored in the SSPs (Kriegler et al, 2012; Riahi et al, 2017). Tied to this synergy is the relationship between economic prosperity and a higher valuation on health and the environment (Rao et al, 2017), supporting the future success of more ambitious carbon mitigation targets.

Recent technological advancements and shifts in fuel sources have countered the effects of population growth and industrialization in the electric power generation sector. The inadvertent result of this, however, is that transportation sector emissions have replaced power generation as the top emitting economic sector, as of 2016 (Randall, 2017). Increases in economic prosperity and population have resulted in a corresponding increase in vehicle miles travelled (VMT); the outcome is the highest-ever fossil fuel emissions from vehicles (EPA, 2017). Fortunately, the same methodology can be applied to mobile source emissions to counter the growing vehicle fleets and emissions.

Projections from the U.S. Energy Information Administration through 2040 show the highest energy consumption source as petroleum and other liquid fuels (Conti, 2016), consistent with the transportation sector having a leading impact on overall emissions for the coming decade. Furthermore, the Organization for Economic Cooperation and Development projects that transport emissions will double by 2050 (Marchal et al., 2012), and the World Bank estimates that

transportation will be the single largest source of global GHG emissions by 2035 and 80% of total emissions by 2050 (Kopp et al., 2013).

To achieve the low temperature anomaly target outlined in the IPCC Special Report, substantial changes in the transportation sector are required. For example, electric vehicles would need to replace internal combustion engines sometime between 2035 and 2050. Although electrification is a promising path for increasing the fuel economy of the light-duty fleet, this pathway may not be viable for heavy-duty vehicles (HDV), which are responsible for almost half of global on-road emissions. HDV are the largest class of vehicles and are used mainly for freight shipping. These vehicles have a disproportionately high environmental impact compared to their share of use, and only four nations (U.S., Canada, China, and Japan) have HDV fuel economy standards (Kodjak, 2015). In the U.S., phase 2 emissions regulations for new HDV require CO_2 per ton-mile to reduce by 12-27% from model years 2018 to 2027 (EPA, 2016; Sharpe et al, 2016).

Nevertheless, the moderate emissions reductions from HDV achieved through standards of only a few nations fall short of a global impact, as the U.S. Energy Information Administration predicts an increase in VMT from HDV of approximately 100 billion miles from 2016 to 2040 (Conti et al, 2016). U.S. freight transport grew by 50% between 1990 and 2013 and is expected to surpass passenger vehicle emissions by 2030 (SmartWay, 2017).

The global HDV fleet comprises some 20 million vehicles and is projected to grow to 45 million vehicles by 2030, with a respective emissions growth of 230% (Enkvist et al, 2007). Emissions from heavy-duty freight transport will likely increase two- to three-fold from now until 2050 (Gota et al, 2016). Due to their low fuel economy, limited existing regulations, and projections that show HDV emissions increasing through 2040 (Law et al, 2011; EIA, 2017), long-haul freight trucking represents an important opportunity for improvement in emissions.

5.1.3 Technology and Policy Strategies for Decarbonization

Historically, road freight transport is linked to economic development, making it especially challenging to reduce these emissions without compromising economic prosperity (Hill et al, 2011). One tactic for reducing freight shipping emissions without a significant economic burden is through a policy instrument, such as a carbon tax, which could be implemented immediately with very low capital expenditures, would generate revenue while spurring transformational shifts in technology, and is the easiest global decarbonization strategy (Kaufman & Gordon, 2018). A successful carbon tax would be based on the historic economic prosperity and current growth rate of each individual nation, permitting sustainable and synergistic global decarbonization while also spurring transformational technology shifts and supporting emerging low-carbon technologies.

The U.S. made a step towards this future in 2018, with the enactment of tax code section 45Q, which provides credits for capturing and storing CO_2. The available credit is prorated until 2025, after which the tax credit will be \$35/tCO_2 for enhanced oil recovery (EOR) or \$50/tCO_2 for saline storage (I.R.C. § 45Q, 2018). The lower price for EOR reflects the marketable product created when CO_2 is used to increase oil production, estimated at an additional \$20/tCO_2 (Godec, 2011).

A carbon tax policy instrument is the enabling arm to most emissions reductions; under the SSP2 pathway, carbon capture and storage (CCS) is implemented widely throughout the century. The year 2100 cumulative CO_2 emissions avoided through CCS totals 414 GtCO_2 (IPCC, 2018), with the majority of capture occurring in the power generation sector. However, CCS could easily be applied to transportation.

Alternative emissions reductions strategies for the transportation sector include light-duty electric vehicles (EVs), car sharing, automation, biodiesel, logistical optimization, electrification

of HDV using overhead power lines, VMT reduction via remote work and education, and light-weighting of aircraft (IPCC, 2018). Collectively, these options comprise a broad approach to mobile source emissions reductions but not without significant barriers in technology advancement, public support, and infrastructure costs. The most promising alternative, EVs, have had significant barriers to growth, historically limited by the cost of battery storage per unit of energy, with an upper threshold target of $150/kWh for commercialization. Market leaders in battery technology, including the Department of Energy, estimate that batteries for EVs will reach the commercialization threshold between 2020 and 2025 (Nykvist & Nilsson, 2015).

Some countries have already implemented national plans to phase out ICE vehicles: China is currently targeting 20% of all new vehicle sales as electric, while India has an all-electric sales goal by 2032 (IPCC, 2018). Globally, EVs have recently begun a transformational market shift, evident by the increase in EV sales of 42% for 2015-2016 and the ever-decreasing battery cost per kilowatt-hour (kWh) (IPCC, 2018).

Ideally, the growth of EV sales would occur concurrently with a shift to renewable energy in the power generation sector, since the electric grid mix of the region is the predominant factor in EV emissions intensity. For a fossil-fuel heavy region, emissions are ~300 grams of CO_2-equivalents per kilometer (gCO_2-e/km) while low-carbon regions achieve ~80 gCO_2-e/km (Wilson, 2013). Collectively, electrification and ride sharing have the potential to reduce CO_2 emissions in urban areas by up to 85% by 2050 (Fulton et al, 2017). A joint study by the Electric Power Research Institute and the Natural Resources Defense Council found that GHG emissions in 2050 could be reduced by 48-70% over 2015 levels with the electrification of the transportation sector (Tonachel, 2015). While the future of passenger transport is increasingly electrified, the same cannot be said for freight transport.

The large size and payload mass of HDV make electrification a daunting challenge. Recent efforts by Tesla and Daimler, however, have illustrated pilot/prototype all-electric freight trucks (with plans to commercialize the technology post-2020) but there are concerns regarding range, cost, charging time, and cargo limitations (Lambert, 2018). Instead, the electric power could be supplied via overhead catenary or in-road inductive charging, but this transformative technology would require substantial capital investments over decades to build a standardized, nationwide travel network prior to deployment. This prerequisite means a delay in market growth, with estimates of 15% of sales in 2050 for catenary electric compared to 50% for traditional passenger EVs (Moultak, Lutsey, & Hall, 2017).

An alternative opportunity exists to decarbonize the HDV fleet: carbon capture using porous solid adsorbents that selectively remove carbon dioxide gas from vehicle exhaust. In mobile carbon capture (MCC), the exhaust would exit the tailpipe under normal vehicle operation and then enter a vessel packed with adsorbent, where the CO_2 would be captured within the solid framework. The resulting CO_2-lean or CO_2-free gas would then be emitted to the atmosphere, while the CO_2-laden adsorbent would be regenerated to siphon off the captured CO_2 and prepare the material for another adsorption cycle.

Carbon capture using physical adsorption is an established technology and presents a unique opportunity to potentially retrofit existing HDV with MCC (HDVCC) to avoid current carbon emissions. Compared to an average vehicle lifetime of 8 years for passenger cars, HDV are typically driven over 20 years (Law et al, 2011). The slow fleet turnover, combined with anticipated increases in HDV freight shipping, means that even widespread electrification after 2020 would not result in reduced CO_2 emissions in 2050 compared to 2015 (Moultak, Lutsey, &

Hall, 2017). HDVCC, specifically if implemented in complement to vehicle electrification, would spur HDV decarbonization by 2050.

5.2 Methodology

5.2.1 Environmental Impacts using a Simple Climate Model

The transient climate response to cumulative carbon emissions (TCRE) provides the framework for an evaluation of climate change futures based on the cumulative anthropogenic CO_2 emitted since industrialization began in 1870 (IPCC, 2013). Estimates of TCRE, calculated from state-of-the-art climate and Earth system models, vary from 1.0-2.1ºC per 1000 GtC (3667 $GtCO_2$) (Matthews et al, 2009), with more recent estimates at the higher end of this range. The median 50% of models suggest that at most 355 to 461 GtC (1300 to 1690 $GtCO_2$) of remaining fossil fuel reserves can be combusted to keep global warming under 2°C (Marcucci, Kypreos, & Panos, 2017; IPCC, 2018).

The TCRE allows a direct relationship to be made between peak CO_2-induced warming and future emissions, regardless of emissions timing or peak rate. A summary of TCRE, computed from various climate models, is shown in Figure 5.2; the unavoidable warming from 1000 GtC of emissions is 2ºC, with a 5-95% confidence interval of 1.3-3.9 ºC (Allen et al, 2009). Cumulative emissions to date are approximately 460 GtC (Le Quéré et al, 2017), or about half of carbon budget for 2ºC peak warming.

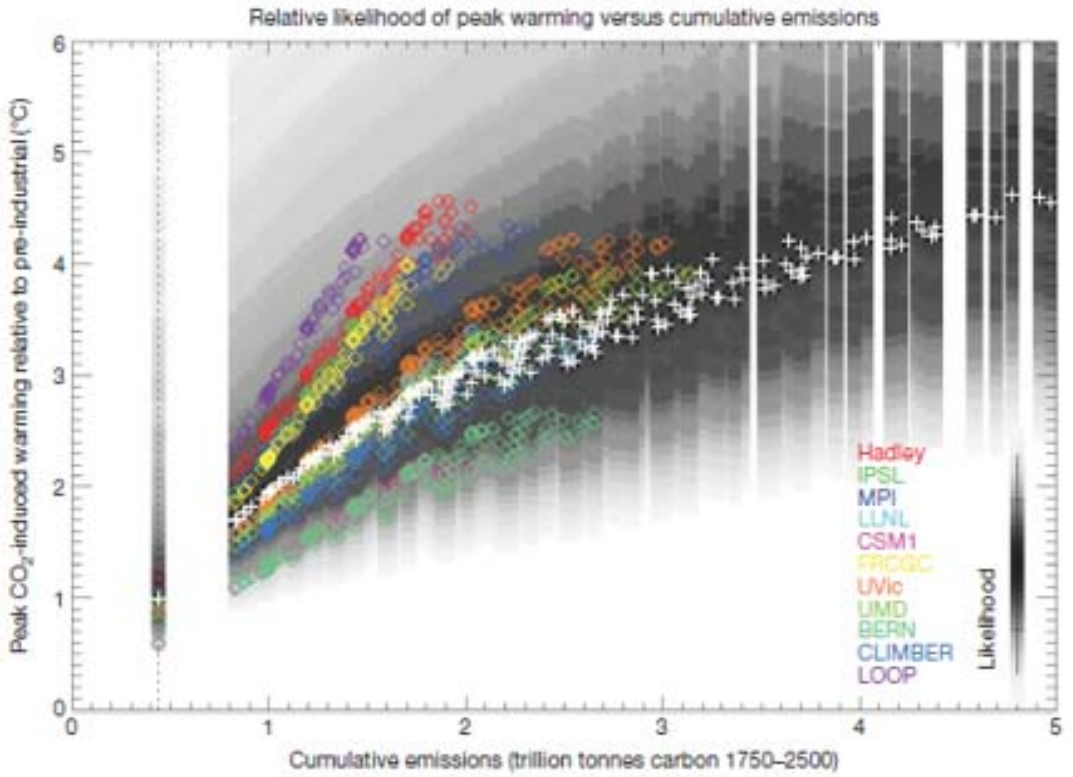

Figure 5.2 | Peak CO_2-induced temperature change as a function of cumulative emissions (white crosses show best-fit values and shading shows likelihood) (Allen et al, 2009)

The open-source simple climate model Hector, developed by Pacific Northwest National Laboratory, was used to assess climate impacts of total global anthropogenic CO_2 emissions resulting from HDVCC. Hector uses a well-mixed globally averaged atmosphere, forced with a broad range of emissions (Hartin et al, 2015). While traditional global climate models are complex and lengthy in run time, Hector is fast-executing with variables that are easy to alter.

In many climate models, the temperature response from non-CO_2 gases and aerosols are assumed to negate each other (Allen et al, 2009), simplifying the relationship between carbon budget and peak warming. This is not true for most future emissions pathways (Tokarska et al, 2018), where the result of non-CO_2 forcings is net warming. The relationship between temperature

anomaly and forcings was evaluated by running duplicate model scenarios that differed in emissions: (1) all forcings included, (2) CO_2 only (all other forcings set to zero), and (3) all non-CO_2 forcings (with CO_2 set to zero). For all scenarios, anthropogenic carbon emissions [1765-2017] follow records from the Global Carbon Project and the Carbon Dioxide Information Analysis Center (Le Quéré et al, 2017; CDIAC, 2017) while non-CO_2 forcings follow SSP2 [1765-2100].

5.2.2 Economic Benefits using the Social Cost of Carbon

The TCRE relates avoided carbon emissions to the environmental impact, while the economic impact is evaluated using a cost-benefit analysis. This cost of HDVCC is estimated in chapter 4, whereas the benefit of avoided CO_2 emissions is assessed using the social cost of carbon (SCC), which represents the present value for all future damages resulting from one additional unit of carbon emissions. The damages include human health, infrastructure, agricultural productivity, diminished biodiversity, and extreme weather events.

The U.S. EPA initially estimated the SCC at $46 in 2025 and $69 in 2050 (2007 USD per ton of CO_2 using a 3% discount rate) (IAWG, 2013). Many experts argue that this estimate is far lower than the true cost of carbon pollution, as it omits widely-accepted scientific and economic impacts of climate change (EDF, 2017). When this uncertainty is included in the SCC estimation, the cost increases to $130 in 2025 and $220 in 2050 (2005 USD per ton of CO_2 using a 2.7% discount rate) (Newbold et al, 2010).

Both estimations for SCC were used to establish certain (IAWG, 2013) and uncertain (Newbold et al, 2010) future economic benefits, based on the avoided emissions ($GtCO_2$) from pursuing HDVCC from 2025 to 2100. Published SCC estimates end around 2050, so each data set

is extrapolated to 2100. Certain and uncertain values are converted to 2018 USD from their respective 2007 or 2005 amounts using annual inflation rates (Amadeo, 2019).

5.2.3 Societal Effect using a Transformative Technology Framework

The role and potential of mobile carbon capture as an emerging, transformative technology for the global HDV fleet is promising, but requires a thorough understanding of the design factors surrounding the capture system, supporting infrastructure, and disruption to existing HDV operations. A framework for establishing the intrinsic, indirect, and external factors (Figure 5.3) is used to inform early design and development of HDVCC (Miller & Keoleian, 2015); important design factors are evaluated for each category, and those design considerations are then used to compare competing technologies from the perspective of a consumer interested in purchasing a new HDV.

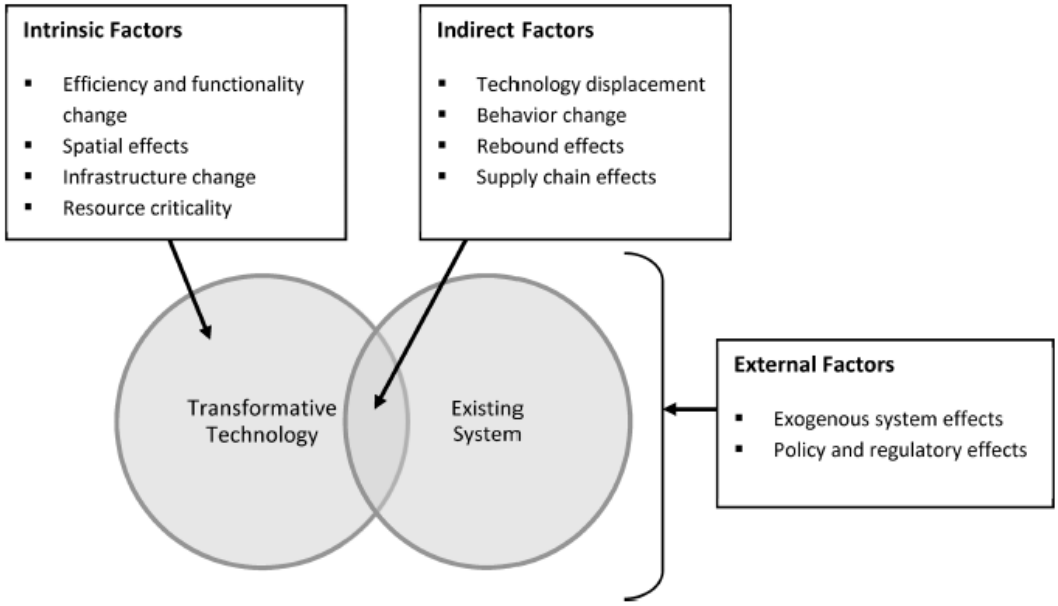

Figure 5.3 | Schematic of the ten factors with the greatest influence on the life cycle of a transformative technology (Miller & Keolian, 2015)

5.3 Results

5.3.1 Establishing the Market Potential of HDVCC

Using SSP2 as our business-as-usual scenario for future emissions, Figure 5.4 illustrates CO_2 emissions (GtC/yr) for the total globe, transportation sector (both taken from SSP2), and heavy-duty freight shipping. Transportation sector emissions peak in 2050 and then decline in emissions at historic rates. By 2070, the transportation share of total emissions reaches a minimum around 20% before increasing to almost 50% by 2100 (Riahi et al, 2017). The share of emissions for HDV freight increases 2.5-fold from 2015 to 2050 (Gota et al, 2016), reaching 56% of transportation sector emissions by mid-century. HDV freight is then assumed to remain at this share of transportation emissions through 2100.

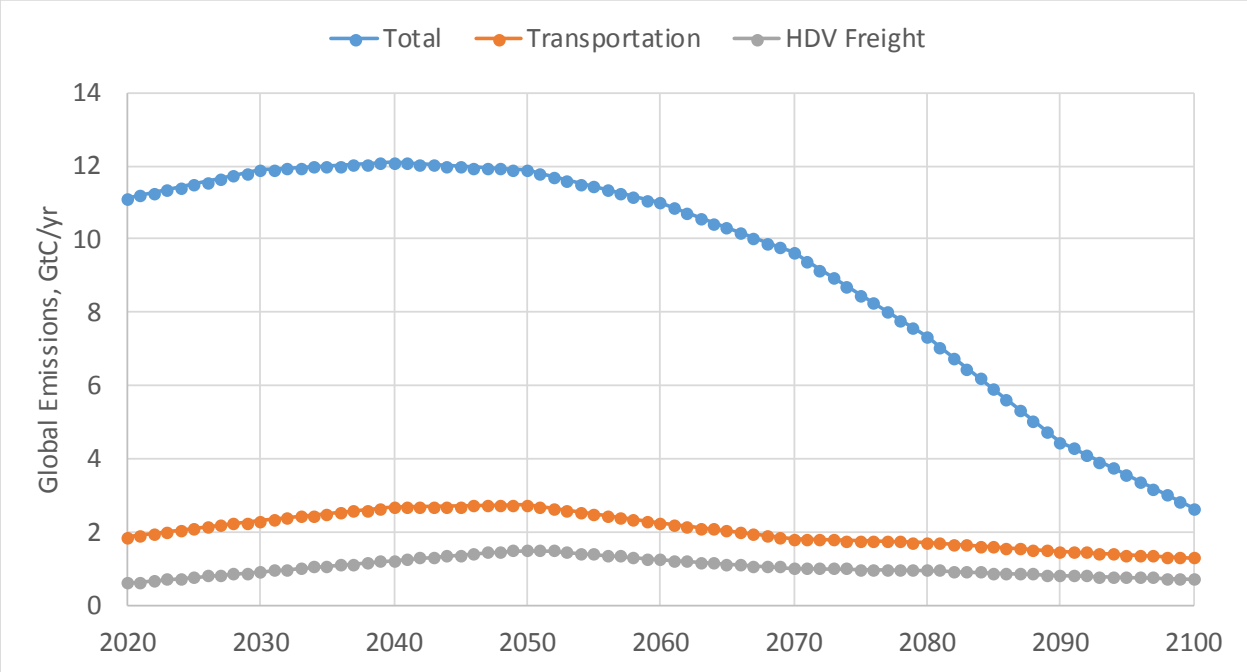

Figure 5.4 | SSP2 annual CO_2 emissions: total, transportation, and on-road HDV freight

An analysis of annualized HDV emissions from 2020 to 2100 (grey line in Figures 5.4-5.5) gives a baseline for total market potential of HDV freight decarbonization. Cumulative emissions (yellow line) reach 33 GtC in 2050 and 84 GtC in 2100.

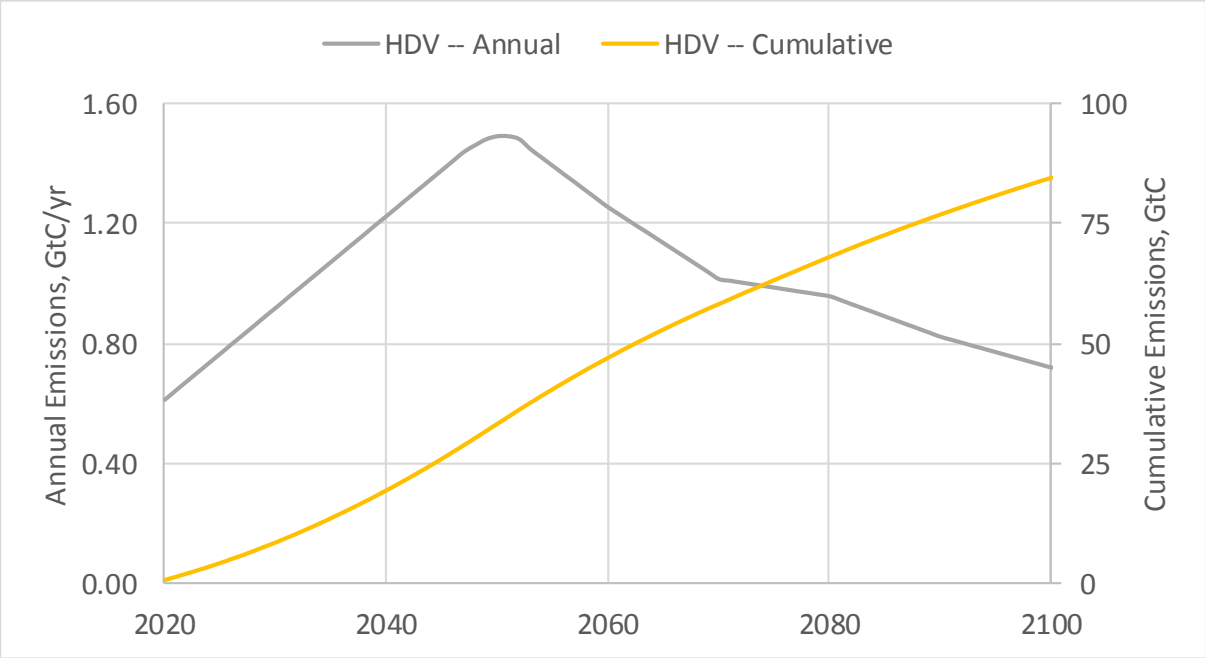

Figure 5.5 | Annual and cumulative emissions from HDV freight, 2020-2100

The Hector model was run with various potential emissions reduction pathways for heavy-duty freight based on different starting dates. While realistic technology implementation would involve a slow ramp-up to full market potential, the starting dates here reflects 100% of the market so the corresponding mass of CO_2 (GtC) is the maximum carbon pollution avoided. The average TCRE computed across all model runs is approximately 1.8°C per 1000 GtC of anthropogenic CO_2 emissions. MCC from HDV freight results in a century-end temperature avoidance of 0.12°C if implemented by 2040 and 0.15ºC if implemented by 2025. This avoidance is approximately 10% of the remaining temperature change for a 2°C peak warming target.

In all scenarios, the longevity of CO_2 dissipation results in a delay in CO_2-induced peak warming that begins approximately 10 years after emissions reductions commence (Ricke & Caldiera, 2014). Therefore, an analysis of the 2050 temperature is futile for all but the earliest actions. Instead, the TCRE provides the time-independent temperature impact of pursuing HD-MCC. The observed trend across increasing carbon budgets is an increasing TCRE; the more CO_2 avoided, the greater the normalized impact on temperature.

5.3.2 Cost-Benefit Analysis

The difference in annualized social benefit of HDVCC between the low and high SCC estimates increases exponentially as the century progresses (Figure 5.6). The rapid growth after 2050 and the increasing disparity between certain and uncertain estimates is yet another motivation for an immediate reduction in emissions.

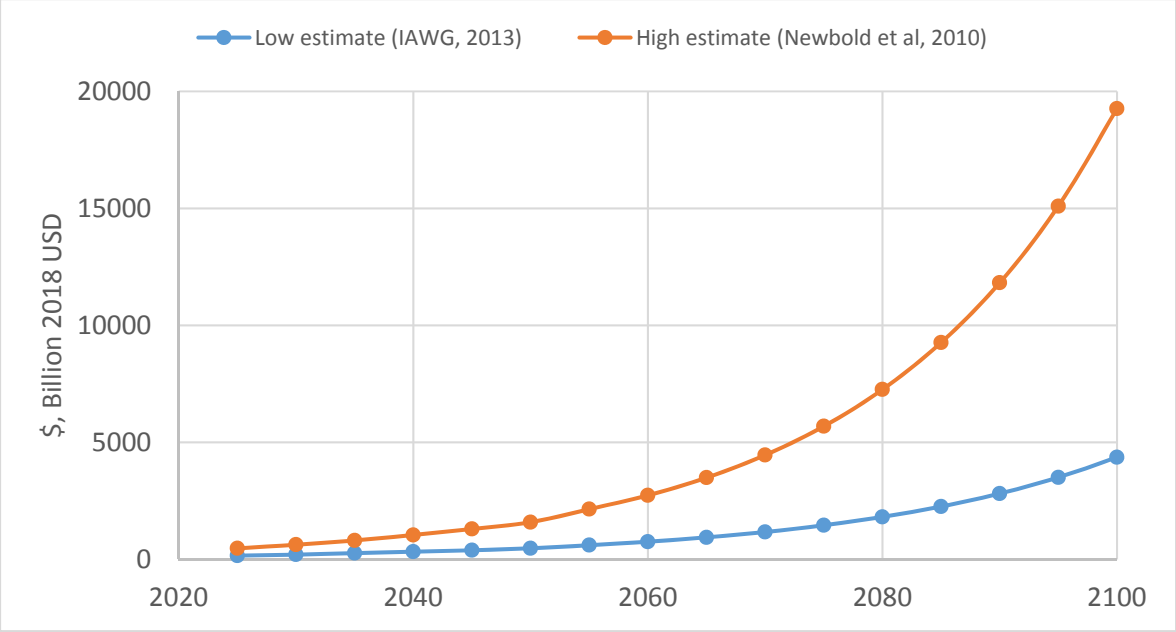

Figure 5.6 | High (Newbold et al, 2010) and low (IAWG, 2013) SCC estimates showing the annualized benefit of HDVCC, with annual values based on cumulative emissions from HDVCC and adjusted to 2018 USD

Cumulative savings in 2050 range from $8-$25 trillion 2018 USD for an emissions avoidance of 80 GtC, giving a normalized benefit per ton of CO_2 emissions mitigated of $71-$228 (2018 USD). The lower (more certain) range of this estimate is similar in price to the carbon abatement cost estimate for heavy-duty vehicular carbon capture of $100/t$CO_2$ (at 100% capital costs), making the future social benefit of HDVCC nearly equal to the current cost of abatement. This represents a conservative estimate since we have assumed the cost is constant over time, even though improvements in technology and efficiency would reduce future abatement costs.

With amended section 45Q of the U.S. tax code and estimates for the financial return on CO_2 for EOR (I.R.C. § 45Q, 2018; Godec, 2011), the mitigated emissions result in an additional positive return of ~$50/t$CO_2$. In comparing these options, it is important to note that the societal benefit is an implied amount, whereas the tax rebates and EOR-CO_2 return are tangible benefits. If only the former are considered, then the cost of HDVCC implementation is ~$25/t$CO_2$ avoided.

5.3.3 Decision-making for Consumers

Intrinsic factors for HDVCC include a decrease in fuel economy, limited adsorbent supply, widespread adopter location, lower CO_2 emissions, system cyclic capacity (lifetime), and infrastructure availability for adsorbent regeneration. Indirect factors at the intersection of traditional HDV and HDVCC include driver behavioral changes, miles travelled, and energy requirements. External factors affecting the entire HDV fleet include a regulations and policies affecting transportation emissions and vehicle efficiency.

Aside from the large capital infrastructure investment, the relevant hurdle for technology deployment of HDVCC, like that of traditional EVs, is public perception. For a consumer interested in purchasing a new HDV for long-haul freight shipping (in a future where all

technologies are available commercially), there are three alternatives to consider: a traditional HDV, one fitted with HDVCC, or an all-electric HDV relying on overhead catenary or in-road inductive charging. The radar plot in Figure 5.7 serves as a decision-making matrix; each option is ranked 1-5 for each decision, and each decision must have a preferred (rank 5, perimeter) and not preferred (rank 1, center) option.

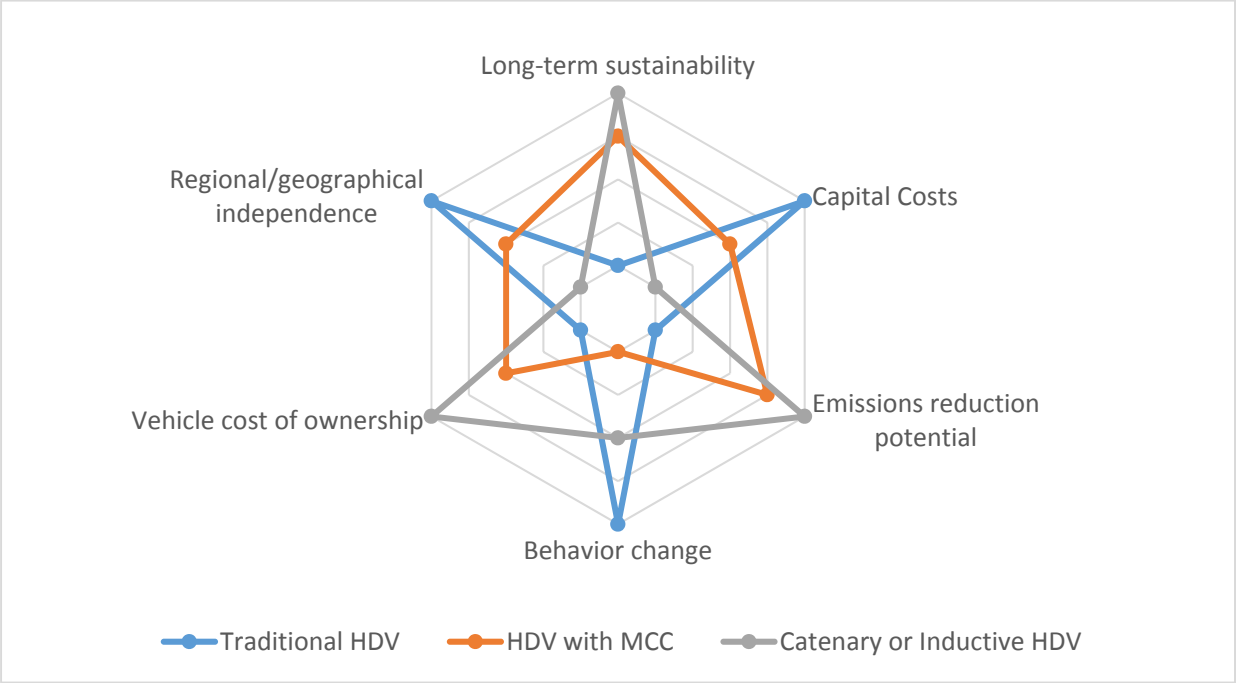

Figure 5.7 | Comparison of alternatives for HDV freight decarbonization alternatives: traditional diesel HDV, HDV with MCC, or all-electric using catenary or inductive charging

A traditional HDV is not the preferred option when it comes to emissions reduction potential (low or non-existent), long-term sustainability (since it will continue to burn fossil fuels and is not well-regulated), and vehicle cost of ownership (since fuel prices and more stringent standards will increase owner costs over time). Similarly, electric HDV are not preferred in terms of geographical independence (range is dependent on charging infrastructure) and capital costs

(since the required infrastructure network is expansive). A HDV outfitted with MCC technology would require the most significant changes in behavior, as the driver would need to regenerate the adsorbent bed periodically and the process lasts longer than refilling a fuel tank.

The results of the radar plot can be interpreted in several ways: The fleet owner (consumer) can consider only those decisions deemed important, or each decision can be weighted based on their relative priority, or the sum of all decisions can be used to select the best option. For primary concerns regarding long-term sustainability, CO_2-free emissions, and low vehicle cost of ownership, electric HDV is the preferred option but comes with high upfront capital investments (estimates at +$150 billion (Moultak, Lutsey, & Hall, 2017)) and a geographical dependence on a nationwide charging network.

Traditional HDV is preferable to avoid infrastructure investments, changes in behavior, and geographical dependence, but at the ultimate cost of continued carbon emissions and eventual higher vehicle costs as regulations become more stringent. The middle ground then becomes HDVCC, which would require a somewhat geographically dependent change in behavior similar to an EV (intermittent charging/regeneration) but would reduce emissions with lower capital costs than catenary electric and an eventual lower cost of vehicle ownership than traditional HDV.

5.4 Conclusions

Despite the slow growth of EVs, global transformational shifts in transportation and freight have occurred on decadal time scales: automobiles replaced horses in 20 years (Carlisle, 2016), the U.S. Interstate Highway system was built in 35 years (Neuharth, 2006), and shipping containers replaced bulk cargo in 30 years (Levinson, 2013). Mobile carbon capture from heavy-duty freight shipping has the potential to reduce transportation sector emissions drastically, with a market

potential upwards of 80 GtC through 2100. The corresponding temperature avoidance is 0.12-0.15°C, corresponding to 10% of the warming remaining for a 2°C target. The economic burden (with a tax rebate) is \$25/tCO_2 and the societal benefit is ~\$75/tCO_2 avoided. There is precedent and opportunity now to alter the heavy-duty freight industry to substantially reduce carbon emissions and become part of the solution to climate change.

Chapter 6

Concluding Remarks

6.1 Summary and Contribution

Climate change mitigation, in the form of reduced emissions, is necessary for a sustainable future that ensures equality and quality of life for all. To achieve significant reductions in fossil fuel emissions, carbon dioxide must not exist in excess in our atmosphere. In an ideal world, carbon capture would not be necessary because fossil fuel combustion would not be our primary source of energy. Unfortunately, existing infrastructure and sunken costs ensure a near-term future powered by carbon fuels. If we tackle the problem at the source, before it becomes diluted in the atmosphere, we can minimize the cost of separation and maximize the emissions reductions.

Post-combustion carbon capture is an effective tool for emissions mitigation, permitting the selective removal of carbon dioxide from exhaust gases using porous solid materials. Stationary carbon capture from power generation facilities is well-studied and is piloted at

industrial sites around the globe. Mobile carbon capture, however, has been largely overlooked or dismissed in research.

This work serves as a first step toward understanding the technical feasibility of carbon dioxide capture from vehicle exhaust, specifically those coming from heavy-duty vehicles in the freight shipping industry. It explores how CO_2 could effectively be removed using affordable commercial materials, what conditions would be optimal for capture, and what constraints would be placed on a widespread HDVCC system. In addition to the technical component, a complementary exploration was made into the social science surrounding a sustainable HDVCC program, which includes work in the environmental (using a simple climate model), economic (based on energy requirements and using comparable estimates from literature), and social (using a design framework for emerging technology) impacts.

Zeolites are a class of materials that function as molecular sieves. They are affordable, available in a range of sizes, and are not dangerous. They can effectively capture CO_2 at over 20 weight percent, but their storage capacity decreases as temperature increases (chapter 2). Under dynamic gas flow from complex representative exhaust steams (chapter 3), storage capacity is again compromised. However, the use of a heat exchanger prior to the MCC unit would simultaneously reduce the temperature and condense entrained water vapor. The result (Figure 6.1) is realistic CO_2 storage capacity near optimal.

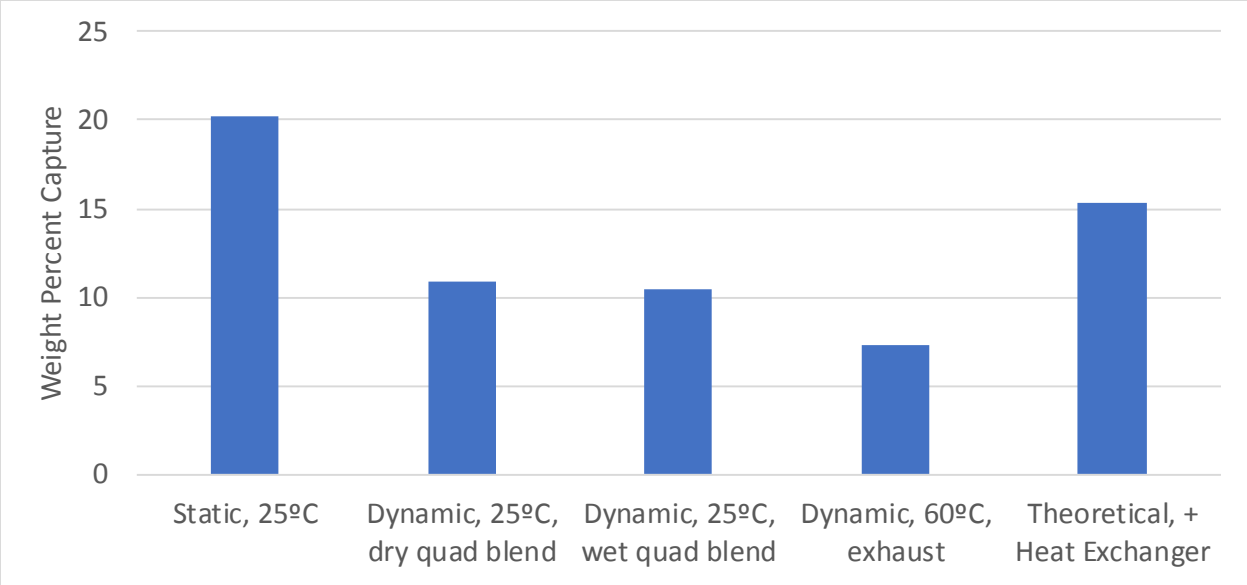

Figure 6.1 | Weight percent capture from 12% CO_2 exhaust using Zeolite 5A

Mobile carbon capture is technically feasible. It is not overly complicated or challenging and presents a unique opportunity to reduce carbon emissions while still combusting fossil fuels. While the installation of a heat exchanger and adsorbent vessel would be simple and low-cost, the necessary infrastructure to compress, transport, and store captured CO_2 is not an easy endeavor. It would ideally be operated in tandem with stationary carbon capture and/or enhanced oil recovery facilities nationwide, minimizing costs and avoiding redundancies.

Beyond the feasibility of this technology lies a more interesting question that is often overlooked in science and engineering studies: should we pursue HDVCC as a practical emissions reduction strategy? To answer this question, we must explore the main pillars of sustainability. First, an energetic-economic evaluation (chapter 4) explored the carbon abatement cost of a hypothetical MCC program for both passenger cars and freight trucks. For either case, MCC was found to be cost-competitive (at ~\$100/tCO_2) with stationary CCS and passenger electric vehicles, and significantly less than direct air capture.

Secondly, the environmental impact of this hypothetical system was explored (chapter 5) based on a likely future emissions pathway; the expected electrification of passenger vehicles exacerbates the role of unchecked freight emissions, which are projected to increase in the coming decades. The market potential of MCC for the HDV freight industry from 2030 to 2100 represents an avoided warming over 0.12°C. Finally, the social impact of HDVCC as an emerging technology was examined (chapter 5) using design factors at the intersection of traditional HDV and overhead catenary electric (as the alternative decarbonization strategy). The result is an informative decision-making tool meant for consumers/drivers planning to purchase a new HDV.

HDVCC is a technically feasible, cost-competitive, effective mitigation strategy that could reduce near-term emissions from the transportation sector. It has the potential to vastly reduce emissions from freight shipping and could be expanded to marine vessels (cargo and cruise ships) to further reduce transportation sector emissions.

6.2 Opportunities for Future Research

Research into MCC, and specifically that from HDV freight shipping, is in its infancy, so the avenues for future research are abundant. The following is in no manner a comprehensive list; instead, it is an exploration into the breadth of future work related to mobile carbon capture.

1. Materials for MCC:
    a. The discovery of an ideal solid adsorbent (which very likely already exists) with extremely high storage CO_2 storage capacity and unaffected by water vapor
    b. The mass production of an ideal adsorbent with tailored sizing or one binded onto a monolith that maximizes contact area

c. A life cycle analysis of the capture unit that includes details on the adsorbent and its cyclic capacity

2. The design of an MCC capture unit:
    a. Heat exchanger configuration and sizing should simultaneously reduce exhaust temperature, remove moisture, and slow gas flow
    b. Adsorbent vessel configuration and sizing should maximize uptake of CO_2 while minimizing parasitic mass
3. Optimal conditions for regeneration:
    a. Minimum temperature and timing necessary for full gas desorption and adsorbent regeneration
    b. Appropriate methods for regeneration that minimize energy requirements, cost, and timing
4. The design of an MCC adsorption-desorption coupled system:
    a. Regeneration system location and methods that minimize infrastructure investments and are most convenient for customers
    b. The integration of infrastructure with existing stationary CCS and EOR operations
5. Pilot testing of HDVCC:
    a. Partnerships to test MCC along freight corridors (end-to-end regeneration) or on city buses using a single regeneration hub
    b. The design and build of a prototype capture system onboard a HDV truck or bus, along with a compatible regeneration system
6. MCC from marine vessels:
    a. Mass, volume, pressure, and temperature restrictions on cargo and cruise ships

b. Ocean storage of CO_2, which would be ideal considering capture location

7. Public policy:
    a. Barriers to the adoption of CCS and vehicle electrification (LDV and HDV)
    b. Support for regulations that limit vehicle emissions
    c. Grassroots movements that promote action to mitigate emissions
8. Sustainability:
    a. Advanced climate modeling to show the role of MCC in relation to stationary CCS, widespread EV adoption, and other low-carbon technologies explored under SSP2
    b. Economic evaluations based on results from pilot/prototype testing
    c. Social explorations (surveys, interviews, workshops) that explore how the general public would interact with HDVCC, increase their understanding of the technology, and attempt to quantify their willingness to pursue/fund

Appendix A

Included herein is the isotherm, isostere, and isobar plots for all seven compounds (ELM-11 is excluded and Zeolite 5A is shown previously in Figures 2.10-2.12) along with a table for each (starting with Zeolite 5A in Table A.1) showing the derivative of the best fit equation using regression modeling. The bottom row of each table shows the triple product for a sample point; with results having an average root mean square error of 7%. The best-fit line was selected from linear, natural log, or exponential growth using the maximum r-squared value for each iso-plot.

Table A.1 | Derivatives of equations for best fit lines for Zeolite 5A at set pressure (P), temperature (T), and uptake capacity (Q), along with the triple product validation at a sample point (bottom row)

P = 14.5 kPa	$y' = -2.268$
28.5 kPa	$y' = -1.952$
56.5 kPa	$y' = -1.682$
101 kPa	$y' = -1.528$
T = 298 K	$y' = 0.000007\, e^{0.05745x}$
313 K	$y' = 0.000281\, e^{0.04385x}$
328 K	$y' = 0.00309\, e^{0.03873x}$
343 K	$y' = 0.01514\, e^{0.03052x}$
Q = 125 mg/g	$y' = 23.76/x$
150 mg/g	$y' = 18.6/x$
175 mg/g	$y' = 14.77/x$
200 mg/g	$y' = 12.96/x$
P | T | Q = 101 | 298 | 238	**xyz = -1.1176**

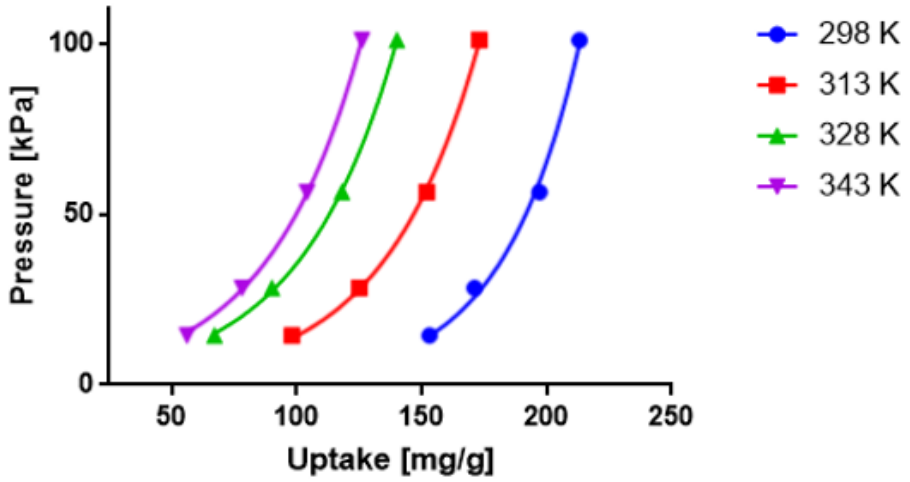

Figure A.1 | Isotherm and regression lines for Zeolite 13X

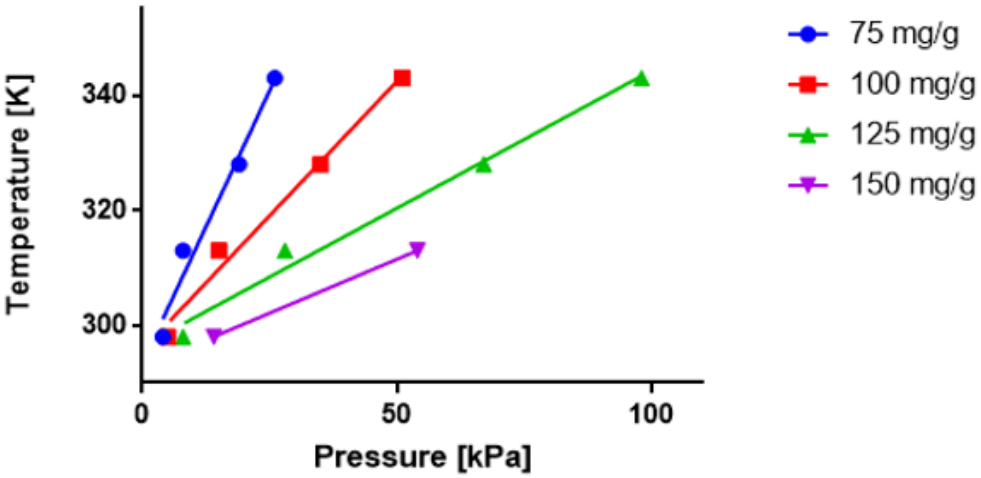

Figure A.2 | Isostere and regression lines for Zeolite 13X

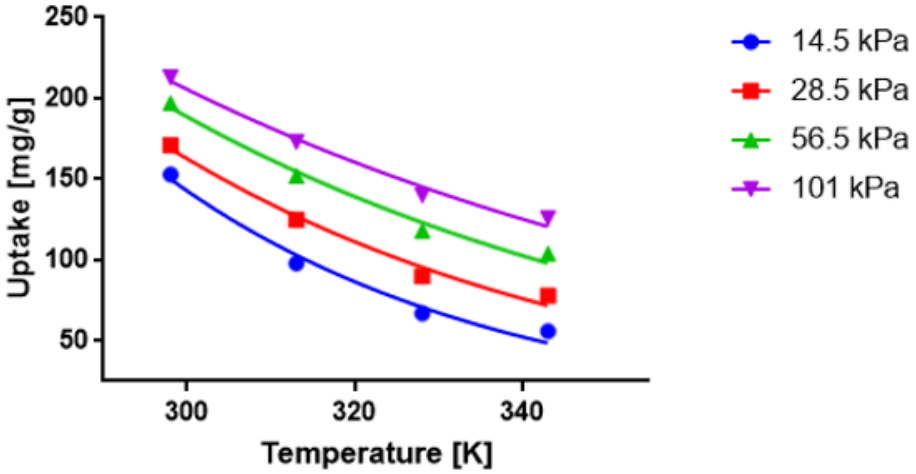

Figure A.3 | Isobar and regression lines for Zeolite 13X

Table A.2 | Derivatives of equations for best fit lines for Zeolite 13X at set pressure (P), temperature (T), and uptake capacity (Q), along with the triple product validation at a sample point (bottom row)

P = 14.5 kPa	$y' = -6497\, e^{-0.02502x}$
28.5 kPa	$y' = -921\, e^{-0.01899x}$
56.5 kPa	$y' = -273\, e^{-0.01519x}$
101 kPa	$y' = -104\, e^{-0.01237x}$
T = 298 K	$y' = 0.0034\, e^{0.03222x}$
313 K	$y' = 0.027\, e^{0.02656x}$
328 K	$y' = 0.069\, e^{0.02597x}$
343 K	$y' = 0.0929\, e^{0.02677x}$
Q = 75 mg/g	$y' = 1.895$
100 mg/g	$y' = 0.9353$
125 mg/g	$y' = 0.4787$
150 mg/g	$y' = 0.375$
P | T | Q = 28.5 | 313 | 125	**xyz = -0.8633**

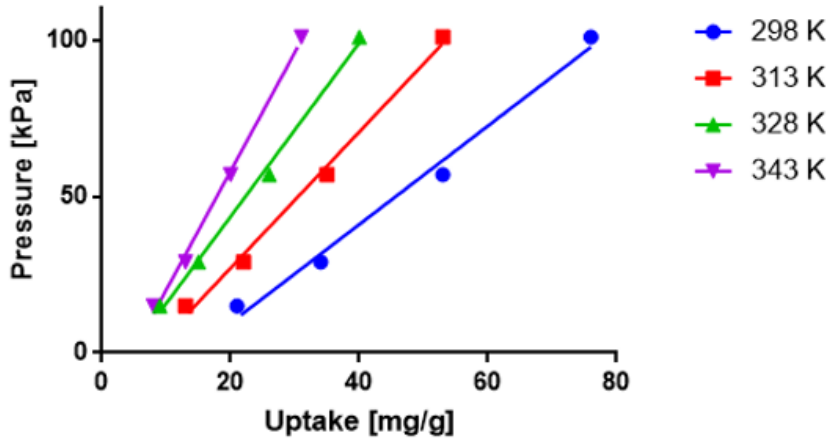

Figure A.4 | Isotherm and regression lines for BPL GAC

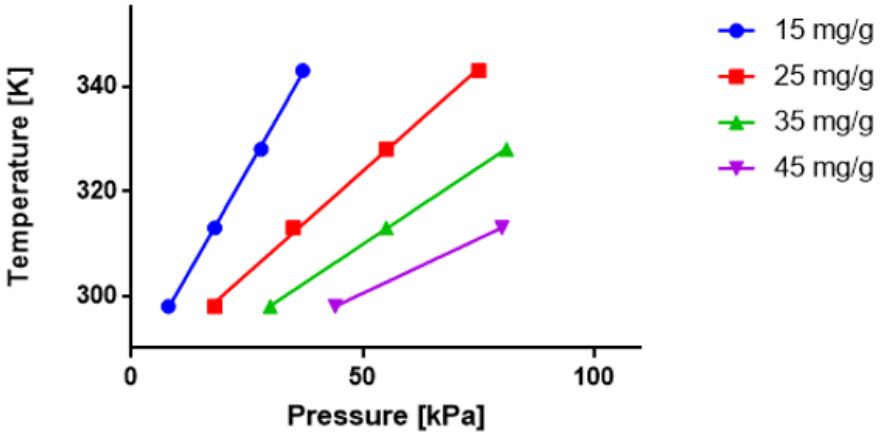

Figure A.5 | Isostere and regression lines for BPL GAC

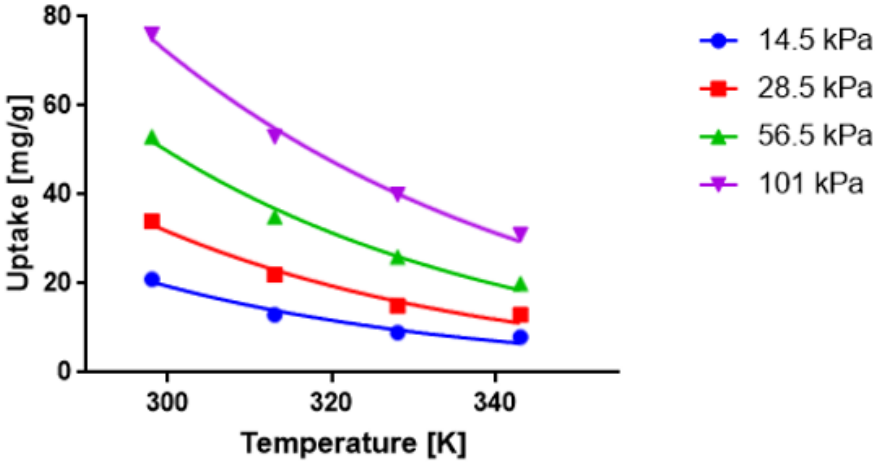

Figure A.6 | Isobar and regression lines for BPL GAC

Table A.3 | Derivatives of equations for best fit lines for BPL GAC at set pressure (P), temperature (T), and uptake capacity (Q), along with the triple product validation at a sample point (bottom row)

P = 14.5 kPa	$y' = -872.5\, e^{-0.02498x}$
28.5 kPa	$y' = -1115\, e^{-0.02426x}$
56.5 kPa	$y' = -1104\, e^{-0.02292x}$
101 kPa	$y' = -744.7\, e^{-0.02071x}$
T = 298 K	$y' = 1.575$
313 K	$y' = 2.177$
328 K	$y' = 2.777$
343 K	$y' = 3.799$
Q = 15 mg/g	$y' = 1.545$
25 mg/g	$y' = 0.7842$
35 mg/g	$y' = 0.5882$
45 mg/g	$y' = 0.4167$
P | T | Q = 101 | 328 | 40	**xyz = -0.9667**

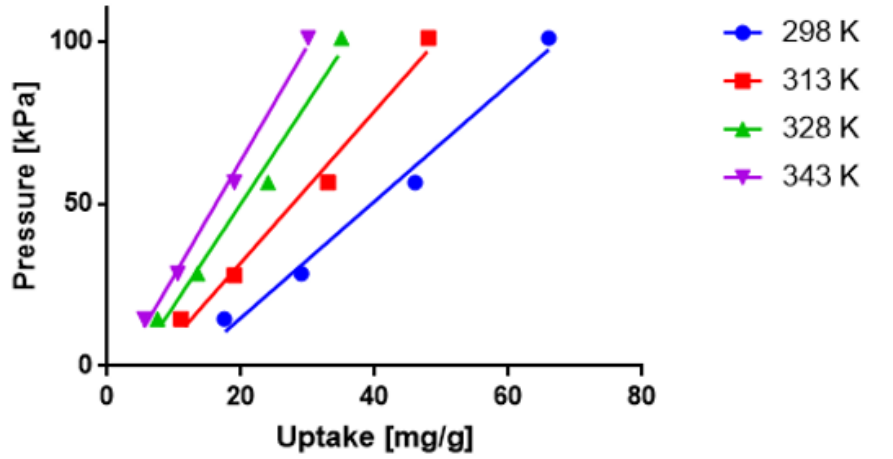

Figure A.7 | Isotherm and regression lines for Darco KB-M PAC

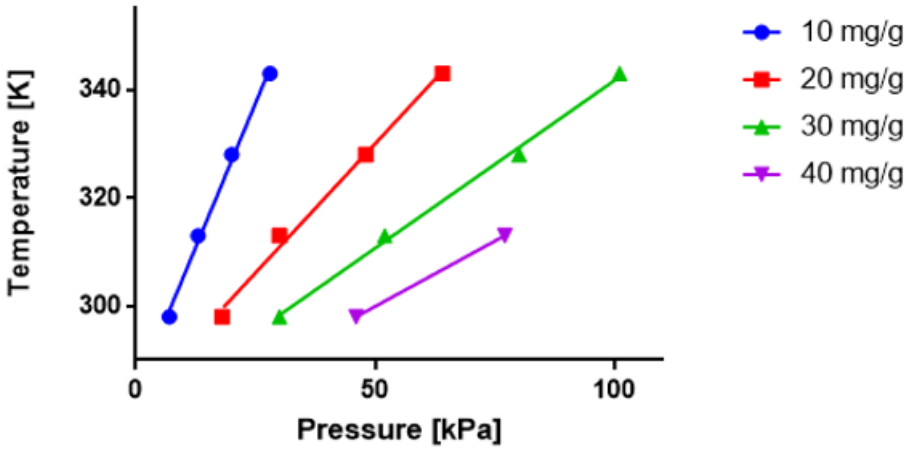

Figure A.8 | Isostere and regression lines for Darco KB-M PAC

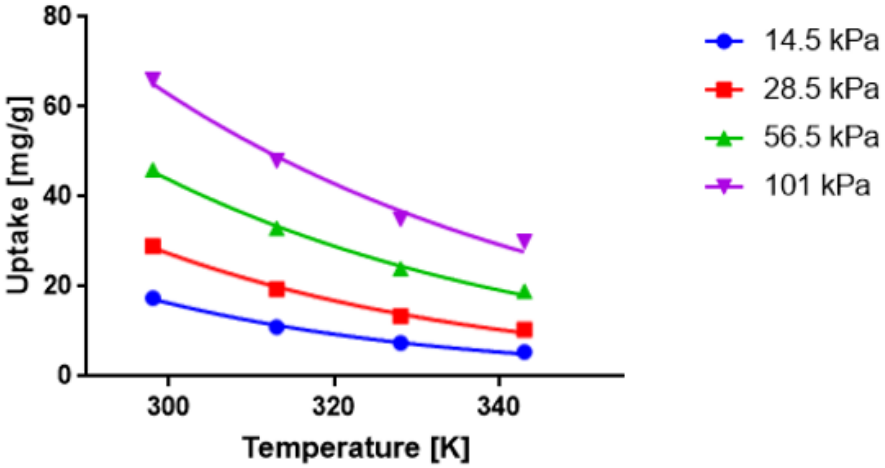

Figure A.9 | Isobar and regression lines for Darco KB-M PAC

Table A.4 | Derivatives of equations for best fit lines for Darco KB-M PAC at set pressure (P), temperature (T), and uptake capacity (Q), along with the triple product validation at a sample point (bottom row)

P = 14.5 kPa	$y' = -1643\, e^{-0.02736x}$
28.5 kPa	$y' = -891.9\, e^{-0.02404x}$
56.5 kPa	$y' = -427.8\, e^{-0.02055x}$
101 kPa	$y' = -352\, e^{-0.01897x}$
T = 298 K	$y' = 1.793$
313 K	$y' = 2.333$
328 K	$y' = 3.127$
343 K	$y' = 3.546$
Q = 10 mg/g	$y' = 2.134$
20 mg/g	$y' = 0.9559$
30 mg/g	$y' = 0.6205$
40 mg/g	$y' = 0.4839$
P | T | Q = 56.5 | 313 | 30	**xyz = -0.9964**

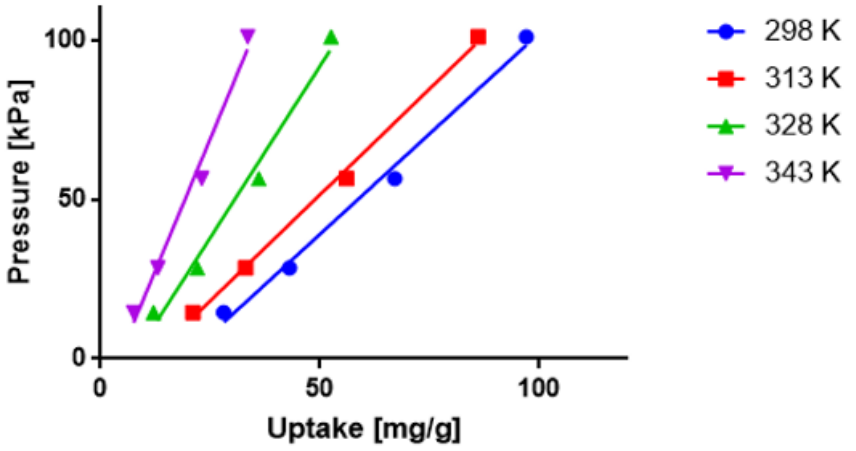

Figure A.10 | Isotherm and regression lines for MIL-53

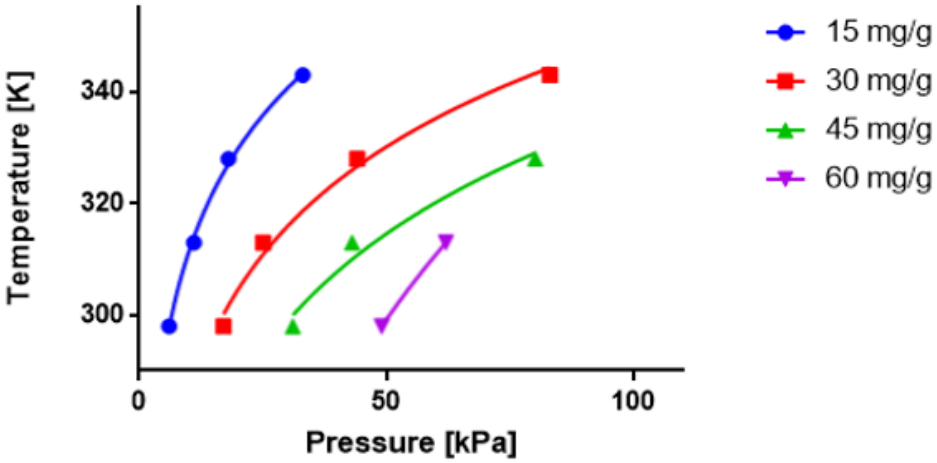

Figure A.11 | Isostere and regression lines for MIL-53

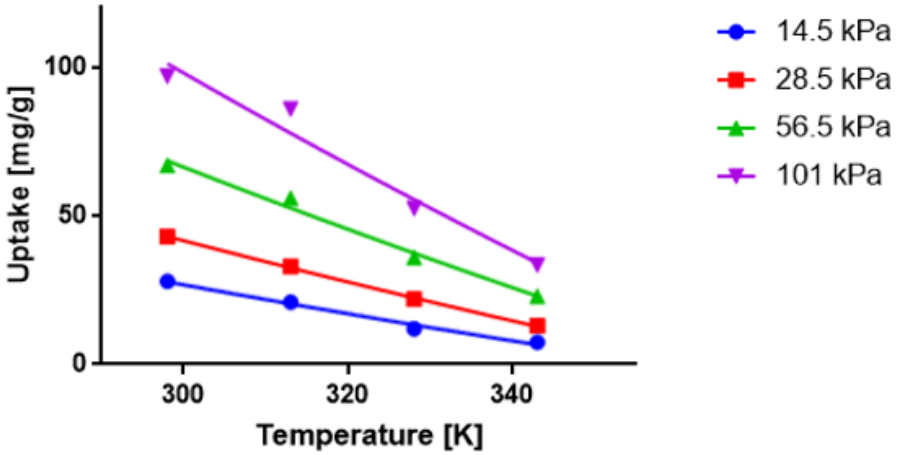

Figure A.12 | Isobar and regression lines for MIL-53

Table A.5 | Derivatives of equations for best fit lines for MIL-53 at set pressure (P), temperature (T), and uptake capacity (Q), along with the triple product validation at a sample point (bottom row)

P = 14.5 kPa	$y' = -150.6/x$
28.5 kPa	$y' = -215.5/x$
56.5 kPa	$y' = -323.9/x$
101 kPa	$y' = -476.9/x$
T = 298 K	$y' = 1.261$
313 K	$y' = 1.331$
328 K	$y' = 2.151$
343 K	$y' = 3.304$
Q = 15 mg/g	$y' = 26.71/x$
30 mg/g	$y' = 27.87/x$
45 mg/g	$y' = 30.66/x$
60 mg/g	$y' = 63.74/x$
P | T | Q = 28.5 | 298 | 43	**xyz = -0.9810**

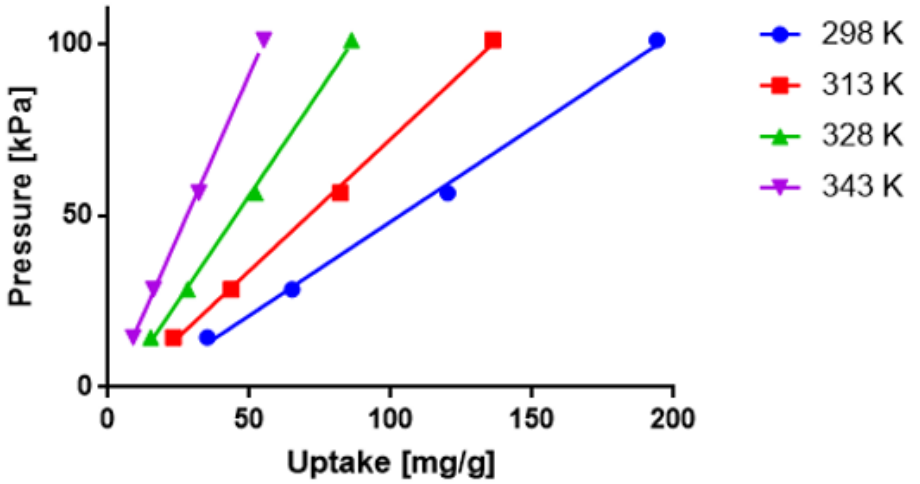

Figure A.13 | Isotherm and regression lines for HKUST-1

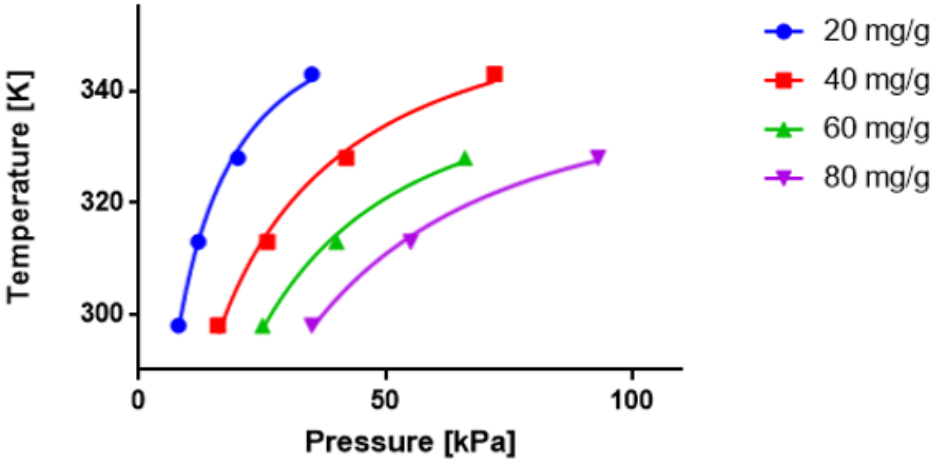

Figure A.14 | Isostere and regression lines for HKUST-1

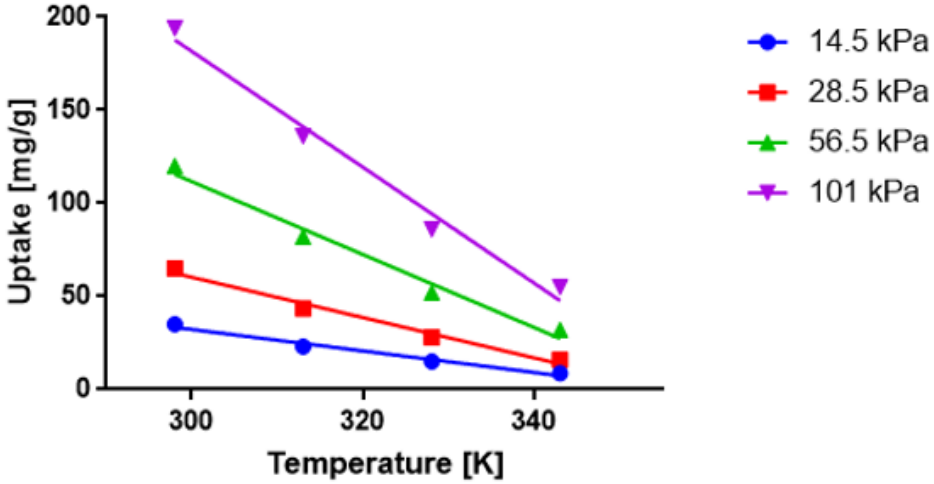

Figure A.15 | Isobar and regression lines for HKUST-1

Table A.6 | Derivatives of equations for best fit lines for HKUST-1 at set pressure (P), temperature (T), and uptake capacity (Q), along with the triple product validation at a sample point (bottom row)

P = 14.5 kPa	$y' = -0.577$
28.5 kPa	$y' = -1.083$
56.5 kPa	$y' = -1.960$
101 kPa	$y' = -3.113$
T = 298 K	$y' = 0.545$
313 K	$y' = 0.767$
328 K	$y' = 1.222$
343 K	$y' = 1.863$
Q = 20 mg/g	$y' = 30.22/x$
40 mg/g	$y' = 30.03/x$
60 mg/g	$y' = 30.89/x$
80 mg/g	$y' = 30.64/x$
P | T | Q = 28.5 | 313 | 43.5	**xyz = -0.8755**

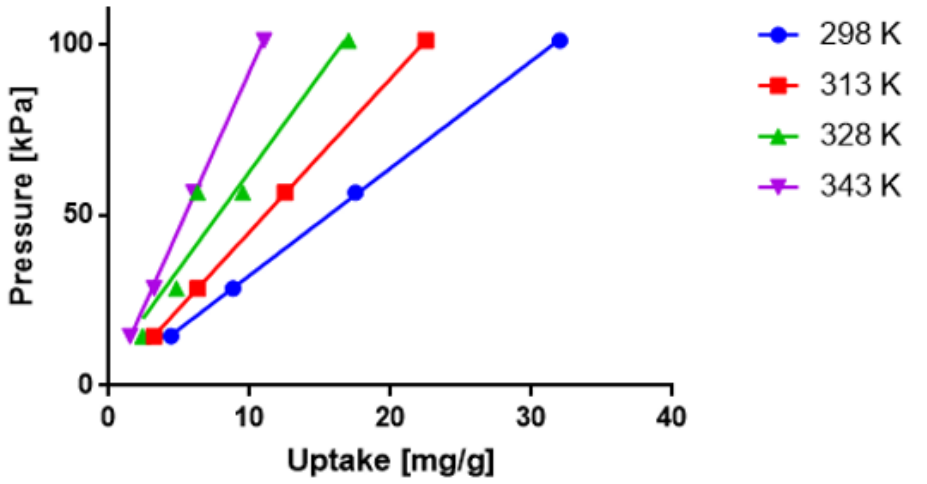

Figure A.16 | Isotherm and regression lines for ZIF-8

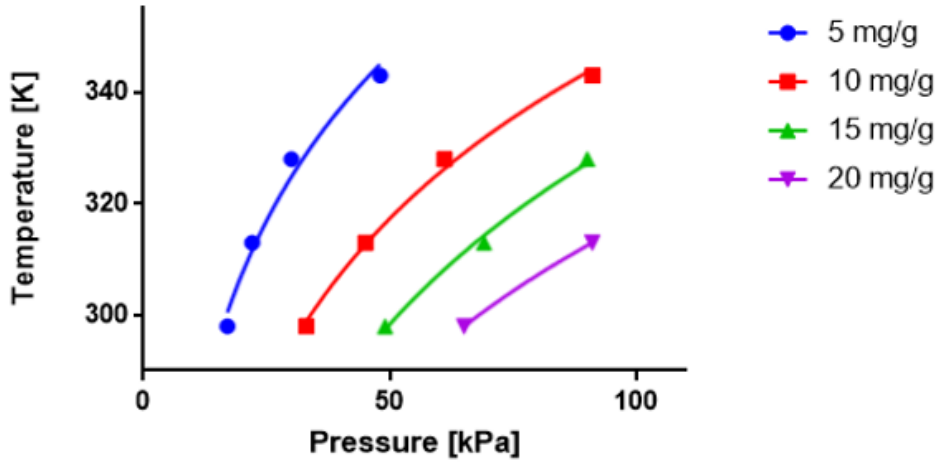

Figure A.17 | Isostere and regression lines for ZIF-8

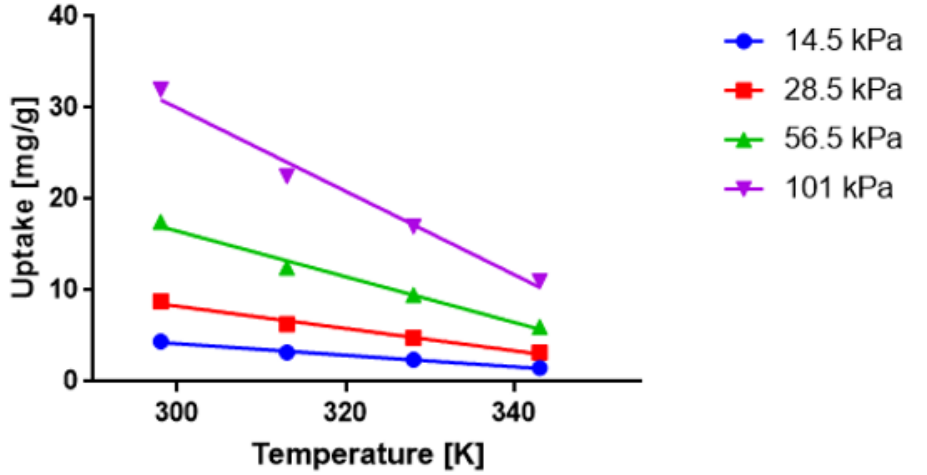

Figure A.18 | Isobar and regression lines for ZIF-8

Table A.7 | Derivatives of equations for best fit lines for ZIF-8 at set pressure (P), temperature (T), and uptake capacity (Q), along with the triple product validation at a sample point (bottom row)

P = 14.5 kPa	$y' = -0.063$
28.5 kPa	$y' = -0.122$
56.5 kPa	$y' = -0.250$
101 kPa	$y' = -0.457$
T = 298 K	$y' = 3.135$
313 K	$y' = 4.482$
328 K	$y' = 5.678$
343 K	$y' = 9.180$
Q = 5 mg/g	$y' = 42.94/x$
10 mg/g	$y' = 44.61/x$
15 mg/g	$y' = 49.08/x$
20 mg/g	$y' = 44.58/x$
P | T | Q = 56.5 | 313 | 12.5	**xyz = -0.9733**

The following graphs show the natural log of pressure plotted against inverse temperature. The slope of the best fit line is used in the Clausius-Clapeyron equation to calculate the isosteric heat of adsorption at various loading fractions. Zeolite 5A is shown in Figure 2.13.

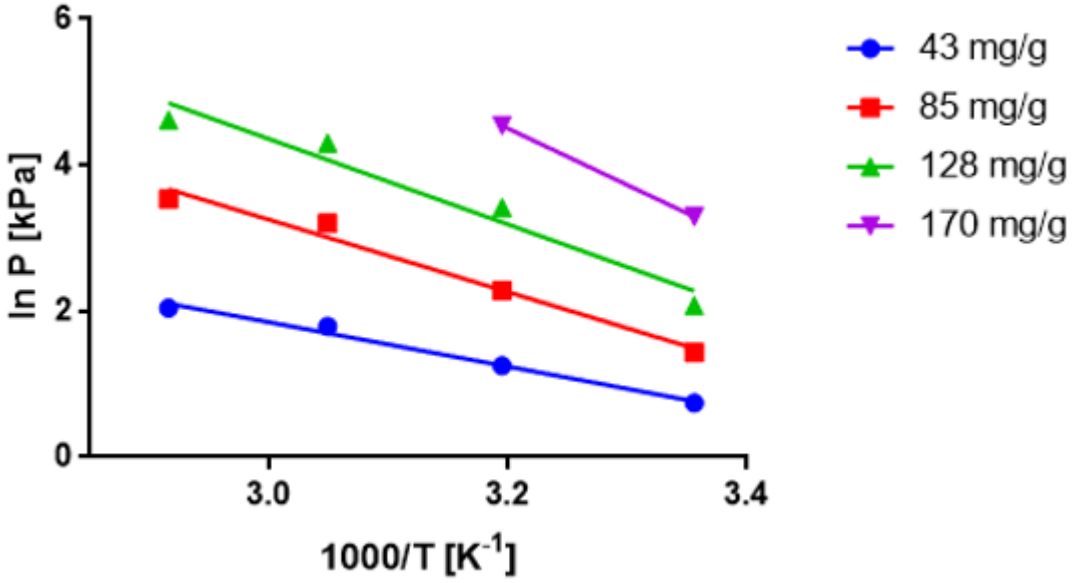

Figure A.19 | Natural log of pressure versus inverse temperature at constant loading for Zeolite 13X

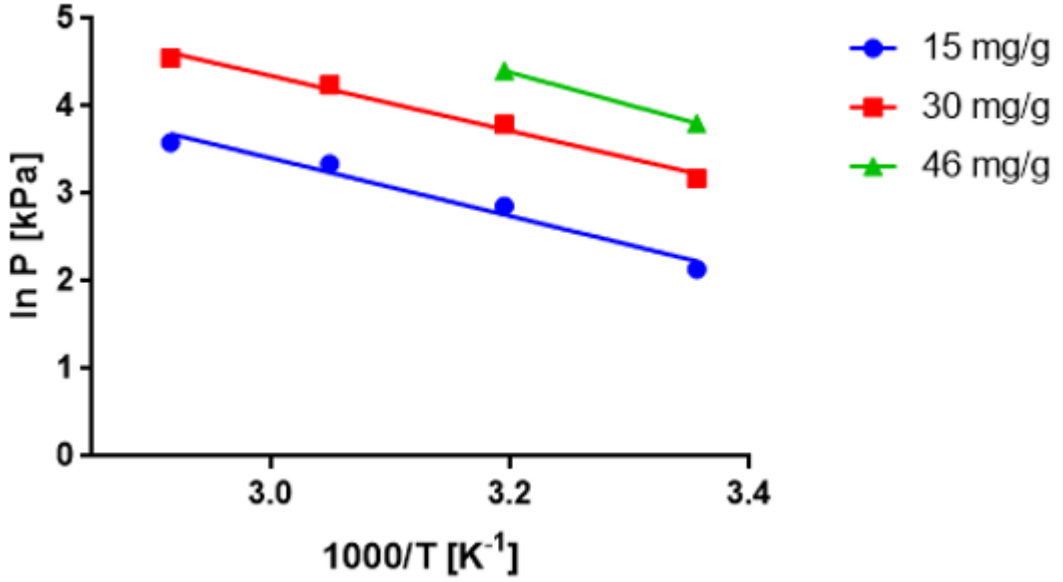

Figure A.20 | Natural log of pressure versus inverse temperature at constant loading for BPL GAC

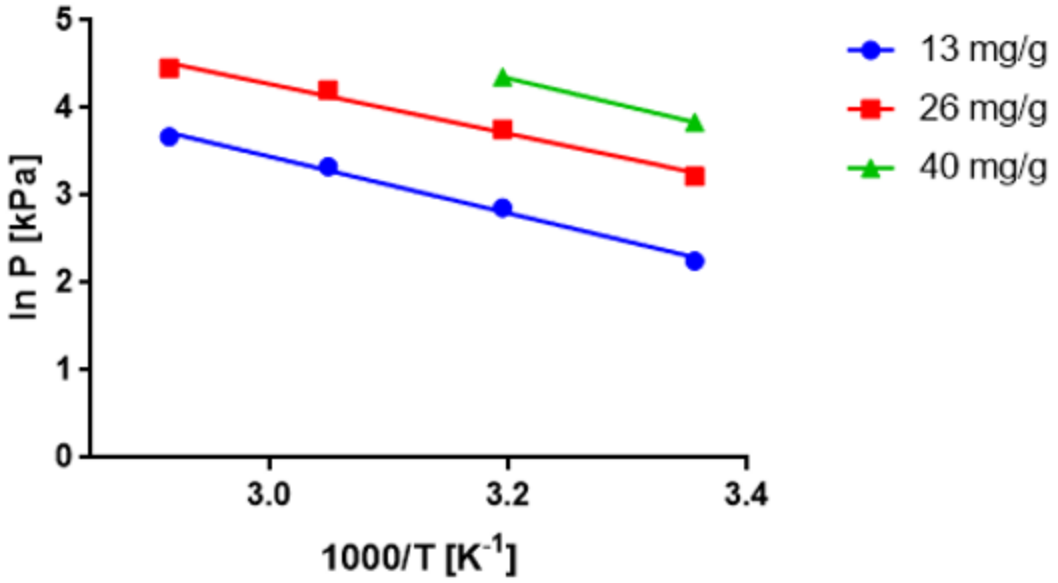

Figure A.21 | Natural log of pressure versus inverse temperature at constant loading for Darco KB-M PAC

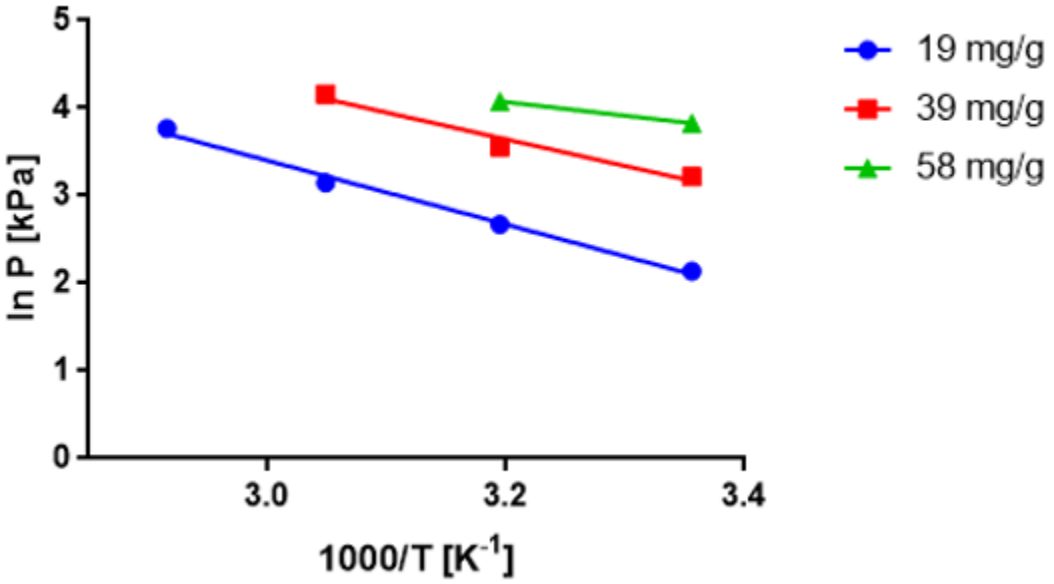

Figure A.22 | Natural log of pressure versus inverse temperature at constant loading for MIL-53

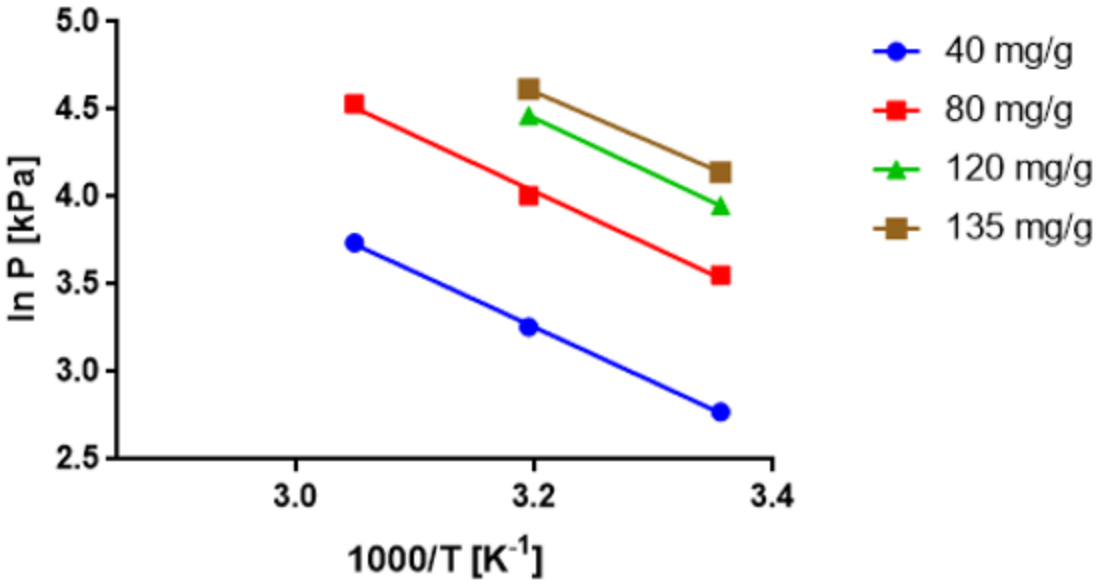

Figure A.23 | Natural log of pressure versus inverse temperature at constant loading for HKUST-1

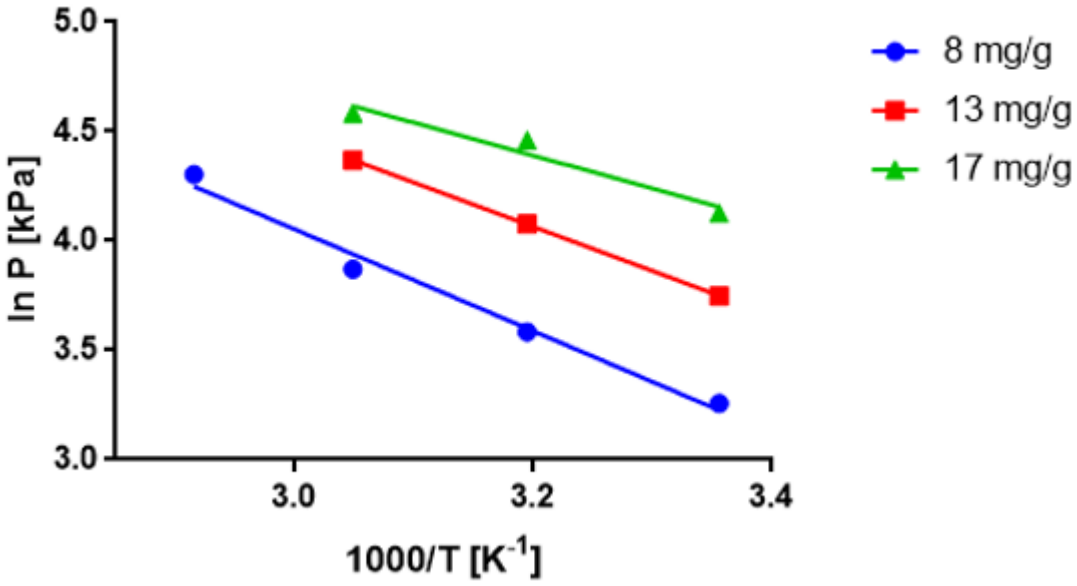

Figure A.24 | Natural log of pressure versus inverse temperature at constant loading for ZIF-8

References

26 U.S.C. § 45Q (as amended in 2018)

Abid, H. R., Rada, Z. H., Shang, J., & Wang, S. (2016). Synthesis, characterization, and CO2 adsorption of three metal-organic frameworks (MOFs): MIL-53, MIL-96, and amino-MIL-53. *Polyhedron*, 120, 103-111.

Aldy, J. E., Barrett, S., & Stavins, R. N. (2003). Thirteen plus one: a comparison of global climate policy architectures. *Climate policy, 3*(4), 373-397.

Allen, M. R., Frame, D. J., Huntingford, C., Jones, C. D., Lowe, J. A., Meinshausen, M., & Meinshausen, N. (2009). Warming caused by cumulative carbon emissions towards the trillionth tonne. *Nature*, 458(7242), 1163.

Amadeo, K. (2019). U.S. Inflation Rate by Year from 1929 to 2020: How Bad is Inflation? Past, Present, Future. *The Balance.*

An, F., & Santini, D.J. (2004). Mass Impacts on Fuel Economies of Conventional vs. Hybrid Electric Vehicles. *SAE Technical Paper* (SAE International).

Arora, V. K., Scinocca, J. F., Boer, G. J., Christian, J. R., Denman, K. L., Flato, G. M., ... & Merryfield, W. J. (2011). Carbon emission limits required to satisfy future representative concentration pathways of greenhouse gases. *Geophysical Research Letters*, 38(5).

Baciocchi, R., Storti, G., & Mazzotti, M. (2006). Process design and energy requirements for the capture of carbon dioxide from air. *Chemical Engineering and Processing: Process Intensification, 45*(12), 1047–1058.

Bahamon, D., & Vega, L. F. (2016). Systematic evaluation of materials for post-combustion CO2 capture in a Temperature Swing Adsorption process. *Chemical Engineering Journal*, 284, 438-447.

Banerjee, R., Phan, A., Wang, B., Knobler, C., Furukawa, H., O'Keeffe, M., & Yaghi, O. M. (2008). High-throughput synthesis of zeolitic imidazolate frameworks and application to CO_2 capture. *Science*, *319*(5865), 939–943.

Bilger, R.W., & Wu, Z. (2009). Carbon Capture for Automobiles Using Internal Combustion Rankine Cycle Engines. *Journal of Engineering for Gas Turbines and Power*, *131*(3), 34502.

Birol, F. (2014). *World Energy Outlook*. International Energy Agency.

Boot-Handford, M. E., Abanades, J. C., Anthony, E. J., Blunt, M. J., Brandani, S., Mac Dowell, N., ... & Haszeldine, R. S. (2014). Carbon capture and storage update. *Energy & Environmental Science*, *7*(1), 130-189.

Bordoff, J. & Larsen, J. (2018). US Carbon Tax Design: Options and Implications. Columbia University Center on Global Energy Policy.

Boutin, A., Coudert, F. X., Springuel-Huet, M. A., Neimark, A. V., Férey, G., & Fuchs, A. H. (2010). The behavior of flexible MIL-53(Al) upon CH4 and CO2 adsorption. *The Journal of Physical Chemistry C*, 114(50), 22237-22244.

Brandani, S. (2012). Carbon Dioxide Capture from Air: A Simple Analysis. *Energy & Environment, 23*(2–3), 319–328.

Brooker, A. D., Ward, J., & Wang, L. (2013). Lightweighting impacts on fuel economy, cost, and component losses (No. 2013-01-0381). *SAE Technical Paper.*

Burchell, T. D., Judkins, R. R., Rogers, M. R., & Williams, A. M. (1997). A novel process and material for the separation of carbon dioxide and hydrogen sulfide gas mixtures. *Carbon*, 35(9), 1279-1294.

Carlisle, S. (2016). We traded carriages for cars – let's embrace the next disruption. *The Globe and Mail.* Retrieved from https://www.theglobeandmail.com/report-on-business/rob-commentary/we-traded-carriages-for-cars-lets-embrace-the-next-disruption/article29782316/.

CDIAC. (2017). Carbon Dioxide Information Analysis Center. Retrieved from http://cdiac.ornl.gov/.

Cheah, L., & Heywood, J. (2011). Meeting U.S. passenger vehicle fuel economy standards in 2016 and beyond. *Energy Policy*, *39*(1), 454-466.

Cheng, Y., Kajiro, H., Noguchi, H., Kondo, A., Ohba, T., Hattori, Y., … Kanoh, H. (2011). Tuning of gate opening of an elastic layered structure MOF in CO_2 sorption with a trace of alcohol molecules. *Langmuir*, *27*(11), 6905–6909.

Cheng, Y., Kondo, A., Noguchi, H., Kajiro, H., Urita, K., Ohba, T., ... & Kanoh, H. (2009). Reversible structural change of Cu-MOF on exposure to water and its CO_2 adsorptivity. *Langmuir*, *25*(8), 4510-4513.

CO2CRC. (2017). Cooperative Research Centre for Greenhouse Gas Technologies. Retrieved from http://www.co2crc.com.au/.

Conti, J., Holtberg, P., Diefenderfer, J., LaRose, A., Turnure, J. T., & Westfall, L. (2016). International Energy Outlook, with projections to 2040. US DOE Energy Information Administration (EIA), Office of Energy Analysis.

Couck, S., Denayer, J. F. M., Baron, G. V, Rémy, T., Gascon, J., & Kapteijn, F. (2009). An amine-functionalized MIL-53 metal-organic framework with large separation power for CO_2 and CH_4. *Journal of the American Chemical Society*, *131*(18), 6326–7.

Cuéllar-Franca, R. M., & Azapagic, A. (2014). Carbon capture, storage and utilisation technologies: A critical analysis and comparison of their life cycle environmental impacts. *Journal of CO2 Utilization*, *9*, 82–102.

Damm, D. L., & Fedorov, A. G. (2008). Conceptual study of distributed CO_2 capture and the sustainable carbon economy. *Energy Conversion and Management*, 49(6), 1674–1683.

David, J., & Herzog, H. (2000). The cost of carbon capture. F*ifth International Conference on Greenhouse Gas Control Technologies*.

DeCicco, J. M. (2015). The liquid carbon challenge: evolving views on transportation fuels and climate. *Wiley Interdisciplinary Reviews: Energy and Environment*, *4*(1), 98–114.

Delft, C.E. (2012). Marginal abatement cost curves for heavy duty vehicles. Background report, Arno Schroten, Geert Warringa and Mart Bles*, Delft.*

Delgado, J. a., Uguina, M. a., Sotelo, J. L., Ruíz, B., & Gómez, J. M. (2006). Fixed-bed adsorption of carbon dioxide/methane mixtures on silicalite pellets. *Adsorption*, *12*(1), 5–18.

Deng, H., Yi, H., Tang, X., Yu, Q., Ning, P., & Yang, L. (2012). Adsorption equilibrium for sulfur dioxide, nitric oxide, carbon dioxide, nitrogen on 13X and 5A zeolites. *Chemical Engineering Journal, 188*, 77-85.

Dirar, Q. H., & Loughlin, K. F. (2013). Intrinsic adsorption properties of CO2 on 5A and 13X zeolite. *Adsorption*, 19(6), 1149-1163.

DOE. (2016). Carbon Dioxide Information Analysis Center. Retrieved from http://cdiac.ornl.gov/.

Dooley, J. J., Dahowski, R. T., & Davidson, C. L. (2008). On the Long-Term Average Cost of CO_2 Transport and Storage. *Pacific Northwest National Laboratory.*

DOT FHA. (2005). Logistic Costs and U.S. Gross Domestic Product. *U.S. Department of Transportation Federal Highway Administration.*

DOT. (2009). National Household Travel Survey. *U.S. Department of Transportation Federal Highway Administration*.

Eddaoudi, M., Moler, D. B., Li, H., Chen, B., Reineke, T. M., O'Keeffe, M., & Yaghi, O. M. (2001). Modular Chemistry: Secondary Building Units as a Basis for the Design of Highly Porous and Robust Metal−Organic Carboxylate Frameworks. *Accounts of Chemical Research*, *34*(4), 319–330.

EDF. (2017). The true cost of carbon pollution. *Environmental Defense Fund.* Retrieved from https://www.edf.org/true-cost-carbon-pollution.

EIA. (2017). Annual Energy Outlook 2017 with projections to 2050. *U.S. Energy Information Administration Office of Integrated and International Energy Analysis*, 1–64.

EIA. (2017). Power sector carbon dioxide emissions fall below transportation sector emissions. *U.S. Energy Information Administration.*

EIA. (2018). Short-Term Energy Outlook. *U.S. Energy Information Administration*.

Enkvist, P., Nauclér, T., & Rosander, J. (2007). A cost curve for greenhouse gas reduction. *McKinsey Quarterly*, *1*, 34.

EPA OTAQ. (2008). Average In-Use Emissions from Heavy-Duty Trucks. *U.S. Environmental Protection Agency Office of Transportation and Air Quality.*

EPA OTAQ. (2016). EPA and NHTSA Adopt Standards to Reduce Greenhouse Gas Emissions and Improve Fuel Efficiency of Medium- and Heavy-Duty Vehicles for Model Year 2018 and Beyond. *U.S. Environmental Protection Agency Office of Transportation and Air Quality.*

EPA, U.S. (2012). EPA and NHTSA Set Standards to Reduce Greenhouse Gases and Improve Fuel Economy for Model Years 2017-2025 Cars and Light Trucks. *U.S. Environmental Protection Agency.*

EPA, U.S. (2014). Control of air pollution from motor vehicles: Tier 3 motor vehicle emission and fuel standards. Retrieved from www.gpo.gov/fdsys/pkg/FR-2014-04- 28/pdf/2014-06954.pdf.

EPA, U.S. (2015). Clean Power Plan for Existing Power Plants. *U.S. Environmental Protection Agency.*

EPA, U.S. (2016). Greenhouse Gas Emissions and Fuel Efficiency Standards for Medium- and Heavy-Duty Engines and Vehicles—Phase 2. *U.S. Environmental Protection Agency.*

EPA, U.S. (2017.). Inventory of U.S. Greenhouse Gas Emissions and Sinks, 1990-2016 (Rep. No. 430-R-18-003). *United States Environmental Protection Agency*.

EPA, U.S. (2018). Greenhouse Gas Emissions from a Typical Passenger Vehicle. *U.S. Environmental Protection Agency.*

EPA, U.S. (2018). Inventory of U.S. Greenhouse Gas Emissions and Sinks, 1990-2017. *United States Environmental Protection Agency*.

Fairen-Jimenez, D., Moggach, S. a., Wharmby, M. T., Wright, P. a., Parsons, S., & Düren, T. (2011). Opening the gate: Framework flexibility in ZIF-8 explored by experiments and simulations. *Journal of the American Chemical Society*, *133*(23), 8900–8902.

FHA. (2017). Moving 12-Month Total Vehicle Miles Traveled. *U.S. Federal Highway Administration*.

Figueroa, J. D., Fout, T., Plasynski, S., McIlvried, H., & Srivastava, R. D. (2008). Advances in CO_2 capture technology—The U.S. Department of Energy's Carbon Sequestration Program. *International Journal of Greenhouse Gas Control*, *2*(1), 9–20.

Fracaroli, A. M., Furukawa, H., Suzuki, M., Dodd, M., Okajima, S., Gándara, F., … Yaghi, O. M. (2014). Metal-organic frameworks with precisely designed interior for carbon dioxide capture in the presence of water. *Journal of the American Chemical Society*, *136*(25), 8863–8866.

Fricko, O., Havlik, P., Rogelj, J., Klimont, Z., Gusti, M., Johnson, N., ... & Ermolieva, T. (2017). The marker quantification of the Shared Socioeconomic Pathway 2: A middle-of-the-road scenario for the 21st century. *Global Environmental Change*, *42*, 251-267.

Friedrich, J., Ge, M., & Pickens, A. (2017). This Interactive Chart Explains World's Top 10 Emitters, and How They've Changed. World Resources Institute. Retrieved from https://www.wri.org/blog/2017/04/interactive-chart-explains-worlds-top-10-emitters-and-how-theyve-changed.

Fulton, L., Mason, J., & Meroux, D. (2017). Three Revolutions in Urban Transportation: How to achieve the full potential of vehicle electrification, automation, and shared mobility in urban transportation systems around the world by 2050. *Institute for Transportation and Development Policy.*

Furukawa, H., Ko, N., Go, Y. B., Aratani, N., Choi, S. B., Choi, E., ... & Yaghi, O. M. (2010). Ultrahigh porosity in metal-organic frameworks. *Science*, *329*(5990), 424-428.

GCP. (2016). 10 Years of Advancing Knowledge on the Global Carbon Cycle and its Management. *The Global Carbon Project*.

Godec, M. L. (2011). Global technology roadmap for CCS in industry sectoral assessment CO2 enhanced oil recovery. *Global CCS Institute*. Arlington, Virginia.

Goeppert, A., Czaun, M., Prakash, G. S., & Olah, G. A. (2012). Air as the renewable carbon source of the future: an overview of CO_2 capture from the atmosphere. *Energy & Environmental Science*, *5*(7), 7833-7853.

Gota, S., Huizenga, C., & Peet, K. (2016). Implications of 2DS and 1.5 DS for land transport carbon emissions in 2050. *Partnership for Sustainable Low-Carbon Transportation*, PPMC.

Grant, T., Morgan, D., & Gerdes, K. (2013). Carbon dioxide transport and storage costs in NETL studies. *NETL Laboratory, U.S. Department of Energy.*

H.R. 6463. (2018). Modernizing America with Rebuilding to Kickstart the Economy of the Twenty-first Century with a Historic Infrastructure-Centered Expansion Act. House of Representative, 115th Congress, 2nd session.

Hao, G.-P., Li, W.-C., & Lu, A.-H. (2011). Novel porous solids for carbon dioxide capture. *Journal of Materials Chemistry*, *21*(18), 6447.

Hartin, C. a., Patel, P., Schwarber, a., Link, R. P., & Bond-Lamberty, B. P. (2015). A simple object-oriented and open-source model for scientific and policy analyses of the global climate system - Hector v1.0. *Geoscientific Model Development*, *8*(4), 939–955.

Hausfather, Z. (2018). Explainer: How 'Shared Socioeconomic Pathways' explore future climate change. *CarbonBrief.*

Herzog, H. J. (2001). What Future for Carbon Capture and Sequestration? *Environmental Science & Technology*, 35(7), 148–153.

Hill, N., Finnegan, S., Norris, J., Brannigan, C., Wynn, D., Baker, H., & Skinner, I. (2011). Reduction and testing of greenhouse gas (GHG) emissions from heavy duty vehicles–Lot 1: strategy. *Final report to the European Commission–DG Climate Action. AEA Technology*.

Holmes, G., & Keith, D. W. (2012). An air–liquid contactor for large-scale capture of CO_2 from air. *Philosophical Transactions of the Royal Society A*, *370*(1974), 4380-4403.

House, K. Z., Baclig, A. C., Ranjan, M., van Nierop, E. A., Wilcox, J., & Herzog, H. J. (2011). Economic and energetic analysis of capturing CO_2 from ambient air. *Proceedings of the National Academy of Sciences*, *108*(51), 20428-20433.

IAWG, US. (2013). Technical support document: Technical update of the social cost of carbon for regulatory impact analysis under executive order 12866. *Interagency Working Group on Social Cost of Carbon*, United States Government, Washington, DC.

IPCC. (2013). Summary for Policymakers. Climate Change 2013: The Physical Science Basis. Contribution of Working Group I. *Fifth Assessment Report of the Intergovernmental Panel on Climate Change (IPCC AR5).*

IPCC. (2018). Global Warming of 1.5ºC: an IPCC special report on the impacts of global warming of 1.5ºC above pre-industrial levels and related global greenhouse gas emissions pathways, in the context of strengthening the global response to the threat of climate change, sustainable development, and efforts to eradicate poverty. Intergovernmental Panel on Climate Change.

Kanoh, H., Kondo, A., Noguchi, H., Kajiro, H., Tohdoh, A., Hattori, Y., … Kaneko, K. (2009). Elastic layer-structured metal organic frameworks (ELMs). *Journal of Colloid and Interface Science*, *334*(1), 1–7.

Kaplan, W. (2002). *Advanced calculus*.

Karplus, V. J., Paltsev, S., Babiker, M., & Reilly, J. M. (2013). Should a vehicle fuel economy standard be combined with an economy-wide greenhouse gas emissions constraint? Implications for energy and climate policy in the United States. *Energy Economics*, *36*, 322-333.

Kaufman, N. & Gordon, K. (2018). The Energy, Economic, and Emissions Impacts of a Federal US Carbon Tax. Columbia University Center on Global Energy Policy.

Kaufman, N., Larsen, J., Mohan, S., Herndon, W., Marsters, P., Diamon, J., Zodrow, G. (2018). Emissions, Energy, and Economic Implications of the Curbelo Carbon Tax Proposal. Columbia University Center on Global Energy Policy.

Keith, D. W., Ha-Duong, M., & Stolaroff, J. K. (2006). Climate strategy with CO_2 capture from the air. *Climatic Change*, *74*(1), 17-45.

Keskin, S., van Heest, T. M., & Sholl, D. S. (2010). Can Metal–Organic Framework Materials Play a Useful Role in Large-Scale Carbon Dioxide Separations. *Chemistry and Sustainability, 3*(8), 879-891.

Kim, J. H., Lee, C. H., Kim, W. S., Lee, J. S., Kim, J. T., Suh, J. K., & Lee, J. M. (2003). Adsorption equilibria of water vapor on alumina, zeolite 13X, and a zeolite X/activated carbon composite. *Journal of Chemical & Engineering Data*, *48*(1), 137-141.

Kitagawa, S., Kitaura, R., & Noro, S. (2004). Functional porous coordination polymers. *Angewandte Chemie (International Ed. in English)*, *43*(18), 2334–75.

Kizzie, A. C., Wong-Foy, A. G., & Matzger, A. J. (2011). Effect of humidity on the performance of microporous coordination polymers as adsorbents for CO_2 capture. *Langmuir*, *27*(10), 6368-6373.

Kodjak, D. (2015). Policies to reduce fuel consumption, air pollution, and carbon emissions from vehicles in G20 nations. *The International Council on Clean Transportation*.

Kopp, A., Block, R. I., & Iimi, A. (2013). Turning the right corner: Ensuring development through a low-carbon transport sector. *World Bank Publications.*

Kriegler, E., O'Neill, B. C., Hallegatte, S., Kram, T., Lempert, R. J., Moss, R. H., & Wilbanks, T. (2012). The need for and use of socio-economic scenarios for climate change analysis: a new approach based on shared socio-economic pathways. *Global Environmental Change*, *22*(4), 807-822.

Krumm, J. (2012). How People Use Their Vehicles: Statistics from the 2009 National Household Travel Survey. *SAE 2012 World Congress & Exhibition*, 1–12.

Lackner, K. S., Grimes, P., & Ziock, H. J. (2001). Capturing carbon dioxide from air. *Carbon Capture and Storage: CO2 Management Technologies.*

Lambert, F. (2018). Tesla Semi is not scaring Daimler, CEO throws cold water and says they will dominate electric trucks. Retrieved from https://electrek.co/2018/11/05/tesla-semi-daimler-ceo-electric-trucks/.

Landrigan, P. J., Fuller, R., Acosta, N. J., Adeyi, O., Arnold, R., Baldé, A. B., ... & Chiles, T. (2017). The Lancet Commission on pollution and health. *The Lancet.*

Lastoskie, C. (2010). Caging carbon dioxide. *Science*, *330*(6004), 595–596.

Law, K., Jackson, M., & Chan, M. (2011). European Union greenhouse gas reduction potential for heavy-duty vehicles. Cupertino, CA, *TIAX LLC*.

Le Quéré, C., Andrew, R. M., Friedlingstein, P., Sitch, S., Pongratz, J., Manning, A. C., ... & Boden, T. A. (2017). Global carbon budget 2017. Earth System Science Data Discussions, 1-79.

Lee, J. S., Kim, J. H., Kim, J. T., Suh, J. K., Lee, J. M., & Lee, C. H. (2002). Adsorption equilibria of CO_2 on zeolite 13X and zeolite X/activated carbon composite. *Journal of Chemical & Engineering Data*, *47*(5), 1237-1242.

Levinson, Marc. (2013). The Box: How the Shipping Container Made the World Smaller and the World Economy Bigger. *Princeton University Press.*

Li, G., Xiao, P., Webley, P., Zhang, J., Singh, R., & Marshall, M. (2008). Capture of CO_2 from high humidity flue gas by vacuum swing adsorption with zeolite 13X. *Adsorption*, *14*(2-3), 415-422.

Li, J. R., Ma, Y., McCarthy, M. C., Sculley, J., Yu, J., Jeong, H. K., … Zhou, H. C. (2011). Carbon dioxide capture-related gas adsorption and separation in metal-organic frameworks. *Coordination Chemistry Reviews*, *255*(15–16), 1791–1823.

Liu, J., Wang, Y., Benin, A. I., Jakubczak, P., Willis, R. R., & LeVan, M. D. (2010). CO_2/H_2O adsorption equilibrium and rates on metal− organic frameworks: HKUST-1 and Ni/DOBDC. *Langmuir*, *26*(17), 14301-14307.

Lutsey, N., & Sperling, D. (2009). Greenhouse gas mitigation supply curve for the United States for transport versus other sectors. *Transportation Research Part D: Transport and Environment*, 14(3), 222–229.

Lynas, M. (2008). *Six Degrees to a Hotter Planet*.

Marchal, V., Dellink, R., van Vuuren, D., Clapp, C., Château, J., Lanzi, E., ... & van Vliet, J. (2012). OECD Environmental Outlook to 2050: The consequences of inaction. *The Organization for Economic Cooperation and Development.*

Marcucci, A., Kypreos, S., & Panos, E. (2017). The road to achieving the long-term Paris targets: energy transition and the role of direct air capture. *Climatic Change*, *144*(2), 181-193

Martín, C. F., Stöckel, E., Clowes, R., Adams, D. J., Cooper, A. I., Pis, J. J., ... & Pevida, C. (2011). Hypercrosslinked organic polymer networks as potential adsorbents for pre-combustion CO2 capture. *Journal of Materials Chemistry*, 21(14), 5475-5483.

Mason, J. A., McDonald, T. M., Bae, T. H., Bachman, J. E., Sumida, K., Dutton, J. J., ... & Long, J. R. (2015). Application of a high-throughput analyzer in evaluating solid adsorbents for post-combustion carbon capture via multicomponent adsorption of CO_2, N_2, and H_2O. *Journal of the American Chemical Society*, *137*(14), 4787-4803.

Matthews, H. D., N. P. Gillett, P. A. Stott, and K. Zickfeld. (2009). The proportionality of global warming to cumulative carbon emissions. Nature, 459 (829–832).

McCollum, D., & Yang, C. (2009). Achieving deep reductions in US transport greenhouse gas emissions: Scenario analysis and policy implications. Energy Policy, 37(12), 5580-5596.

McCoy, S. T., & Rubin, E. S. (2008). An engineering-economic model of pipeline transport of CO_2 with application to carbon capture and storage. *International Journal of Greenhouse Gas Control*, *2*(2), 219-229.

McEwen, J., Hayman, J.-D., & Ozgur Yazaydin, A. (2013). A comparative study of CO_2, CH_4 and N_2 adsorption in ZIF-8, Zeolite-13X and BPL activated carbon. *Chemical Physics*, *412*, 72–76.

Metz, B., Davidson, O., De Coninck, H., Loos, M., & Meyer, L. (2012). Carbon dioxide capture and storage. *IPCC Special Report*.

Miller, S. A., & Keoleian, G. A. (2015). Framework for analyzing transformative technologies in life cycle assessment. *Environmental science & technology*, *49*(5), 3067-3075.

Moultak, M., Lutsey, N., & Hall, D. (2017). Transitioning to zero-emission heavy-duty freight vehicles. *International Council on Clean Transportation: Washington, DC, USA*.

Mulloth, L. M., & Finn, J. E. (1998). Carbon dioxide adsorption on a 5A zeolite designed for CO2 removal in spacecraft cabins. *NASA*.

NAS. (2013). Transitions to alternative vehicles and fuels. National Research Council, National Academies Press.

National Academies of Sciences, Engineering, and Medicine. (2018). Direct Air Capture and Mineral Carbonation Approaches for Carbon Dioxide Removal and Reliable Sequestration: Proceedings of a Workshop- in Brief. *The National Academies Press.*

National Research Council. (2015). Climate intervention: Carbon Dioxide Removal and Reliable Sequestration. *The National Academies Press.*

Nauclér, T., & Enkvist, P. (2009). Pathways to a low-carbon economy: Version 2 of the global greenhouse gas abatement cost curve. *McKinsey & Company, 192*.

Neuharth, A. (2006). Traveling interstates is our sixth freedom. *USA Today*. Retrieved from https://usatoday30.usatoday.com/news/opinion/columnist/neuharth/2006-06-22-interstates_x.htm.

Newbold, S. C., Griffiths, C., Moore, C., Wolverton, A., & Kopits, E. (2010). The "social cost of carbon" made simple. *Environmental Protection Agency National Center for Environmental Economics*. Working Paper Series, (10-07).

Nguyen, N. T. T., Furukawa, H., Gándara, F., Nguyen, H. T., Cordova, K. E., & Yaghi, O. M. (2014). Selective capture of carbon dioxide under humid conditions by hydrophobic chabazite-type zeolitic imidazolate frameworks. *Angewandte Chemie - International Edition*, *53*(40), 10645–10648.

NOAA (2019). National Centers for Environmental Information, State of the Climate: Global Climate Report for Annual 2018. *National Oceanic & Atmospheric Administration.*

Nykvist, B., & Nilsson, M. (2015). Rapidly falling costs of battery packs for electric vehicles. *nature climate change*, *5*(4), 329.

OICA. (2017). 2005-2016 Sales Statistics. *International Organization of Motor Vehicle Manufacturers*. Retrieved from http://www.oica.net/category/sales-statistics/

Pan, H., Ritter, J. A., & Balbuena, P. B. (1998). Examination of the approximations used in determining the isosteric heat of adsorption from the Clausius−Clapeyron equation. *Langmuir*, 14(21), 6323-6327.

Perez, M. L., Susa, M. R., Pellerano, M., & Delebarre, A. (2012). Technico-economical evaluation of CO_2 transport in an adsorbed phase. *Low Carbon Economy*, 21-33.

Phan, a, Doonan, C. J., Uribe-Romo, F. J., Knobler, C. B., O'Keeffe, M., & Yaghi, O. M. (2010). Synthesis, Structure, and Carbon Dioxide Capture Properties of Zeolitic Imidazolate Frameworks. *Accounts of Chemical Research*, *43*(1), 58–67.

Pielke, R. A. (2009). An idealized assessment of the economics of air capture of carbon dioxide in mitigation policy. *Environmental Science & Policy*, *12*(3), 216-225.

Pires, J. C. M., Martins, F. G., Alvim-Ferraz, M. C. M., & Simões, M. (2011). Recent developments on carbon capture and storage: An overview. *Chemical Engineering Research and Design*, *89*(9), 1446–1460.

Pritchard, C., Yang, A., Holmes, P., & Wilkinson, M. (2015). Thermodynamics, economics and systems thinking: What role for air capture of CO_2? *Process Safety and Environmental Protection*, *94*, 188-195.

Randall, T. (2017). Transport Sector Now Largest Source of Greenhouse Gas Pollution in US. Retrieved from https://www.ttnews.com/articles/transport-sector-now-largest-source-greenhouse-gas-pollution-us.

Ranjan, M., & Herzog, H. J. (2011). Feasibility of air capture. *Energy Procedia*, *4*, 2869-2876.

Rao, S., Klimont, Z., Smith, S. J., Van Dingenen, R., Dentener, F., Bouwman, L., ... & Reis, L. A. (2017). Future air pollution in the Shared Socio-economic Pathways. Global Environmental Change, 42, 346-358.

Reinhart, T. E. (2015). Commercial medium-and heavy-duty truck fuel efficiency technology study-Report# 1 *U.S. Department of Transportation.* (No. DOT HS 812 146).

Riahi, K., Rao, S., Krey, V., Cho, C., Chirkov, V., Fischer, G., ... & Rafaj, P. (2011). RCP 8.5—A scenario of comparatively high greenhouse gas emissions. *Climatic Change*, *109*(1-2), 33.

Riahi, K., Van Vuuren, D. P., Kriegler, E., Edmonds, J., O'neill, B. C., Fujimori, S., ... & Lutz, W. (2017). The shared socioeconomic pathways and their energy, land use, and greenhouse gas emissions implications: an overview. Global Environmental Change, 42, 153-168.

Ricke, K. L., & Caldeira, K. (2014). Maximum warming occurs about one decade after a carbon dioxide emission. *Environmental Research Letters*, *9*(12), 124002.

Ritchie, H., & Roser, M. (2019). Fossil Fuels. Retrieved from https://ourworldindata.org/fossil-fuels.

Ruthven, D. M. (2014). CO_2 capture: Value functions, separative work and process economics. *Chemical Engineering Science*, *114*.

Saha, D., Bao, Z., Jia, F., & Deng, S. (2010). Adsorption of CO2, CH4, N2O, and N2 on MOF-5, MOF-177, and zeolite 5A. *Environmental science & technology*, *44*(5), 1820-1826.

Sharpe, B., Lutsey, N., Delgado, O., & Muncrief, R. (2016). United States efficiency and greenhouse gas emission regulations for model year 2018-2027 heavy-duty vehicles, engines, and trailers. *International Council on Clean Transportation.*

Shen, D., Bülow, M., Siperstein, F., Engelhard, M., & Myers, A. L. (2000). Comparison of experimental techniques for measuring isosteric heat of adsorption. *Adsorption*, 6(4), 275-286.

Singh, V. K., & Kumar, E. A. (2016). Comparative studies on CO2 adsorption kinetics by solid adsorbents. *Energy Procedia*, 90, 316-325.

SmartWay. (2017). *United States Environmental Protection Agency SmartWay Program*. Retrieved from https://www.epa.gov/smartway/learn-about-smartway.

Smith, S. J., Edmonds, J., Hartin, C. A., Mundra, A., & Calvin, K. (2015). Near-term acceleration in the rate of temperature change. Nature Climate Change, 5(4), 333.

Socolow, R., Desmond, M., Aines, R., Blackstock, J., Bolland, O., Kaarsberg, T., ... & Siirola, J. (2011). Direct air capture of CO_2 with chemicals: a technology assessment for the APS Panel on Public Affairs. *American Physical Society.*

Song, H. K., & Lee, K. H. (1998). Adsorption of carbon dioxide on chemically modified carbon adsorbents. *Separation science and technology*, 33(13), 2039-2057.

Sotomayor, F.J. (2016). Carbon Capture: Materials and Strategies (Doctoral thesis). *University of Michigan.*

Soubeyrand-Lenoir, E., Vagner, C., Yoon, J. W., Bazin, P., Ragon, F., Hwang, Y. K., ... & Llewellyn, P. L. (2012). How water fosters a remarkable 5-fold increase in low-pressure CO_2 uptake within mesoporous MIL-100 (Fe). *Journal of the American Chemical Society*, *134*(24), 10174-10181.

Sullivan, J. M., & Sivak, M. (2012). Carbon capture in vehicles: A review of general support, available mechanisms, and consumer acceptance issues. *University of Michigan Transportation Research Institute.*

Sullivan, J. M., Sivak, M., & Schoettle, B. (2013). A survey of driver opinion about carbon capture in vehicles. *University of Michigan Transportation Research Institute*.

Sun, Y., Wang, Y., Zhang, Y., Zhou, Y., & Zhou, L. (2007). CO 2 sorption in activated carbon in the presence of water. *Chemical physics letters*, 437(1), 14-16.

Supekar, S. D., & Skerlos, S. J. (2015). Reassessing the Efficiency Penalty from Carbon Capture in Coal-Fired Power Plants. *Environmental Science & Technology*, *49*(20).

Supekar, S. D., & Skerlos, S. J. (2017). Analysis of Costs and Time Frame for Reducing CO2 Emissions by 70% in the US Auto and Energy Sectors by 2050. *Environmental Science & Technology,* 51(19), 10932-10942.

Tokarska, K. B., Gillett, N. P., Arora, V. K., Lee, W. G., & Zickfeld, K. (2018). The influence of non-CO2 forcings on cumulative carbon emissions budgets. Environmental Research Letters, 13(3), 034039.

Tonachel, L. (2015). Study: Electric Vehicles Can Dramatically Reduce Carbon Pollution from Transportation and Improve Air Quality. Retrieved from https://www.nrdc.org/experts/luke-tonachel/study-electric-vehicles-can-dramatically-reduce-carbon-pollution.

Trigg, T., Telleen, P., Boyd, R., Cuenot, F., D'Ambrosio, D., Gaghen, R., ... & Kaneko, H. (2013). Global EV Outlook: Understanding the Electric Vehicle Landscape to 2020. *International Energy Agency.*

UN. (2012). World Population Prospects: the 2012 Revision. *The United Nations*.

UNFCC. (2016) Paris Agreement. United Nations Treaty Collection. *United Nations Framework Convention on Climate Change.*

Van Vuuren, D. P., Edmonds, J., Kainuma, M., Riahi, K., Thomson, A., Hibbard, K., … Rose, S. K. (2011). The representative concentration pathways: An overview. *Climatic Change*, *109*(1), 5–31.

Van Vuuren, D. P., Stehfest, E., Gernaat, D. E., Doelman, J. C., Van den Berg, M., Harmsen, M., ... & Girod, B. (2017). Energy, land-use and greenhouse gas emissions trajectories under a green growth paradigm. Global Environmental Change, 42, 237-250.

Wallace, M., Goudarzi, L., Callahan, K., & Wallace, R. (2015). A Review of the CO_2 Pipeline Infrastructure in the U.S. *Department of Energy National Energy Technology Laboratory.*

Wang, B., Côté, A. P., Furukawa, H., O'Keeffe, M., & Yaghi, O. M. (2008). Colossal cages in zeolitic imidazolate frameworks as selective carbon dioxide reservoirs. *Nature*, *453*(7192), 207–211.

Wang, Y., & LeVan, M. D. (2009). Adsorption equilibrium of carbon dioxide and water vapor on zeolites 5A and 13X and silica gel: pure components. *Journal of Chemical & Engineering Data*, *54*(10), 2839-2844.

Wennersten, R., Sun, Q., & Li, H. (2014). The future potential for Carbon Capture and Storage in climate change mitigation – an overview from perspectives of technology, economy and risk. *Journal of Cleaner Production*, *103*, 724–736.

White House. (2014). Fact Sheet: U.S.-China Joint Announcement on Climate Change and Clean Energy Cooperation. Retrieved from https://www.whitehouse.gov/the-press-office/2014/11/11/fact-sheet-us-china-joint-announcement-climate-change-and-clean-energy-c.

White House. (2016). U.S. Leadership and the Historic Paris Agreement to Combat Climate Change. Retrieved from https://www.whitehouse.gov/the-press-office/2015/12/12/us-leadership-and-historic-paris-agreement-combat-climate-change.

Wilcox, J. (2012). *Carbon capture*. Springer Science & Business Media.

Wilcox, J., Psarras, P. C., & Liguori, S. (2017). Assessment of reasonable opportunities for direct air capture. *Environmental Research Letters*, 12(6), 065001.

Wilson, L. (2013). Shades of Green: Electric Cars' Carbon Emissions Around the Globe. Retrieved from http://shrinkthatfootprint.com/wp-content/uploads/2013/02/Shades-of-Green-Full-Report.pdf.

Wong, S. (2005). CO2 compression and transportation to storage reservoir. Building capacity for CO2 capture and storage in the APEC region. *A training manual for policy makers and practitioners*. Singapore: APEC.

World Bank. (2019). World Bank Open Data. *The World Bank.* Retrieved from https://data.worldbank.org.

Yazaydın, A. O., Snurr, R. Q., Park, T. H., Koh, K., Liu, J., LeVan, M. D., ... & Low, J. J. (2009). Screening of metal− organic frameworks for carbon dioxide capture from flue gas using a combined experimental and modeling approach. *Journal of the American Chemical Society*, 131(51), 18198-18199. https://doi.org/10.1021/ja9057234

Yong, Z., Mata, V. G., & Rodrigues, A. E. (2001). Adsorption of carbon dioxide on chemically modified high surface area carbon-based adsorbents at high temperature. *Adsorption*, 7(1), 41-50.

Zeman, F. (2007). Energy and material balance of CO_2 capture from ambient air. *Environmental science & technology*, *41*(21), 7558-7563.

Zeman, F. (2014). Reducing the cost of Ca-based CO_2. *Environmental science & technology*, *48*(19), 11730-11735.